INSIDE TRACK with **MINDSPEED TECHNOLOGIES'** RUPERT BAINES p32

EVALUATE DIFFERENT **EM** SIMULATORS p62

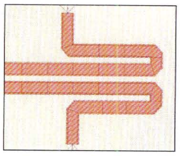

TAKE A MEASURE OF **THERMAL** MANAGEMENT p50

MicroWaves&RF

APRIL 2012 TRUSTED ENGINEERING RESOURCE FOR 50 YEARS www.MWRF.com

AMPLIFIERS & OSCILLATORS ISSUE

Tx/Rx Chips Communicate at 60 GHz

A PENTON PUBLICATION
Periodicals Postage Paid • USPS 100 Approved Poly

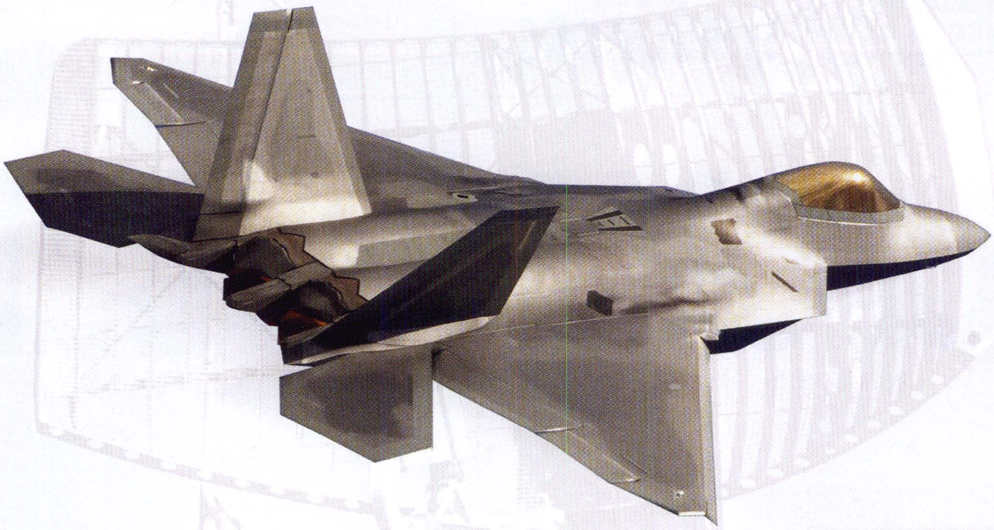

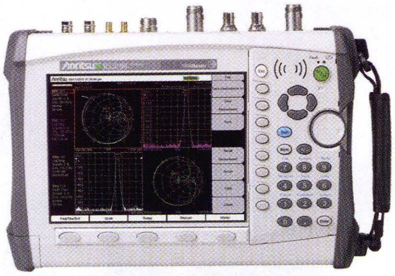

More Than Just Low Noise AMPLIFIERS

- Cryogenic
- Limiting
- Variable Gain
- Limiter Input
- TTL Controlled
- High Dynamic Range
- Equalized Gain
- Built-in Test
- Detected Output
- Military Versions
- Space Qualified
- Super Low Noise

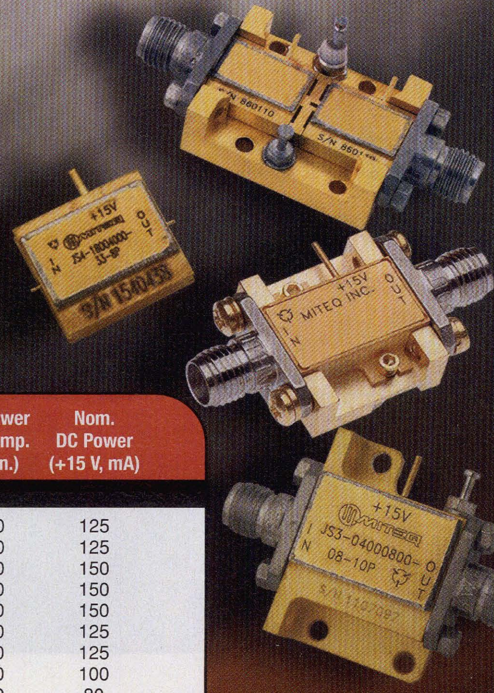

Model Number	Frequency Range (GHz)	Gain (Min./Max.) (dB)	Gain Flatness (±dB)	Noise Figure (dB, Max.)	VSWR IN/OUT (Max.)	Output Power @ 1 dB Comp. (dBm, Min.)	Nom. DC Power (+15 V, mA)
OCTAVE BAND AMPLIFIERS							
AFS3-00120025-09-10P-4	0.12-.25	38	0.50	0.9	2.0:1	+10	125
AFS3-00250050-08-10P-4	0.25-0.5	38	0.50	0.8	2.0:1	+10	125
AFS3-00500100-06-10P-6	0.5-1	38	0.75	0.6	2.0:1/1.5:1	+10	150
AFS3-01000200-05-10P-6	1-2	38	1.00	0.5	2.0:1	+10	150
AFS3-01200240-06-10P-6	1.2-2.4	34	1.00	0.6	2.0:1	+10	150
AFS3-02000400-06-10P-4	2-4	32	1.00	0.6	2.0:1	+10	125
AFS3-02600520-10-10P-4	2.6-5.2	28	1.00	1.0	2.0:1	+10	125
AFS3-04000800-07-10P-4	4-8	32	1.00	0.7	2.0:1	+10	100
AFS3-08001200-09-10P-4	8-12	28	1.00	0.9	2.0:1	+10	80
AFS3-08001600-15-8P-4	8-16	28	1.00	1.5	2.0:1	+8	100
AFS4-12001800-18-10P-4	12-18	28	1.50	1.8	2.0:1	+10	125
JS4-18002600-22-10P	18-26	35	1.50	2.2	2.0:1	+10	200
JS3-18004000-40-15P	18-40	32	2.70	4.0	2.6:1	+15	400*
JS4-18004000-30-5P	18-40	23	2.50	3.0	2.5:1	+5	200
JS42-18004000-31-8P	18-40	35	3.50	3.1	2.5:1	+8	300
JS1-26004000-100-19P	26-40	17	2.50	10.0	2.5:1	+19	400*
JS4-26004000-30-8P	26-40	23	2.50	3.0	2.5:1	+8	200
JS42-26004000-31-8P	26-40	37	3.50	3.1	2.5:1	+8	300
MULTIOCTAVE BAND AMPLIFIERS							
AFS3-00500200-08-15P-4	0.5-2	38	1.00	0.8	2.0:1	+15	125
AFS3-01000400-10-10P-4	1-4	30	1.50	1.0	2.0:1	+10	125
AFS3-02000800-09-10P-4	2-8	26	1.00	0.9	2.0:1	+10	125
AFS4-02001800-24-10P-4	2-18	35	2.50	2.4	2.5:1	+10	175
AFS4-06001800-22-10P-4	6-18	25	2.00	2.2	2.0:1	+10	125
AFS4-08001800-22-10P-4	8-18	28	2.00	2.2	2.0:1	+10	125
ULTRA WIDEBAND AMPLIFIERS							
AFS3-00100100-09-10P-4	0.1-1	38	1.00	0.9	2.0:1	+10	125
AFS3-00100200-10-15P-4	0.1-2	38	1.00	1.0	2.0:1	+15	150
AFS3-00100300-12-10P-4	0.1-3	34	1.00	1.2	2.0:1	+10	125
AFS3-00100400-13-10P-4	0.1-4	30	1.00	1.3	2.0:1	+10	125
AFS3-00100600-13-10P-4	0.1-6	30	1.25	1.3	2.0:1	+10	125
AFS3-00100800-14-10P-4	0.1-8	28	1.50	1.4	2.0:1	+10	125
AFS4-00101200-22-10P-4	0.1-12	30	1.50	2.2	2.0:1	+10	150
JS4-00102000-25-10P	0.1-20	29	2.00	2.5**	2.5:1	+10	200
JS4-00102600-30-10P	0.1-26	28	2.50	3.0**	2.5:1	+10	200
JS4-00104000-54-5P	0.1-40	30	3.00	5.4**	2.5:1	+5	200

Noise figure increases below 500 MHz.
* Dual Voltage, -8V@50 mA. ** Above 800 mHz.

3 YEAR WARRANTY

ISO 9001 Registered · ANAB Accredited · AS9100 Registered

RoHS compliant Available

This is only a small sample of our extensive list of standard catalog items. Please contact our Sales Department at (631) 439-9220 or e-mail components@miteq.com for additional information or to discuss your custom requirements.

MITEQ®

100 Davids Drive, Hauppauge, NY 11788
TEL.: (631) 436-7400 • FAX: (631) 436-7430
www.miteq.com

APRIL 2012
Volume 51, Issue 4

MicroWaves&RF

CONTENTS

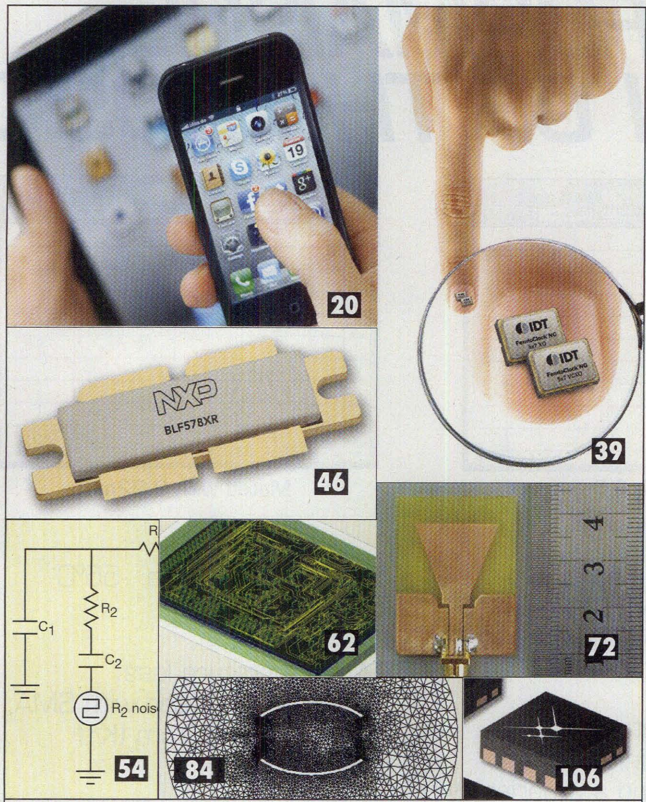

INDUSTRY TRENDS AND ANALYSIS

DESIGN FEATURES

COVER STORY

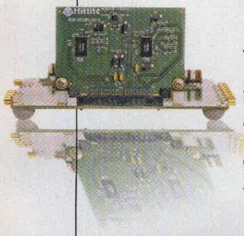

PRODUCT TECHNOLOGY

NEWS & COLUMNS

SPECIAL SECTION

Defense Electronics

Starts after **p. 72**

Penton
Electronics Group

HIGH POWER

PRODUCTS

POWER DIVIDERS

Model #	Frequency (MHz)	Insertion Loss (dB) [Typ./Max.] ◊	Amplitude Unbalance (dB) [Typ./Max.]	Phase Unbalance (Deg.) [Typ./Max.]	Isolation (dB) [Typ./Min.]	VSWR (Typ)	Input Power (Watts) [Max.] ▫	Package
2-WAY								
DSK-729S	800 - 2200	0.5 / 0.8	0.05 / 0.4	1 / 2	25 / 20	1.3:1	10	215
DSK-H3N	800 - 2400	0.5 / 0.8	0.25 / 0.5	1 / 4	23 / 18	1.5:1	30	220
P2D100800	1000 - 8000	0.6 / 1.1	0.05 / 0.2	1 / 2	28 / 22	1.2:1	5	329
DSK100800	1000 - 8000	0.6 / 1.1	0.05 / 0.2	1 / 2	28 / 22	1.2:1	20	330
DHK-H1N	1700 - 2200	0.3 / 0.4	0.1 / 0.3	1 / 3	20 / 18	1.3:1	100	220
P2D180900L	1800 - 9000	0.4 / 0.8	0.05 / 0.2	1 / 2	27 / 23	1.2:1	5	331
DSK180900	1800 - 9000	0.4 / 0.8	0.05 / 0.2	1 / 2	27 / 23	1.2:1	20	330
3-WAY								
S3D1723	1700 - 2300	0.2 / 0.35	0.3 / 0.6	2 / 3	22 / 16	1.3:1	5	316

◊ In excess of theoretical split loss of 3.0 dB
▫ With matched operating conditions

HYBRIDS

Model #	Frequency (MHz)	Insertion Loss (dB) [Typ./Max.] ◊	Amplitude Unbalance (dB) [Typ./Max.]	Phase Unbalance (Deg.) [Typ./Max.]	Isolation (dB) [Typ./Min.]	VSWR (Typ)	Input Power (Watts) [Max.]	Package
90°								
DQS-30-90	30 - 90	0.3 / 0.6	0.8 / 1.2	1 / 3	23 / 18	1.35:1	25	102SLF
DQS-3-11-10	30 - 110	0.5 / 0.8	0.6 / 0.9	1 / 3	30 / 20	1.30:1	10	102SLF
DQS-30-450	30 - 450	1.2 / 1.7	1 / 1.5	4 / 6	23 / 18	1.40:1	5	102SLF
DQS-118-174	118 - 174	0.3 / 0.6	0.4 / 1	1 / 3	23 / 18	1.35:1	25	102SLF
DQK80300	800 - 3000	0.2 / 0.4	0.5 / 0.8	2 / 5	20 / 18	1.30:1	40	113LF
MSQ80300	800 - 3000	0.2 / 0.4	0.5 / 0.8	2 / 5	20 / 18	1.30:1	40	325
DQK100800	1000 - 8000	0.8 / 1.6	1 / 1.6	1 / 4	22 / 20	1.20:1	40	326
MSQ100800	1000 - 8000	0.8 / 1.6	1 / 1.6	1 / 4	22 / 20	1.20:1	40	346
MSQ-8012	800 - 1200	0.2 / 0.3	0.2 / 0.4	2 / 3	22 / 18	1.20:1	50	226
180° (4-PORTS)								
DJS-345	30 - 450	0.75 / 1.2	0.3 / 0.8	2.5 / 4	23 / 18	1.25:1	5	301LF-1

◊ In excess of theoretical coupling loss of 3.0 dB

COUPLERS

Model #	Frequency (MHz)	Coupling (dB) [Nom]	Coupling Flatness (dB)	Mainline Loss (dB) [Typ./Max.]	Directivity (dB) [Typ./Min.]	Input Power (Watts) [Max.] ▫	Package
KDS-30-30	30 - 512	27.5 ±0.8	±0.75	0.2 / 0.28	23 / 15	50	255 *
KBS-10-225	225 - 400	10.5 ±1.0	±0.5	0.6 / 0.7	25 / 18	50	255 *
KDS-20-225	225 - 400	20 ±1.0	±0.5	0.2 / 0.4	25 / 18	50	255 *
KBK-10-225N	225 - 400	10.5 ±1.0	±0.5	0.6 / 0.7	25 / 18	50	110N *
KDK-20-225N	225 - 400	20 ±1.0	±0.5	0.2 / 0.4	25 / 18	50	110N *
KEK-704H	850 - 960	30 ±0.75	±0.25	0.08 / 0.2	38 / 30	500	207
SCS100800-10	1000 - 8000	10.5 ±1.5	±2.0	1.2 / 1.8	8 / 5	25	361
KBK100800-10	1000 - 8000	10.5 ±1.5	±2.0	1.2 / 1.8	8 / 5	25	322
SCS100800-16	1000 - 7800	16.8 ±1.5	±2.8	0.7 / 1	14 / 5	25	321
KDK100800-16	1000 - 7800	16.8 ±1.5	±2.8	0.7 / 1	14 / 5	25	322
SCS100800-20	1000 - 7800	20.5 ±2.0	±2.0	0.45 / 0.75	12 / 5	25	321
KDK100800-20	1000 - 7800	20.5 ±2.0	±2.0	0.45 / 0.75	14 / 5	25	322

* Add suffix - LF to the part number for RoHS compliant version.
▫ With matched operating conditions

Unless noted, products are RoHS compliant.

SYNERGY®
MICROWAVE CORPORATION

Phone: (973) 881-8800 | Fax: (973) 881-8361
E-mail: sales@synergymwave.com
Web: WWW.SYNERGYMWAVE.COM
Mail: 201 McLean Boulevard, Paterson, NJ 07504

MicroWaves&RF ON THE WEB

MWRF.com

Optimize Spectrum-Analyzer Settings For TOI Measurements

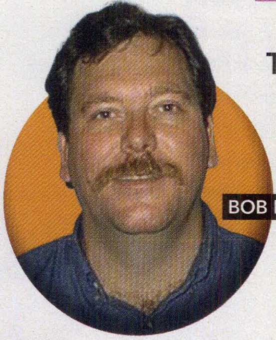
BOB NELSON

THIRD-ORDER-INTERCEPT (TOI) point is a parameter used to evaluate the linearity of components utilized in applications where nonlinear effects can cause distortion—for example, in digitally modulated signals. This measurement can be challenging, as uncertainties vary significantly based on a spectrum analyzer's settings. In this web-exclusive article, Agilent Technologies' Bob Nelson investigates whether a better way exists.

To read the article in its entirety, *visit www.mwrf.com.*

VIDEO FOCUS: IMS2011

Held in Baltimore June 5 to 10, IMS2011 lived up to its billing as the must-attend microwave event of the year. But if you weren't able to make the trip to Charm City this time around, never fear: *Microwaves & RF's* correspondents were pounding the pavement, interviewing industry luminaries and getting the scoop on the hottest new product offerings. Visit www.engineeringtv.com to check out dozens of exclusive videos from the show floor.

Microwaves for the World — IMS2011 Baltimore

engineering tv

NEWS UPDATES Sent To Your Desktop

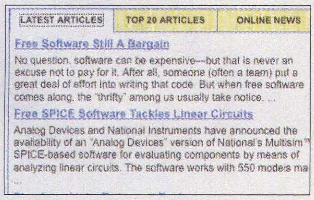
LATEST ARTICLES | TOP 20 ARTICLES | ONLINE NEWS

Free Software Still A Bargain

No question, software can be expensive—but that is never an excuse not to pay for it. After all, someone (often a team) put a great deal of effort into writing that code. But when free software comes along, the "thrifty" among us usually take notice. ...

Free SPICE Software Tackles Linear Circuits

Analog Devices and National Instruments have announced the availability of an "Analog Devices" version of National's Multisim™ SPICE-based software for evaluating components by means of analyzing linear circuits. The software works with 550 models ma ...

Don't believe everything you read, unless it's in the latest issue of *Microwaves & RF UPDATE*. The industry's longest-running weekly e-mail newsletter, it combines insightful commentary with the latest product and industry business news. It is sent directly to your computer desktop each week, and often contains the little things that engineers love, such as links to free white papers and even design software. If you're not already reading it, subscriptions are free, and available from the *Microwaves & RF* website at www.mwrf.com.

MWRF.com has archives of print and online articles dating back to October 2002. Visit MWRF.com today and click the "Back Issues" link. And while you're taking a look around the site, click on "Product Directory" to gain access to our complete directory of products and suppliers.

SHARE YOUR THOUGHTS with QUICK POLLS

Quick polls allow you to regularly share your opinion on a wide range of topics.

LATEST POLL RESULT:

Is passive intermodulation (PIM) a real threat to cellular communications system performance that requires a redesign of many passive components?

62% YES

23% NO

15% Don't Know

NEW POLL QUESTION:

Can you still design an RF/microwave circuit without the help of computer-aided-engineering (CAE) software?

YES NO

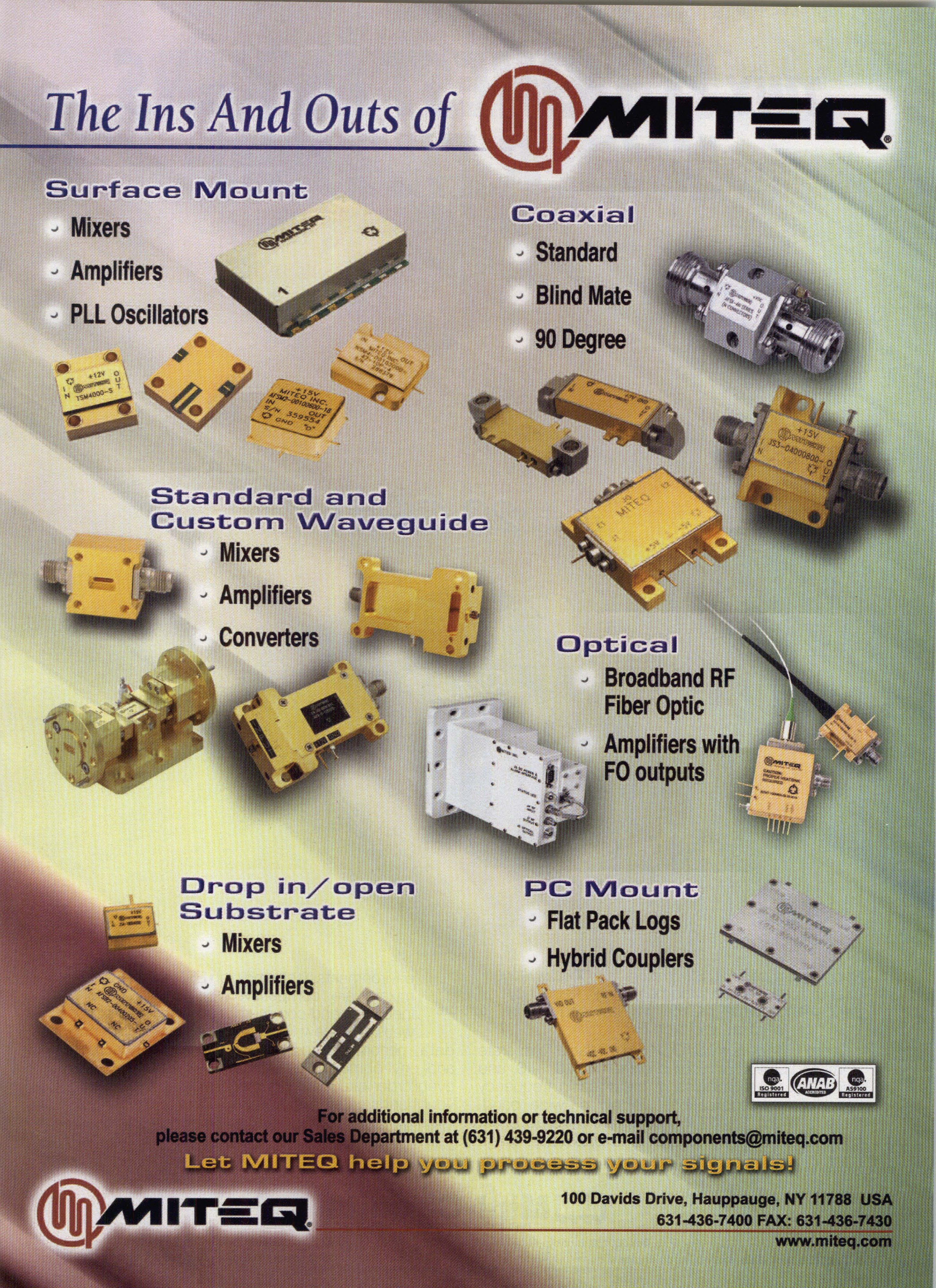

The Ins And Outs of MITEQ
Surface Mount
Mixers
Amplifiers
PLL Oscillators
Coaxial
Standard
Blind Mate
90 Degree
Standard and Custom Waveguide
Mixers
Amplifiers
Converters
Optical
Broadband RF Fiber Optic
Amplifiers with FO outputs
Drop in/open Substrate
Mixers
Amplifiers
PC Mount
Flat Pack Logs
Hybrid Couplers
ISO 9001 Registered
ANAB
AS9100 Registered
For additional information or technical support,
please contact our Sales Department at (631) 439-9220 or e-mail components@miteq.com
Let MITEQ help you process your signals!
MITEQ
100 Davids Drive, Hauppauge, NY 11788 USA
631-436-7400 FAX: 631-436-7430
www.miteq.com

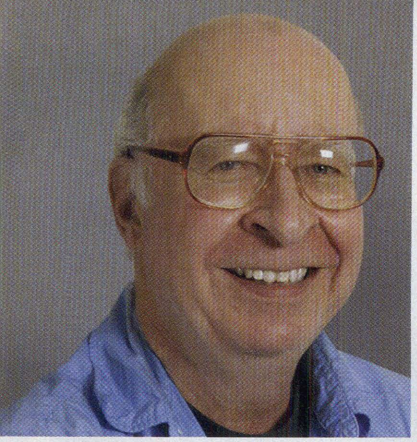

From the
Editor

Tracking Oscillator Trends

WHILE OSCILLATOR TECHNOLOGY makes gains from year to year, the progress is often deliberate—and typically, motivated by the needs of different markets. One recent trend in oscillator design (as noted in this month's Special Report, beginning on p. 39) is that oscillators are getting smaller and lighter, whether they are fixed crystal oscillators or tunable voltage-controlled oscillators (VCOs). Yet, even as crystal oscillators squeeze into surface-mount packages that are only 5 x 7 mm, they must still deliver high output levels and avoid phase noise.

Oscillator circuits have been refined over the years, with designers taking full advantage of the analysis capabilities of different electromagnetic (EM) software simulation tools. But in terms of an oscillator's output power and phase noise, the choice of active device within the oscillator has a great deal of influence on those two performance parameters. For many years, higher-frequency oscillator designers, such as builders of VCOs, YIG-tuned oscillators, or dielectric resonator oscillators (DROs), wrestled with the choice between the lower phase noise of silicon bipolar transistors and the higher-frequency operation of GaAs field-effect transistors (FETs).

In recent years, however, device designers have continued to enhance such technologies as GaAs heterojunction bipolar transistors (HBTs) and silicon-germanium (SiGe) BiCMOS transistors, reaching higher frequencies while benefitting from the low-phase-noise characteristics of these device technologies. A number of organizations have sought cost-effective oscillator designs capable of low-phase-noise performance at millimeter-wave frequencies. And they have looked to the promise of SiGe active device technology as a means of achieving such high-frequency operation.

Such advanced transistor technologies allow fundamental-frequency operation well past 100 GHz, depending upon device dimensions, with acceptably low phase noise. To make full use of newer transistors in EM and circuit simulation software, however, computer models of those transistors are necessary, and these are constructed only through laborious scattering-parameter (S-parameter) measurements. Accurate models allow designers to "experiment" in software with different circuit configurations, to better understand the interaction of a resonant inductive-capacitive (LC) circuit with the active circuit represented by the high-frequency transistor. Low phase noise is an often elusive design goal. But for a growing number of millimeter-wave radar or communications systems applications, lower oscillator phase noise is always better given the large number of digital modulation signal formats that are in use. Such modulation formats rely on maintaining the phase integrity of in-phase (I) and quadrature (Q) signal components, which is easier done with a low-phase noise oscillator at any frequency.

In the end, while oscillator designers are to be commended for their progress in increasing frequencies and decreasing phase noise over the years, just as much credit is due to the active device designers. MWRF

Jack Browne

Technical Contributor

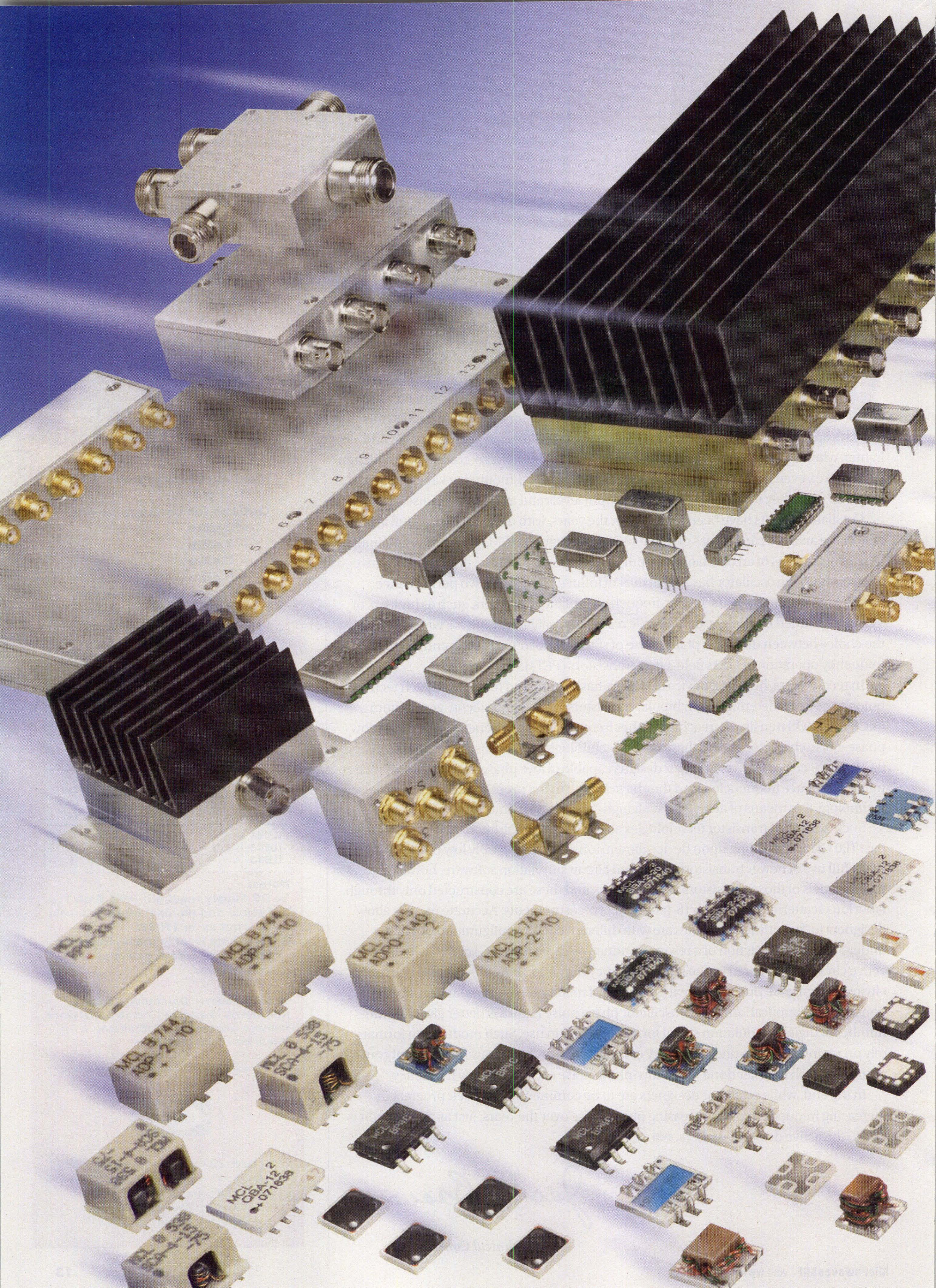

MCL B 744
ADP-2-10
MCL A 745
ADPQ-140
MCL
QBA-12
071838
MCL
BPNC

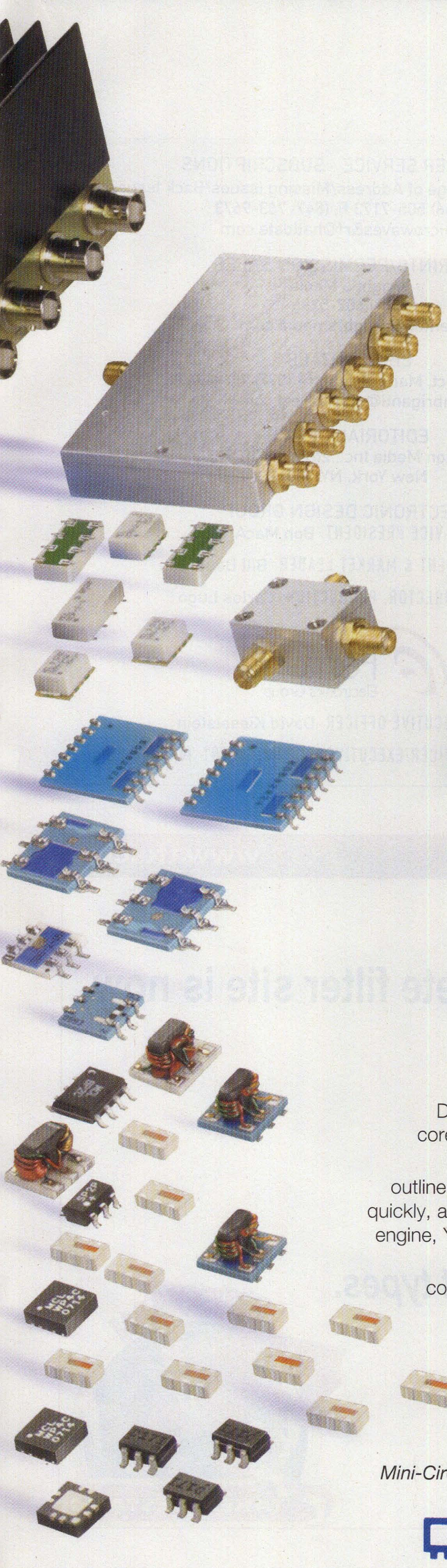

MicroWaves&RF

EDITOR-IN-CHIEF Nancy K. Friedrich
(212) 204-4373
nancy.friedrich@penton.com

TECHNICAL CONTRIBUTOR Jack Browne
(212) 204-4377
jack.browne@penton.com

MANAGING EDITOR Jeremy Cohen
(212) 204-4243
jeremy.cohen@penton.com

EUROPEAN EDITOR Paul Whytock
+44 (0)20 8859 1206
p.whytock@btinternet.com

PRODUCTION

PRODUCTION COORDINATOR Kara Walby
(913) 967-7476

ART DEPARTMENT

ART DIRECTOR/GROUP DESIGN MANAGER
Anthony Vitolo
tony.vitolo@penton.com

SENIOR ARTIST
James M. Miller

STAFF ARTIST
Michael Descul

CUSTOMER SERVICE - SUBSCRIPTIONS

New/Renew/Change of Address/Missing Issues/Back Issues
T: (866) 505-7173 F: (847) 763-9673
E: microwaves&rf@halldata.com

REPRINTS/PERMISSION SALES

Wright's Media
(877) 652-5295
penton@wrightsmedia.com

LIST RENTALS

MeritDirect, Marie Briganti • (877) 796-6947
mbriganti@meritdirect.com

EDITORIAL OFFICE

Penton Media Inc., 249 W. 17th St.
New York, NY 10011

ELECTRONIC DESIGN GROUP

SENIOR VICE PRESIDENT Bob MacArthur

VICE PRESIDENT & MARKET LEADER Bill Baumann

SENIOR DIRECTOR, PRODUCTION Carlos Lugo

Penton
Electronics Group

CHIEF EXECUTIVE OFFICER David Kieselstein

CHIEF FINANCIAL OFFICER/EXECUTIVE VICE PRESIDENT Nicola Allais

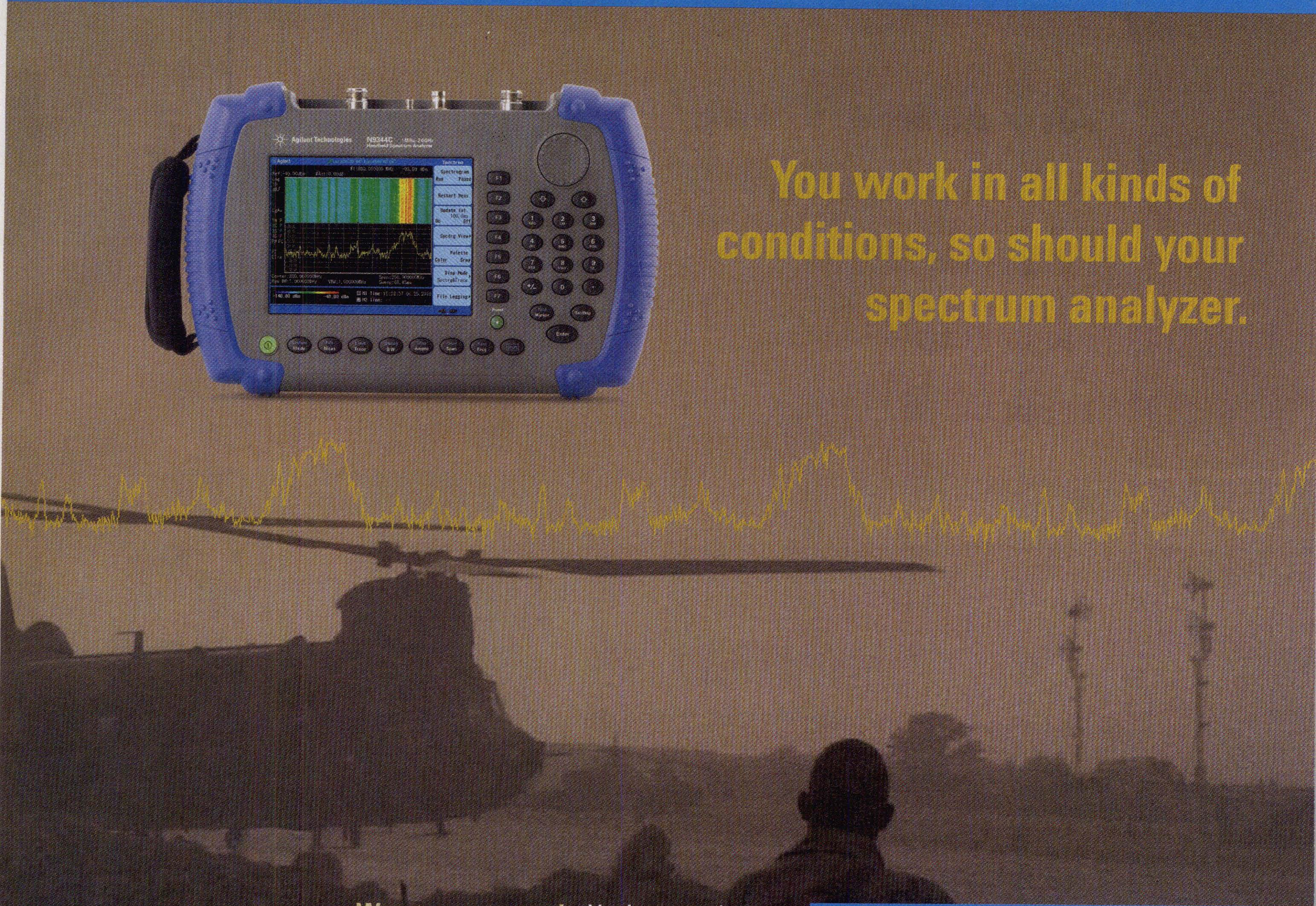

Worst-case scenario: You've got minutes to troubleshoot RF interference that has shut down communications on the ground, at dusk, in the desert.

Best-case scenario: You've got the only spectrum analyzer with benchtop performance in a lightweight MIL-PRF 28800F Class 2 compliant handheld—with secure erase to keep classified data classified.

That's thinking ahead. That's Agilent.

Scan the QR code or visit http://goo.gl/Rfbde to see a HSA N9344C demo guide video

Handheld Spectrum Analyzers (HSA)

Key Specs	N9344C	N9343C	N9342C
Frequency	1 MHz–20 GHz	1 MHz–13.6 GHz	100 kHz–7 GHz
DANL	-155 dBm/Hz	-155 dBm/Hz	-164 dBm/Hz
Sweep time	< 0.9 s	< 0.7 s	< 0.4 s
Weight with battery	3.6 kg (7.9 lbs)	3.6 kg (7.9 lbs)	3.6 kg (7.9 lbs)

Agilent and our Distributor Network
Right Instrument.
Right Expertise.
Delivered Right Now.

ALLIED ELECTRONICS

800-433-5700
www.alliedelec.com/agilent

View online HSA video demos
Download demonstration guides
www.alliedelec.com/lp/agilenthsa/

 (U.S. Army photo by Spc. Patrick Tharpe) (Released)

Agilent Technologies

MORE MIXER NOISE

When you publish in one of the industry's premiere magazines, you open yourself up to criticism such as what was presented in your "Feedback" column (March 2012). The focus of Mr. Polivka's criticism was at the end of the article ("Predict Mixer Noise Behavior," January 2012), in which I commented about the degradation of system noise figure when image noise is not dealt with properly. He contended, quite vigorously, that the noise figure of the system is set by the front-end LNA, independent of whether or not the image noise is rejected.

I was the recipient of numerous demeaning e-mails from Mr. Polivka, in which he ignored all of the published references and measured data that support my position in the article. The following are two well-known published textbook excerpts which I supplied to Mr. Polivka:

"Practical RF Circuit Design for Modern Wireless Systems," by Rowan Gilmore and Les Besser: "Therefore, in a broadband mixer, the noise floor at the image frequency will fold onto the RF signal noise floor when downconverted to the IF, resulting in a 3-dB loss in system sensitivity, no matter how good the preceding component noise figure. The purpose of the preceding RF filter should therefore be to remove as far as possible the effect of the image noise."

"Practical RF System Design," by William F. Egan: "If the circuitry preceding the mixer is high-gain broadband (same gain at all frequencies of importance), the cascade noise figure can increase as much as 3 dB."

The facts that support this aspect of my article (which was not even the main point of the article) are not new, and are not disputed by the engineering community. There will always be those out there who try to hold on to old beliefs, and when confronted with opposing views, lash out with personal attacks instead of presenting a factual basis for their position. I am afraid that Mr. Polivka falls into this category.

ROY MONZELLO

CORRECTION

Owing to editorial error, the article "UWB Lowpass Filter Features Wide Stopband" by Milad Mirzaee (March 2012) did not include the graphic for Fig. 2(c). The corrected article can be viewed online at http://mwrf.com/Articles/ArticleID/23945/23945.html.

Microwaves & RF welcomes mail from its readers. The magazine reserves the right to edit letters appearing in "Feedback." Address letters to:

Nancy Friedrich
Editor-In-Chief
nancy.friedrich@penton.com

Jack Browne
Technical Contributor
jack.browne@penton.com

News

GSMA, WBA Push Wi-Fi Roaming Initiative

The widespread proliferation of smartphones, tablets, and other devices have created the need for a uniform Wi-Fi connectivity protocol.

WITH MORE THAN 6 billion mobile connections worldwide (a number predicted to more than double within the next decade), smartphone and tablet users certainly aren't lacking WiFi hotspots with which to connect.

What they do still lack, however, is a streamlined, uniform process for doing so. Because these devices feature different configurations, different uses of access keys, and different mechanisms for acquiring and paying for connectivity, there is currently no consistency in how they attach to Wi-Fi networks.

The solution may lie in Wi-Fi roaming, an initiative that is being jointly advanced by the GSM Association (GSMA; www.gsma.com) and the Wireless Broadband Alliance (WBA; www.wballiance.com). As theorized, Wi-Fi roaming will bring together the benefits of mobile technology and Wi-Fi networks. The intent is to allow mobile devices to seamlessly connect to a Wi-Fi hotspot using the subscriber-identity-module (SIM) card for authentication, as well as to give mobile operators the ability to uniquely and securely identify users—whether they are on a mobile or Wi-Fi network.

The GSMA and WBA are currently developing technical and commercial frameworks for Wi-Fi roaming. It will be based on the WBA's Next Generation Hotspot program, in addition to the Wi-Fi Alliance's (www.wi-fi.org) Passpoint certification technology and the GSMA's roaming principles.

At press time, both parties have identified and agreed to the basis for a common approach to authenticating mobile devices on Wi-Fi hotspots, automatically and securely. It will now work towards aligning guidelines on security, billing, data offload, device implementation, and network selection to create a consistent solution. This work will build on the GSMA's GPRS Roaming Exchange (GRX) and the WBA's Wireless Roaming Intermediary Exchange (WRIX) roaming models. If successful, billions of consumers around the world will potentially be able to enjoy straightforward Internet connectivity.

LOCKHEED MARTIN Continues SEWS Support

HAVING RECENTLY INKED a follow-up contract with the US Air Force, Lockheed Martin (www.lockheedmartin.com) will continue to provide support for the Shared Early Warning System (SEWS). Currently installed at 37 sites worldwide, SEWS provides support to three different theater areas of responsibility: the US European Command, US Central Command, and US Pacific Command regions. The system distributes data from US missile warning systems to combatant commanders, in addition to select foreign nations.

Per the contract's terms, Lockheed Martin (working in tandem with the SEWS team) will standardize and normalize the system's architecture. Engineering and administrative support will also be provided in the areas of foreign military sales (FMS) case development, international traffic and arms regulations (ITAR)/export control, releasability planning, equipment acquisition, configuration management, equipment installation, maintenance/sustainment, and R&D initiatives.

Awarded by the Air Force's Electronics System Center, Space C2, and Surveillance Division (based out of Peterson Air Force Base in Colorado), the initial contract award is for $21.5 million. Its potential value over a 5-year period is $78 million.

Sizing Up ENERGY HARVESTING

WITH ENERGY HARVESTING techniques continuing to surge in popularity, it's little wonder that tools for gauging their effectiveness have likewise grown in demand. And now, RF designers have a promising new option available for evaluating their applications' energy harvesting wireless solutions.

Jointly released in North America by EnOcean (www.enocean.com) and Future Energy Solutions (FES; www.futureelectronics.com), the new ESK 300C starter kit includes a variety of energy converters and modules. Specifically, it consists of a switch module for building services, components for different switch applications, a temperature sensor module, a Universal-Serial-Bus (USB) gateway, personal-computer (PC) software for visualization, and a sample case for industrial switching solutions.

Using the kit, designers can apply energy harvesting technology to markets ranging from building automation to smart homes and smart metering. The various components allow users to implement switches and interior temperature sensors, in addition to a variety of industrial switches—among them, wireless position switches and solutions to control gates.

KUDOS

LOCKHEED MARTIN—Sonya Stewart, a Vice-President within the company's Information Systems & Global Solutions-Civil Division, has been named a *Washington Business Journal* Minority Business Leader. Stewart, who joined Lockheed Martin in 1992, is one of 25 honorees.

AWR CORP.—Has announced the continuation of its Graduate Gift Initiative, which provides qualified Electrical Engineering graduates with a complimentary, fully-functional 1-year term license of its Microwave Office and Visual System Simulator (VSS) software suites. AWR first launched this initiative in 2010.

RFMD—Has shipped more than one billion cellular power amplifiers (PAs) to handset manufacturers headquartered in China. The company opened its first manufacturing facility in Beijing in 2002.

MARKET QUOTE

According to new data from the Semiconductor Industry Association (SIA; www.sia-online.org), worldwide semiconductor sales in February declined 7.3% from the previous year. The biggest drop was observed in Europe, which posted $2.71 billion in February sales—a 16.4% drop from 1 year ago. Total worldwide semiconductor sales for February were $22.9 billion.

An End To SMARTPHONE SNEAKING?

FOR ALL OF their myriad benefits, smartphones have proven to be a security nightmare in the wrong settings—chief among them, college classrooms (think test-taking), courtrooms, corporate boardrooms, and government secure facilities. In an effort to curb illegal and/or unsecure cell phone use, Berkeley Varitronics Systems (www.bvsystems.com) recently released its PocketHound™ cell phone detector **(see photo)**.

Boasting a 75-ft range, the PocketHound's receiver is tuned to the RF signature of all second-generation (2G), third-generation (3G), and fourth-generation (4G) cell phones. Designed to scan for all voice, text, and data transmissions, it applies auto-thresholding technology to compare cellular measurements with the RF noise floor of the environment. Thus, the PocketHound will only be triggered by genuine cell phone use.

Once triggered, alerts can be conveyed via a choice of selectable flashing light-emitting diodes (LEDs) and/or vibrating alerts, enabling the PocketHound to be employed covertly. Smaller than a pack of playing cards, PocketHound's internal lithium polymer battery and Universal-Serial-Bus (USB) charging system allow for as much as two hours of continuous runtime.

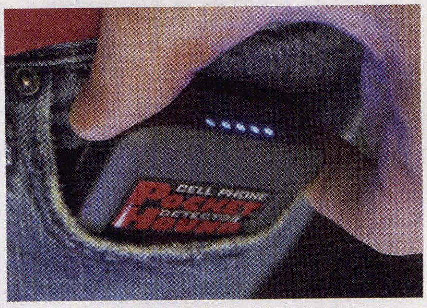

The PocketHound cell phone detector provides a deterrent to illegal and/or unsecure cell phone use in various settings.

BookReview

Klystrons, Traveling Wave Tubes, Magnetrons, Crossed-Field Amplifiers, and Gyrotrons

A.S. GILMOUR, JR.

MICROWAVE VACUUM TUBES come in many shapes, sizes, and output-power ratings. As detailed in *Klystrons, Traveling Wave Tubes, Magnetrons, Crossed-Field Amplifiers, and Gyrotrons* by A.S. Gilmour, Jr., the technologies behind these devices are quite mature, largely dating to the time of and before World War II. Although they are mature, microwave vacuum tubes have proven their reliability. For that reason,

they are often employed in deep-space applications including in satellite communications (satcom) systems. Microwave vacuum tubes are also quite efficient in turning bias energy into high-frequency output power—much more so than their solid-state counterparts.

Gilmour provides a wealth of knowledge pertaining to the vacuum tubes listed in his title, including historical references, cross-sectional diagrams, and circuit equations. In his chapter on traveling-wave tubes (TWTs), for example, he explores the design limitations for peak and average output power levels, for gain, and for efficiency. He also provides examples of the specifications required for these devices when used in different types of applications, such as in electronic-countermeasures (ECM) and radar systems.

For those interested in microwave vacuum tubes, this is 859 pages of invaluable content for any bookshelf. Artech House, 685 Canton St., Norwood, MA 02062; (781) 769-9750, (800) 225-9977, FAX: (781) 769-6334, www.artechhouse.com.

Molex Debuts NEXT-GEN ANTENNA TECHNOLOGY

TRADITIONAL PASSIVE ANTENNA structures are based on meandered antenna patterns. Unfortunately, said patterns are saddled with limitations on manufacturing tolerances and mechanical properties. With its next-generation MobliquA™ antenna technology, Molex (www.molex.com) hopes to circumvent those issues.

Intended for portable electronic devices like cell phones, tablets, and laptops, the MobliquA technology offers a multi-use platform supporting both single and dual feed RF architectures within the same antenna structure. The dual feed configuration can provide at least 20-dB isolation between the input ports, all the while maintaining its bandwidth-enhancing features. The good isolation and bandwidth simplifies optimization of antenna impedances to match different RF engines, thus reducing current consumption and improving power transfer efficiency.

The MobliquA technology provides a high degree of immunity toward insertion of metal objects into the antenna volume. Additionally, it enables utilization of RF decoupled or grounded parts as an integrated component of the antenna system. The technology also provides notable electrostatic discharge (ESD) protection of the front end, owing to a combination of its unique feeding techniques and a direct grounding of the antenna elements.

CHANGING THE WORLD Through Tantalum

BACK IN DECEMBER, AVX Corp. (www.avxcorp.com) announced that its current tantalum powder and wire suppliers were in compliance with the Conflict-Free Smelter Program (CFS). This initiative had been undertaken to combat mineral looting in the Democratic Republic of the Congo (DRC), the proceeds of which are typically used to support war efforts within the country (for more, read "*Look For Positive Changes*" in the January issue of *Microwaves & RF*).

The Solutions for Hope project has provided companies with the infrastructure to procure tantalite ore ethically.

As a follow-up, AVX has now shipped what is being billed as the world's first tantalum products manufactured from validated conflict-free tantalite ore mined in the DRC. This first shipment is the result of Solutions for Hope, an initiative launched by Motorola Solutions (the recipient of the shipment). This initiative demonstrates a process for delivering conflict-free tantalum material from the DRC under the guidelines of the Organization for Economic Cooperation and Development (OECD), and is in full compliance with CFS.

The basis of the process is an AVX-controlled and -funded "closed pipe." Tantalite ore is mined from government-approved concessions within the Katanga Province of the DRC **(see photo)**. It is then traced along its secure closed supply chain to the end customer's equipment in the form of tantalum capacitors. The Solutions for Hope project enables companies to meet the requirements of the impending Dodd-Frank legislation, which states that US companies must fully disclose the use of certain minerals (including tantalum) in their products, as well as describe the purchasing process used.

Editor's Note: For more information about Solutions for Hope, visit http://solutions-network.org/site-solutionsforhope/.

PEOPLE

GENERAL DYNAMICS—The board of directors has promoted PHEBE N. NOVAKOVIC to the roles of President and Chief Operating Officer. Novakovic previously served as Executive Vice-President for the Marine Systems Group.

AGILEX—MARIANNE MEINS has been appointed President of the company's Intel/Defense Sector business. She most recently served as Senior Vice-President for National Security Initiatives at Secure Mission Solutions, as well as Vice-President and General Manager for the company's Systems Engineering and Security Sector business.

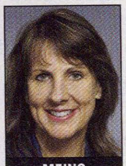

MEINS

LINX TECHNOLOGIES—KRIS LAFKO has joined the company as Director of Worldwide Sales. Lafko has more than 20 years of experience in the semiconductor and sensor industries.

TDS—Has promoted JOSEPH R. HANLEY to Senior Vice-President of Technology, Services, and Strategy. Hanley, who first joined TDS in 1988, most recently served as Vice-President of Technology, Planning, and Services.

HANLEY

LASER SERVICES—Has announced several new additions to its Sales Department. KEN SILBER, PHIL KENDALL, and JAMESE RIVERA have all joined the company as Sales Representatives.

CTIA - THE WIRELESS ASSOCIATION—JOHN MARINHO has been appointed to the newly created role of Vice President of Technology and Cybersecurity. Marinho previously served as Director for Mobility Solutions at Dell.

MARINHO

HEI—Has appointed CHAD RUWE Vice-President and General Manager of its flagship Microelectronic Assembly High Performance Manufacturing business, based out of Victoria, MN. Ruwe most recently served as Chief Operating Officer and Executive Vice-President, Operations at BioDrain Medical.

ENDICOTT INTERCONNECT TECHNOLOGIES—DAVID W. VAN ROSSUM has been appointed Chief Financial Officer. Van Rossum comes to Endicott from Russound, where he served as Chief Financial Officer and Chief Operations Officer.

BARE BOARD GROUP—DAVID DUROSS has joined the company as Engineering Director. Officially known as the "Board Czar," Duross boasts 20 years of printed circuit board fabrication experience.

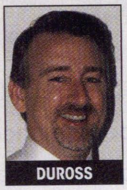

DUROSS

ON SEMICONDUCTOR CORP.—Has announced the additions of TERESA M. RESSEL and BERNARD L. HAN to the company's board of directors. Ressel, who was also appointed to the Audit Committee, most recently served in an executive role for UBS Investment Bank. Han currently serves as Chief Operating Officer of DISH Network Corp. In addition, current board member Atsushi Abe was appointed to both the Audit and Compensation Committees.

RCA - THE COMPETITIVE CARRIERS ASSOCIATION—SANDRA MOTLEY has been appointed to the organization's board of directors. Motley currently serves in the role of Vice-President of Sales, US Wireless Accounts at Alcatel-Lucent.

MOTLEY

IMS2012
MONTRÉAL

MICROWAVES WITHOUT BORDERS
MICRO-ONDES SANS FRONTIÈRES

International Microwave Symposium
IEEE 17-22 June 2012, Montréal, Canada MTT-S
http://ims2012.mtt.org/

MTT IMS
NEW YORK 1952 MONTRÉAL 2012
60 YEARS 60

Look What's Happening at IMS2012!

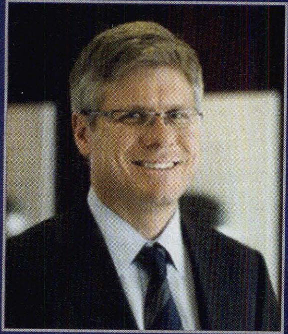

Plenary Session Speaker: Steve Mollenkopf

President and Chief Operating Officer, *Qualcomm*

3G/4G Chipsets and the Mobile Data Explosion

Monday, 18 June 2012
1730-1900

The rapid growth of wireless data and complexity of 3G and 4G chipsets drives new design and deployment challenges for radio and device manufacturers along with carriers. This talk will provide a perspective on the problem from the point of view of a large, worldwide manufacturer of semiconductors and technology for cellular and connected consumer electronics devices. The increase in device and network complexity will result in significant business opportunities for the industry.

Closing Ceremony Speaker: Thomas H. Lee

Professor, *Stanford University*

The Fourth Age of Wireless and the Internet of Everything

Thursday, 21 June 2012
1600-1730

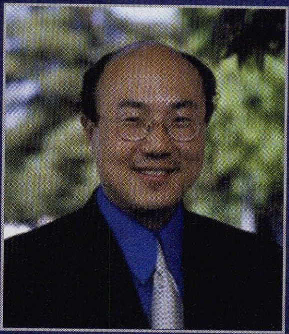

"Making predictions is hard, particularly about the future." The patterns of history are rarely discernible until they're obvious and perhaps irrelevant. Wireless may be an exception, at least in broad outline, for the evolution of wireless has been following a clear pattern that tempts us to extrapolate. Marconi's station-to-station spark telegraphy gave way to a second age dominated by station-to-people broadcasting, and then to today's ubiquitous people-to-people cellular communications. Each new age was marked by vast increases in value as it enlarged the circle of interlocutors. Now, these three ages have covered all combinations of "stations" and "people," so any Fourth Age will have to invite "things" into the mix to provide another stepwise jump in the number of interlocutors. This talk will describe how the inclusion of multiple billions of objects, coupled with a seemingly insatiable demand for ever-higher data rates, will stress an infrastructure built for the Third Age. Overcoming the challenges of the coming Fourth Age of Wireless to create the Internet of Everything represents a huge opportunity for RF engineers. History is not done.

The IMS2012 Housing Bureau and Registration are now open!

Don't miss your chance to see the latest RF/Microwave technology advancements while accessing over 500 companies technologies and services.

Visit http://ims2012.mtt.org for complete details and to download your Program Book. Review technical sessions, workshop descriptions and exhibiting companies so you can make the most of your time at Microwave Week!

MTT-S® **http://ims2012.mtt.org** IEEE

FRESH STARTS

AWR Corp.—Has been issued US Patent No. 8,131,521 for a "block-specific harmonic balance analysis system." The invention, MRHB, addresses circuit simulation using multi-rate harmonic balancing.

Raytheon Co.—MathAlive!, the company's interactive exhibition promoting science, technology, engineering, and mathematics (STEM) education, has opened at the Smithsonian International Gallery in Washington, DC. Following its three-month debut, MathAlive! will embark on a 15-city, multiyear tour to science centers and museums worldwide.

Meru Networks—In conjunction with its local distributor, Wavelink, the company has announced expansion plans in the Australian region. A dedicated Meru technical sales team will target the education, healthcare, enterprise, government, and hospitality markets, among others.

Masimo—Has acquired substantially all of the assets of Spire Semiconductor. Masimo Semiconductor, a newly-formed, wholly-owned subsidiary, will operate the business going forward.

Vaunix—Has hired a new sales representative to handle the company's customer relationships in India. Premier Measurement Solutions is based out of Bangalore.

ZMDI—Has expanded its presence in the US market. The company has opened three new sales offices and engineering application laboratories located in Milpitas, CA; Phoenix, AZ; and Boston, MA.

SIPCO—Has reached a minority ownership agreement with GE and MPEG LA. Financial terms of the transaction were not disclosed.

Texas Instruments—Has opened TI Silicon Valley Labs, a research center located in Santa Clara, CA. The facility has been chartered to conduct R&D initiatives in analog and mixed signal circuits and technologies.

Semiconductor Manufacturing International Corp. (SMIC)—Has founded an integrated-circuit (IC) research program in conjunction with Brite Semiconductor and Zhejiang University. As part of the agreement, SMIC and Brite will provide Zhejiang University graduate students with hands-on training and internship opportunities, while the university will provide a continuing education program for both companies' employees.

Cogo—Founder, CEO, and Chairman Jeffrey Kang has proposed acquiring approximately 30% of the company's assets, liabilities, and revenue. The total purchase price of the transaction—which would take place through Kang's personal investment venture, Envision Global Group—is expected to be between $60 million and $82 million.

CONTRACTS

RAYTHEON
Snares domestic, overseas military deals

LOCKHEED MARTIN
Wins Sniper ATP upgrade contract

Raytheon Co.—Has won a tube-launched, optically tracked, wire-guided (TOW) missile subsystems contract from the US Army. Under the 5-year contract, valued at $77.9 million, Raytheon will provide logistics and engineering support for TOW missile subsystems and associated support equipment. In addition, Raytheon has been chosen by the Netherlands Ministry of Defence to upgrade the air traffic control radar system at the Royal Netherlands Air Force base in Woensdrecht. The company will implement technology to mitigate the adverse effects of wind turbines on radar performance. Finally, Raytheon has won a $7 million contract to upgrade 15 military air traffic landing systems. The company will provide engineering, technical, and depot services both for the Naval Air Systems Command (NAVAIR) and the US Marine Corps.

Mountain Secure Systems (MSS)—Has received additional orders from the city of Denver, CO for its Summit Series wireless network radios. The 35 new radios are intended to expand coverage for a traffic control video surveillance network.

DiViNetworks—Has been selected by ZON, Portugal's leading cable TV provider, to optimize its data link to the Azores Islands, satisfying the growing demand for bandwidth. ZON is utilizing the company's DiViLink offering.

NASA—Has signed an agreement with the government of Bermuda to establish a temporary mobile tracking station on Cooper's Island. The station—which will provide telemetry, meteorological, optical, and command and control services—will support launches from NASA's Wallops Flight Facility in Virginia, including future commercial missions.

QinetiQ North America—Has been awarded a new task order by the Marine Corps Systems Command (MARCORSYSCOM). QinetiQ will support the replacement of 4 40-year-old legacy supply and maintenance information technology systems. The task order has a total potential value of $20 million.

Ruckus Wireless and SmartWave Technologies—Have been selected by the city of San Jose, CA to supply products and services for a new public Wi-Fi network initiative. The outdoor network will cover San Jose's business district, allowing the city to offer free high-speed Wi-Fi services.

Lockheed Martin—Has received an indefinite delivery/indefinite quantity Sniper Advanced Targeting Pod (ATP) Post Production Support (PPS) contract from the US Air Force. Covering a variety of upgrade activities for the legacy Sniper ATP fleet, the contract has a potential value of $841 million over a 7-year period.

OpConnect—Has received a $60,000 order from the US Navy for its electric vehicle charging stations. The OpConnect dual Level I & II units will be installed at Navy facilities in Washington, DC; Indian Head, MD; and San Diego, CA.

API Technologies—Has received a $3.9 million order from an undisclosed defense customer to provide engineered solutions for mission-critical radar systems.

Ceragon Networks—Has won a new $6 million contract from Globacom Nigeria (Glo) for its wireless backhaul solutions and professional services. Ceragon will manage the end-to-end deployment of its FibeAir IP-10 and Evolution IP Long-Haul systems throughout Nigeria, expanding upon the original network it developed for Glo in 2010.

Now! MULTIPLY
UP TO 20 GHz

Frequency Multipliers from $5.95 qty. 10-49

For your leading-edge synthesizers, local oscillators, and Satellite up/down converters, Mini-Circuits offers a large selection of ***broadband doublers, triplers, quadruplers, and x12 frequency multipliers.***

Now generate output frequencies from 100 kHz to 20 GHz with excellent suppression of fundamental frequency and undesired harmonics, as well as spurious. All featuring low conversion loss and designed into a wide array of, off-the-shelf, rugged coaxial, and surface mount packages to meet your requirements.

Visit our website to choose and view comprehensive performance curves, data sheets, pcb layouts, and environmental specifications. And you can even order direct from our web store and have a unit in your hands as early as tomorrow! Mini-Circuits...we're redefining what VALUE is all about!

Mini-Circuits®
ISO 9001 ISO 14001 AS9100

P.O. Box 350166, Brooklyn, New York 11235-0003 (718) 934-4500 Fax (718) 332-4661

YONI2® ***The Design Engineers Search Engine*** *finds the model you need, Instantly* • For detailed performance specs & shopping online see **minicircuits.com**

U.S. Patents 7739260, 7761442

IF/RF MICROWAVE COMPONENTS

455 rev F

Inside Track with Rupert Baines,

Vice-President of Strategic Marketing and Marketing Communications, Mindspeed Technologies

Interview by NANCY FRIEDRICH

NF: With the acquisition of Picochip Ltd., Mindspeed is clearly broadening its focus beyond the more traditional network infrastructure to include smaller cells. How do you envision the network infrastructure of the next five to ten years?

RB: During recent years, wireless phones have become the preferred mode of communication while landline access has decreased. At the same time, most cellular service subscribers now also use the mobile Internet, and many new broadband mobile devices including smartphones, tablets, and laptops with 3G capabilities have been commercialized for applications such as social networking and video on demand. The majority of current 3G cellular networks only support data rates of, at best, a few megabits per second (Mbps) under low-mobility conditions. This is not enough for carriers to support today's escalating growth in mobile device deployment, usage and associated network traffic, while maintaining a competitive price/performance model and ensuring sufficient network performance.

The solution for delivering all of the extra traffic is to deploy many more base stations, closer to the users: the small cell network. Long-Term Evolution (LTE) includes the concept of the Heterogeneous Network (HetNet), which allows networks to efficiently mix traditional, big base stations and small cells. However, for small cells to be sufficiently economical, they need to be cheap to build, and will rely heavily on dual-mode System-on-Chip (SoC) integration. This is a pattern we have seen before—in computers, with the shift from big mainframes to PCs, and in broadband, with the trend to push intelligence to the edge. As in these earlier transitions, the industry will use standardized reference designs and SoCs to drive the economics of high volume.

The Small Cell Forum (www.smallcellforum.org) recently announced a rapid uptake of its small cell LTE application platform interfaces (APIs), showing that the vendor community is rapidly preparing the technology to meet the operator demand. This rapid adoption is being driven by widespread LTE small cell commitments from operators around the world including China Mobile, Vodafone, SK Telecom, and NTT DoCoMo.

NF: What role will small cells in particular play? What kind of data rates do you foresee for these small cells in support of the wireless "connected home"? And do you think that home security systems, such as motion detectors and alarm systems, will be part of the functionality of a small cell in a wireless home?

RB: The adoption of small cells is one of the key prerequisites for LTE deployment. The only way to increase data capacity is to improve the spectrum efficiency of radio technologies while also reducing cell sizes. In addition to helping fuel LTE network deployment, small-cell solutions will also deliver additional value in the wireless connected home. Cellular coverage in the home has always been a challenge because of the combination of high 3G frequencies, high data rates, large cell sizes, and signal impediments inside the home caused by issues such as attenuation from walls. LTE uses even higher frequencies, and more complex coding and modulation schemes. Small cells will solve these coverage problems while offering data rates of tends of Mbps for a variety of broadband applications. It is also likely that small-cell technology will merge with wireline hubs, routers and gateways in the home, which are already being used to provision security, home automation, energy management and other services on a single platform.

NF: Can you provide numbers on how many small cells are currently in use?

RB: Infonetics Research reports that the small cell installed base is widespread and growing fast (http://www.infonetics.com/pr/2011/Carrier-Small-Cell-Deployment-Strategies-Survey-Highlights.asp). Picochip has been the leader in small cell SoC shipments, having shipped more than one million 3G product units with associated physical-layer (PHY) software. According to ABI Research, 4.3 million small cells (including femtocells, picocells and microcells) will be shipped in 2012, rising to 36.8 million shipments in 2016, valued at $20.4 billion.

NF: What about the number or percentage offered by carriers for individual residences? Have they started to be used more widely?

RB: ABI Research finds that residential and enterprise models currently dominate small cell shipments with 62% and 30% respectively. ABI Research's data suggests that by 2016, indoor small cells will be 94% of total shipments and outdoor small cells will make up 64% of the revenue. There are many benefits to small cell adoption in the home, including

"For small cells to be sufficiently economical, they need to be cheap to build, and will rely heavily on SoC integration."

providing a means for carriers to improve service quality. A Parks Associates survey found that 41% of mobile users experiencing dropped calls on a daily basis are likely to switch providers within the next 12 months; 28% of those experiencing dropped calls on a weekly basis are likely to churn. There were similar responses for those with poor voice quality, also.

Operators are starting to have significant promotions for residential small cells. According to Infonetics, Sprint is one of the leading operators for femtocells, with a policy of free devices for any customer with bad service. Another example is OPTUS in Australia, a mobile-only operator that competes with Telstra as the traditional incumbent with both fixed plus mobile. As a competitive technique, OPTUS offers with its femtocell free unlimited calls from your cell phone at home, without counting towards your bucket. As their ads put it, "who needs a fixed line?" FREE in France has perhaps the best broadband offering in the Western world—it is now integrating femtocells with its set-top box and a very aggressive pricing plan.

NF: How do you see a combination of network technologies, ranging from small cells to the more traditional cellular infrastructure, serving fourth-generation (4G) technologies?

RB: As mentioned earlier, the LTE specifications include the concept of the Heterogeneous Network, comprised of many different types of base stations. HetNets will help carriers to avoid exclusive reliance on large macro base stations wherever they need coverage. Instead, smaller cells can be deployed either by the mobile operators or end customers to deliver additional capacity in those locations where it is needed.

NF: Do you think this model can also aid the rollouts of more entry-level services in rural and hard-to-reach areas?

RB: Yes. Small cells can deliver capacity by breaking urban areas into smaller coverage units—or they can extend service to under-served "not spot" or rural areas that have sparse coverage. In the UK, Vodafone has actually used this as a feature of its advertising: guaranteeing the best network.

NF: Both Mindspeed and Picochip are semiconductor-focused companies. What similarities do you have in terms of your technical offerings?

RB: A key rationale behind Mindspeed's acquisition of Picochip was the high level of synergies—including technology and customers—between the two companies. Picochip has the same customers that leverage Mindspeed's wireline products, so the company already has a great channel into these customers including Alcatel-Lucent, Nokia Siemens, Huawei, and major Japanese OEMs. Both companies also have mature platforms based on a multi-core SoC architecture using ARM processors. Picochip has shipped more than 1 million 3G product units with associated field-proven PHY software, and Mindspeed has won nearly 30 customer designs to date for its Transcede platform. By offering the two companies' small-cell technologies in a single, market-leading multi-mode platform, Mindspeed will enable wireless carriers to support both 3G and LTE in a single unit, dramatically improving their business case by delivering twice the benefit at half the traditional per-node opex and capex costs. MWRF

PROCESSOR BOASTS 3 BILLION TRANSISTORS on 9 Copper Layers

INTEGRATION MEANS MANY things to many people. But in the world of high-power, high-speed microprocessors, integration means literally billions of transistors on a chip, as researchers from Intel Corp. (www.intel.com) demonstrated recently. A team led by Reid Riedlinger, Ron Arnold, and Larry Biro (Fort Collins, CO), in addition to Bill Bowhill and associates (Hudson, MA), recently disclosed information on a next generation Intel® Itanium® microprocessor fabricated in a 32-nm silicon CMOS process. The device fits 3.1 billion transistors on a die with 9 layers of copper measuring just 18.2 x 29.9 mm. The processor features 8 multithreaded cores, a ring-based system interface, memory bandwidth to 45 Gb/s, and peak processor-to-processor bandwidth to 128 Gb/s.

This impressive processor incorporates 54 Mb of on-die cache memory distributed throughout the core and system interface. The device uses high-dielectric-constant metal-gate transistors combined with nine layers of copper interconnections to link the multitude of transistors and passive components. Of the more than 3 billion transistors, 720 million devices are allocated to the eight processor cores. The maximum frequency of the input/output ports and memory interfaces is 6.4 billion transfers per second (GT/s).

The aggregate memory and I/O bandwidths of various ports of the processor easily exceed 115 Gb/s, with several different interfaces operating at transfer rates exceeding 4.8 GT/s per lane with power efficiency of 14 mW per GT/s. The analog portion of the microprocessor includes process-, voltage-, and temperature-tolerant circuitry. See "A 32 nm, 3.1 Billion Transistor, 12 Wide Issue Itanium® Processor for Mission-Critical Servers," *IEEE Journal of Solid-State Circuits*, Vol. 47, No. 1, January 2012, p. 177.

WIRELESS GLUCOSE MONITOR Is Integrated Onto Contact Lens

GLUCOSE MONITORING is a powerful weapon in the fight against diabetes, but the usual method of checking a patient's blood sugar levels is through an enzyme-based finger-pricking method. A proposed alternative utilizes a fully integrated active contact lens system, providing wireless monitoring of glucose levels using the tear fluid in the eye.

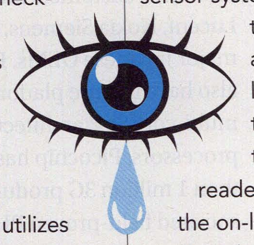

The novel approach was proposed by Yu-Te Liao of the National Chung-Cheng University in Taiwan, along with Huanfen Yao, Andrew Lingley, Babak Parviz, and Brian Otis from the University of Washington (Seattle, WA). Their on-lens glucose sensor system detects the tear glucose level and then wirelessly transmits the information to an external reader. The goal for the on-lens sensor was a noise level of less than 1 nA root mean square (RMS) at a power consumption level of less than 5 μW, in a sensor area of approximately 0.36 mm^2. The sensor IC consists of a power management block, readout circuitry, wireless communications interface, LED driver, and energy storage capacitors in the compact CMOS chip.

A loop antenna was designed with a 5-mm radius and 0.5-mm trace width. Assuming ideal antenna-chip matching, it could provide minimum gain of 1.76 dBi. Experiments were performed for use in the Industrial-Scientific-Medical (ISM) band at 1.8 GHz with good results on power consumption (about 3 μW consumed during operation). See "A 3-μW CMOS Glucose Sensor for Wireless Contact-Lens Tear Glucose Monitoring," *IEEE Journal of Solid-State Circuits*, Vol. 47, No. 1, January 2012, p. 335.

All-Textile PIFA Suits Wireless Body Area Networks

TEXTILE ANTENNAS ARE attractive for emerging applications in "wearable wireless" systems, such as in wireless body-area networks (WBANs). Ping Jack Soh and Guy Vandenbosch of Katholieke Universiteit Leuven (Leuven, Belgium), along with Soo Liam Ooi and Nurul Husna Mohd Rais of Universiti Malaysia Perlis (Perlis, Malaysia), pursued the design and development of an all-textile antenna design based on a planar inverted-F antenna (PIFA) architecture. The team's design featured a slot on the radiator for operation on the 2.45-GHz ISM band.

The antenna was designed and fabricated with two types of conducting textile materials and a 0.035-mm-thick conductive copper foil tape. Both of the commercial conducting textile materials feature high conductivity. The antenna design was based on two conductive layers shorted by a wall. The substrate was a 6-mm-thick felt fabric placed between the ground plane and the radiating patch. The substrate exhibited a relative dielectric constant of 1.43 at 2.4 GHz with loss tangent of 0.025 in the z-direction at the same frequency. The design exhibited a bandwidth as wide as 1200 MHz in free space and as much as 1300 MHz when worn on a body, showing great promise. See "Design of a Broadband All-Textile Slotted PIFA," *IEEE Transactions on Antennas and Propagation*, Vol. 60, No. 1, January 2012, p. 379.

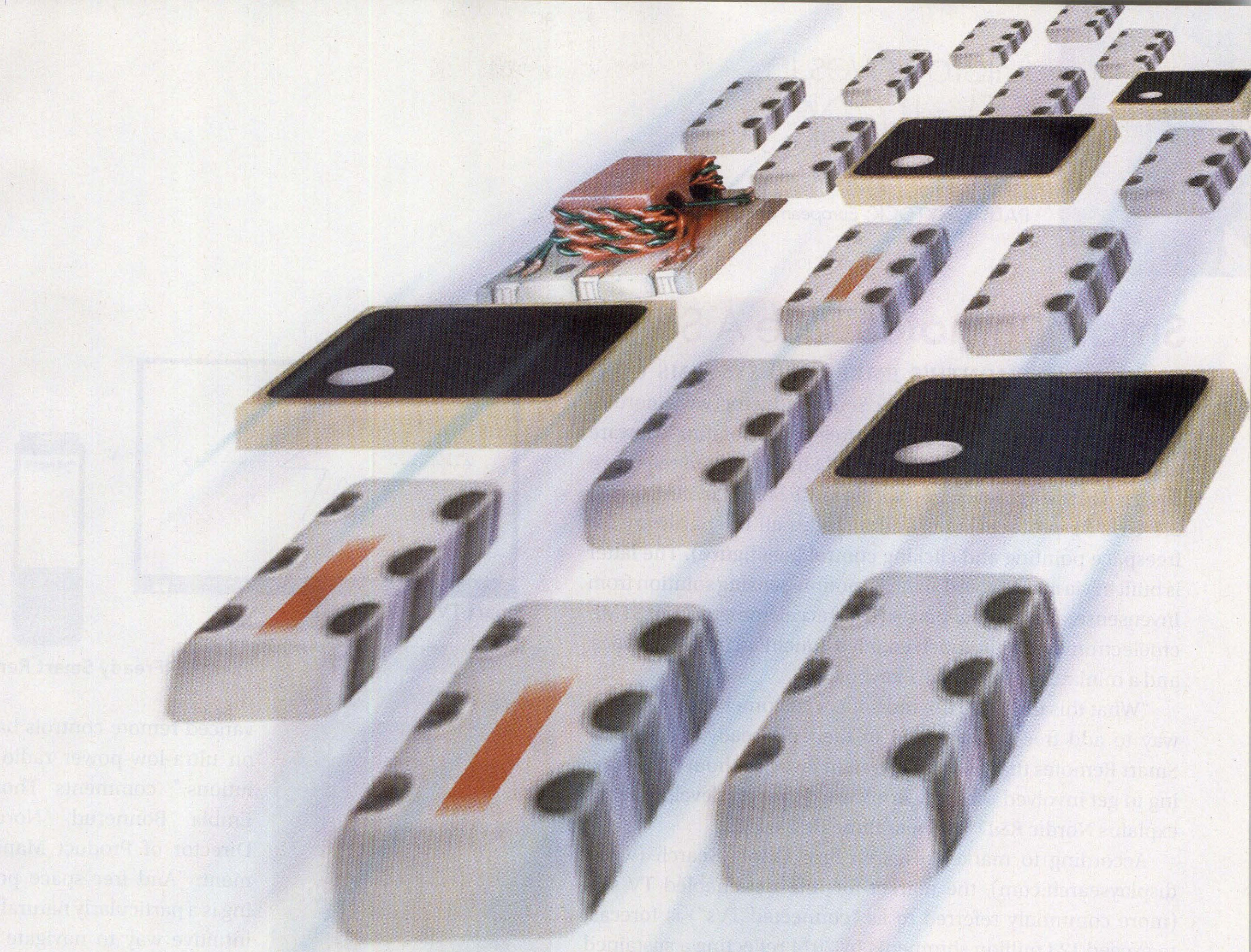

90° SPLITTERS

5 MHz to 8 GHz from $3.95 ea. qty. 20

Two-way 90° power splitters (hybrids) are critical building blocks in a wide array of RF design solutions. That's why Mini-Circuits offers extra-tight phase and amplitude balance, to ensure your expected high-performance design results. Plus, our robust, rugged units deliver repeatable performance and are available in over 70 different SMT models, in the widest range of frequencies in the industry (from 5 MHz to 8 GHz), and in package sizes as small as 0.08" x 0.05".

LTCC models now available in small-quantity reels, with standard counts of 20, 50, 100, 200, 500, 1000, or 2000 *at no extra cost!* For full performance details and product availability, visit our web site **www.minicircuits.com**. You can order online and have units in-hand as soon as next-day.

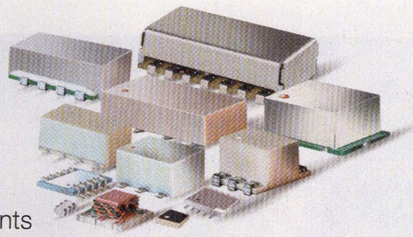

RoHS compliant

Mini-Circuits...we're redefining what VALUE is all about!

Mini-Circuits®

ISO 9001 ISO 14001 AS9100

P.O. Box 350166, Brooklyn, New York 11235-0003 (718) 934-4500 Fax (718) 332-4661

YONI2® U.S. Patents 7739260, 7761442 ***The Design Engineers Search Engine*** *finds the model you need, Instantly* • For detailed performance specs & shopping online see minicircuits.com

IF/RF MICROWAVE COMPONENTS

463 rev G

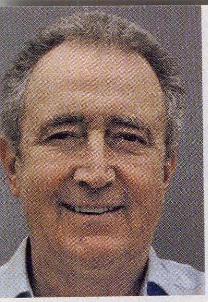

Microwaves in Europe

PAUL WHYTOCK, *European Editor*

Smart Remotes Take A Step Forward

AT LAST MONTH'S EMBEDDED SYSTEMS CONFERENCE (ESC), Nordic Semiconductor (www.nordicsemi.com) demonstrated a free-space pointing firmware upgrade for its nRFready 2.4-GHz RF Smart Remote reference design. This design leverages Nordic's nRF24LE1 SoC and Gazell 2.4-GHz RF protocol stack and includes all the hardware for freespace pointing and clicking control **(see figure)**. The latter is built in via an on-board six-axis motion-sensing solution from Invensense, an ultra-low-power (ULP) accelerometer from STMicroelectronics, a multitouch enabled TouchPad from Synaptics, and a miniaturized QWERTY keyboard.

"What this firmware upgrade offers customers is a fast-track way to add freespace control to their nRFready 2.4-GHz RF Smart Remotes that will work straight away, without them having to get involved with any firmware design or development," explains Nordic R&D Engineer Rune Brandsegg.

According to market research firm DisplaySearch (www.displaysearch.com), the market for Internet-enabled TV sets (more commonly referred to as "connected TVs") is forecast to exceed 123 million shipments by 2014 reflecting a sustained 30% compound annual growth rate over that period. This shipment number does not include other increasingly popular types of Internet-enabled consumer electronics (CE) devices, such as STBs and media players.

An essential part of all these products, however, is the remote control—it enables end users to take advantage of, and enjoy with ease, the full range and potential of digital content and services such products now support.

"With the growing popularity of Internet-enabled TVs and set-top boxes, we are seeing an explosion in demand for advanced remote controls based on ultra-low-power radio solutions," comments Thomas Embla Bonnerud, Nordic's Director of Product Management. "And free-space pointing is a particularly natural and intuitive way to navigate and browse all types of modern digital content and services—including audio, video, gaming, web browsing, social media, and online shopping—as it offers familiar mouse-like PC control without the need for a flat surface."

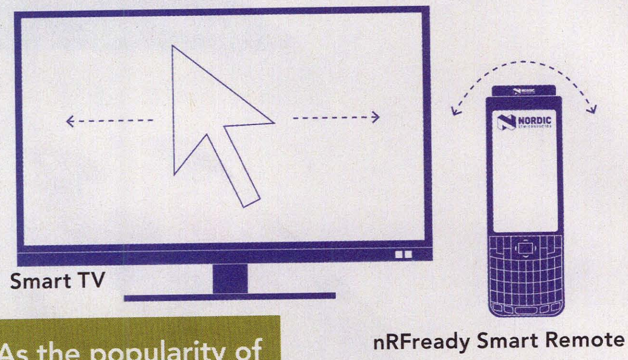

As the popularity of Internet-enabled TVs and set-top boxes grows, there is a demand for advanced remote controls based on ultra-low-power (ULP) radio solutions.

The nRFready 2.4-GHz RF Smart Remote reference design kit includes a Nordic Smart Remote baseboard, Smart Remote 2.4-GHz RF radio module, 2.4-GHz RF USB dongle, programming adapter and a set of design files, software source code, and supporting documentation.

HEARING AIDS EMBRACE WIRELESS SOLUTIONS

IN OTHER NORDIC NEWS, hearing solutions company GN ReSound (www.gnresound.com), has employed the company's nRF24L01+ in its ReSound Alera™ hearing aid. This offering enables users to wirelessly stream audio from consumer electronics devices such as TVs directly to their hearing aid(s) over a range to 20 m **(see figure)**.

In operation, the end user connects a TV or other device—smartphone, desktop personal computer (PC), laptop, tablet, home cinema system, radio, etc.—to a small audio streamer box equipped with a Nordic nRF24L01+ 2.4-GHz transceiver. This pairs with a second nRF24L01+ located in the ReSound Alera hearing aid. When a user wants to watch TV, they simply push a button on the back of the hearing aid. Alternately, an optional remote control can be used to select the device's designated wireless channel (typically between 1 and 3) to immediately stream wireless audio in stereo.

The ReSound Alera™ hearing aid product enables users to wirelessly stream audio from TVs, smartphones, and other electronic devices.

JACK BROWNE | Technical Contributor

Generating Stable RF/Microwave Signals

OSCILLATORS ARE FOLLOWING A TREND OF SMALLER PACKAGES AND LOWER POWER CONSUMPTION WHILE ALSO DELIVERING ENHANCED SPECTRAL PURITY AND LEVERAGING A NUMBER OF DIFFERENT TECHNOLOGIES.

1. These crystal oscillators and VCXOs operate through 1300 MHz in packages measuring only 5 x 7 mm. [Photo courtesy of Integrated Device Technology (www.idt.com).]

OSCILLATORS FULFILL A LARGE NUMBER OF REQUIREMENTS in high-frequency systems, from keeping time to generating and translating the frequency of other signals. Given the number of different oscillator types and technologies currently on the market, making a choice can seem intimidating for someone faced with selecting one for an electronic system. Perhaps the selection can be made a little easier by reviewing the current high-frequency oscillator types and their performance limitations.

In general, high-frequency electronic systems can be thought of as a receiver, a transmitter, or a combination of the two. That is, a system must detect and process signals or generate and send signals. In a radar, the received signals are reflections from targets of signals originally transmitted by the same system. In a satellite communications (satcom) system, a terrestrial earth station sends signals to a space-based satellite and receives return signals from the satellite. Even test equipment, such as a spectrum analyzer, can be thought of as a receiver, with a tunable oscillator and adjustable filters at its core. In all of these systems, the oscillators must meet a certain set of performance parameters for the systems to operate properly.

The most basic of oscillator performance parameters include frequency tuning range (and, for some oscillators that are not tunable, this is a fixed value), output power, output power flatness with frequency and temperature, spurious and harmonic noise, single-sideband (SSB) phase noise, and tuning speed. In some applications, such as in mobile electronic systems, vibration-induced instabilities can be a critical performance parameter, as well as performance over temperature.

In its simplest form, an RF/microwave oscillator consists of a tuned resonant (filter) circuit or element and an active device, such as a transistor, for amplification of the resonant frequencies. Some fixed-frequency oscillators may use passive circuit elements, such as inductors and capacitors, for the tuned circuit, while some will use quartz crystal as the resonant element or resonators based on surface-acoustic-wave (SAW) materials. Tuning circuits with variable elements, such as variable capacitors, also afford a certain amount of frequency tuning. At higher frequencies, yttrium-iron-garnet (YIG) spheres have been used as resonators in YIG-tuned oscillators (YTOs), as have coaxial resonators in coaxial resonator oscillators (CROs) and dielectric materials in dielectric resonator oscillators (DROs). A number of proven oscillator circuits have been developed over the years, often named for their founders (including the Butler, Clapp, Colpitts, Hartley, and Pierce oscillator types).

SURVEYING THE OPTIONS

High-frequency oscillator suppliers are constantly refining their designs for improvements in key performance parameters, such as phase noise, tuning speed, and even physical size, the better to meet the increased demands of modern electronic systems. Phase noise, for example, is a measure of an oscillator's frequency stability and must be minimized in systems that rely on digital modulation based on in-phase (I) and quadrature (Q) signal components to transfer information. It is a critical performance parameter for crystal oscillators serving as a clock or reference oscillator in a communication system or test instrument. The highest grade of stability for a crystal oscillator is a family of components known as oven-controlled crystal oscillators (OCXOs); these feature built-in heating circuits that help maintain the oscillator at a fixed temperature during operation, so as to minimize fluctuations in phase and frequency.

A challenge for designers of these type of oscillators is in maintaining the excellent stability while making them smaller in size. For example, the NV45G OCXO from Bliley Technologies (www.bliley.com) provides 100-MHz sinewave output signals at +7 dBm with phase noise of –130 dBc/Hz offset 100 Hz from the carrier. It exhibits –25 dBc harmonics and –75 dBc spurious levels and operates from a +12 or +15 VDC supply. It fits into a surface-mount package measuring 1 x 1 x 0.53 i222n.

One of the lowest-noise OCXOs in the industry, the 10-MHz model OX-045 from Vectron International (www.vectron.com), is built around a stress-compensated (SC) cut crystal. Although packed into a surface-mount housing measuring only 50 x 50 mm, it achieves impressive phase noise of –113 dBc/Hz offset 1 Hz from the carrier, –140 dBc/Hz offset 10 Hz from the carrier, and a noise floor of –163 dBc/Hz. It boast temperature stability of ±3 ppb from 0 to +70°C and ± 10 ppb from –40 to +70°C. The source offers +10-dBm typical output power with –30 dBc harmonics with an aging rate of only 10 ppb/year.

Even smaller, the model VFOV405 from Valpey Fisher (www.valpeyfisher.com) fits in a surface-mount package that is only 14 x 14 mm and only consumes 0.12 W power from a typical +3.3-VDC supply in steady-state operation. It is available with fixed output frequencies from 5 to 50 MHz at HCMOS/TTL levels. The oscillator features an aging rate of only 0.5 parts per billion per day (0.5 ppb/day). The tiny OCXO exhibits exceptional phase noise, making it ideal as a reference oscillator for phase-lock-loop (PLL) frequency synthesizers. For a 10-MHz oscillator, the SSB phase noise is –90 dBc/Hz offset 1 Hz from the carrier, –125 dBc/Hz offset 10 Hz, –155 dBc/Hz offset 1 kHz, and –165 dBc/Hz offset 10 kHz from the carrier. The OCXO is designed for operating temperatures from –40 to +85°C.

Greenray Industries (www.greenray-industries.com) offers OCXOs with frequencies from 1 to 200 MHz in a range of package styles, including surface-mount and dual-in-line-package (DIP) types. The YH1320 series OCXOs come in a pin package measuring 50.8 x 50.8 x 19.05 mm with HCMOS or sinewave outputs from 10 to 120 MHz. The sources consume 2.5 W during steady-state operation from a +12-VDC supply. They exhibit –20 dBc harmonics and, for a 10-MHz oscillator, phase noise of –125 dBc/Hz offset 10 Hz from the carrier, –160 dBc/Hz offset 1 kHz, and –165 dBc/Hz offset 10 kHz from the carrier.

When a somewhat smaller oscillator package is required, the company recently introduced its T72 series of temperature-compensated crystal oscillators (TCXOs) with clipped sinewave outputs from 10 to 50 MHz. Based on high-performance crystals from Statek (www.statek.com), these oscillators are housed in rugged ceramic packages measuring only 5 x 7 mm. They

are stable within ±0.2 ppm across operating temperatures from –40 to +85°C. They draw only 1 mA current from a +3.3-VDC supply making them suitable for battery-powered wireless applications. They are also resistant to the effects of vibration and feature a phase-noise floor of –159 dBc/Hz for a 10-MHz source.

Integrated Device Technology (www.idt.com) recently introduced its fourth-generation FemtoClock® NG crystal oscillators and voltage-controlled crystal oscillators (VCXOs). Housed in packages measuring 5 x 7 mm **(Fig. 1)**, they can be supplied with programmable output frequencies from 15.476 to 1300 MHz.

Additional suppliers of crystal oscillators include Bomar Crystal (www.bomarcrystal.com), Connor-Winfield Corp. (www.conwin.com), Fox Electronics (www.foxonline.com), Freescale (www.freescale.com), International Crystal Manufacturing (www.icmfg.com), Maxim Integrated Products (www.maxim-ic.com), MMD Components (www.mmdcomp.com), M-tron Industries (www.mtronpti.com), Silicon Labs (www.silabs.com), SiTime (www.sitime.com), and Texas Instruments (www.ti.com).

Voltage-controlled oscillators (VCOs) have long been known for their fast tuning speeds and low phase noise over wide bandwidths. Circuitry for these can be made compact enough to fit surface-mount housings and run at lower supply voltages. For example, reviewing the performance of the model MAOC-009264-PKG003 VCO from M/A-COM Technology Solutions (www.macomtech.com) may help to understand the essential parameters that come into play when comparing and specifying VCOs for applications.

The MAOC-009264-PKG003 operates from 8.8 to 9.8 GHz by means of tuning voltages from 1 to 13 V. Based on an InGaP heterjunction-bipolar-transistor (HBT) low-noise active device, the oscillator is supplied in a RoHS-compliant, 5 x 5 mm 32-lead PQFN package. It is somewhat unique in providing fundamental-frequency output signals and signals divided by 2 (from 4.4 to 4.9 GHz) at a separate port. The oscillator has a integrated buffer amplifier to provide +9 dBm typical output power from 8.8 to 9.8 GHz and +3 dBm typical output power from 4.4 to 4.9 GHz. The phase noise is typically –88 dBc/Hz offset 10 kHz from any carrier in the fundamental-frequency range, and –115 dBc/Hz offset 100 kHz from the carrier.

The 50-Ω oscillator typically draws 165 mA current from a +5-VDC supply, with –25 dBc harmonics at the main port and –24 dBc harmonics at the divided port. It exhibits frequency pushing, or sensitivity to supply voltage, of 20 MHz/V at the main port and 2 MHz/V at the divided port. The

Aethercomm®

We make hardware that saves lives.™

HIGH POWER RF SWITCHES

Aethercomm has been designing and manufacturing solid state high power RF switches for over 12 years for our own high power systems. We are now offering them to the industry as stand alone modules.

Custom Modules Available:

- Different Frequency Ranges
- Smaller Volumes
- Higher Isolation
- Higher Power Levels
- Faster Switching Speeds
- Lower Insertion Loss

Standard Product Offerings Available:

Model Number	Frequency Range	CW Power Rates	Peak Power Handling	Insertion Loss	Isolation	VSWR	Switching Speed	Size
SSHPS 0.96-1.22-3000	960-1220 MHz	250 Watts	3000 Watts	0.8 dB	60 dB	2.0:1	4 µsec	4.5 x 3.5 x 1.0 inches
SSHPS 1.2-1.4-4000	1200-1400 MHz	200 Watts	4000 Watts	0.7 dB	60 dB	1.6:1	4 µsec	4.5 x 3.5 x 1.0 inches
SSHPS 2.7-2.9-1000	2.7-2.9 GHz	100 Watts	1000 Watts	0.8 dB	40 dB	1.7:1	4 µsec	3.5 x 3.5 x 1.0 inches
SSHPS 2.9-3.1-1000	2.9-3.1 GHz	100 Watts	1000 Watts	0.8 dB	40 dB	1.8:1	4 µsec	3.5 x 3.5 x 1.0 inches
SSHPS 2.7-3.5-1000	2.7-3.5 Ghz	50 Watts	1000 Watts	0.9 dB	40 dB	2.0:1	4 µsec	3.5 x 3.5 x 1.0 inches
SSHPS 0.020-1.000-200	20-1000 MHz	200 Watts	1500 Watts	0.7 dB	25 dB	2.0:1	5 µsec	3.0 x 3.0 x 1.0 inches
SSHPS 0.225-0.450-400	225-450 MHz	400 Watts	2000 Watts	0.7 dB	40 dB	2.0:1	5 µsec	3.0 x 3.0 x 1.0 inches
SSHPS 1.0-2.5-200	1000-2500 MHz	200 Watts	1000 Watts	0.9 dB	25 dB	1.5:1	4 µsec	4.0 x 6.0 x 1.3 inches

SSHPS 1.03-1.09-5000 Typical Data

- Operation from 1030-1090 MHz
- Peak Power Handling of 5000 Watts
- Insertion Loss = 0.4 dB nominal
- Isolation = 58 dB typical
- Operation into an Infinite VSWR
- -40C to +70C Operation
- Internal BIT
- < 5µSec Switching Speed
- Return Loss, All Ports = -14 dB nominal
- 4.5" wide x 3.5" long x 1.0" high
- All switches High Power Tested & ESS Screened

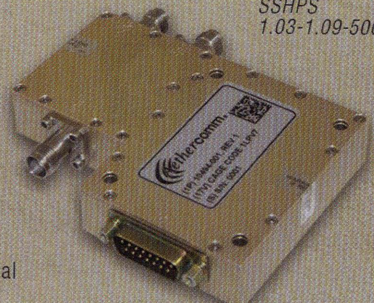

SSHPS 1.03-1.09-5000

Tel 760.208.6002
sales@aethercomm.com

BSI REGISTERED ISO 9001:2008 FM 89386

BSI AS 9100 FM 551035

12 YEARS IN BUSINESS 1999-2011

www.aethercomm.com

frequency drift with temperature from 8.8 to 9.8 GHz is 0.75 MHz/°C from –40 to +85°C. Peak-to-peak frequency pushing is 10.3 MHz for load VSWRs of 1.95:1 to 2.25:1. The one specification not supplied on the VCO's data sheet, tuning speed and/or frequency settling time, may be instrumental in selecting an oscillator for an application that requires rapid changes of frequency.

Synergy Microwave Corp. (www.synergymwave.com), a long-time supplier of microwave VCOs, entered the crystal oscillator market last year with several 10-MHz OCXOs, including model OXO10-1-348. Housed in a compact 25.4 x 22.0 mm surface-mount package, it delivers sinewave outputs with less than –20 dBc harmonics and less than –90 dBc spurious content. It features phase noise of –100 dBc/Hz offset 1 Hz from the carrier, –160 dBc/Hz offset 1 kHz from the carrier, and –165 dBc/Hz offset 10 kHz from the carrier. It consumes less than 200 mA current from a +12-VDC supply during steady-state operation, and has a voltage range of 0 to 5 V for control of a tuning range from ±0.5 to ±1.5 ppm. The OCXO handles operating temperatures from –20 to +70°C.

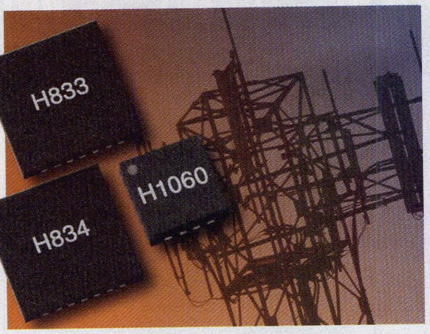

2. This pair of surface-mount PLLs includes integrated VCOs for applications through 6 GHz. [Photo courtesy of Hittite Microwave Corp. (www.hittite.com).]

Mini-Circuits (www.minicircuits.com) offers more than 3000 wideband and linear-tuning VCOs for frequencies from 3 to 7800 MHz in case styles from 0.25 x 0.25 in. to 0.5 x 0.5 in. It provides surface-mount-packaged VCOs at frequencies from 24 to 6840 MHz. One example, model ROS-2600-119+, tunes from 1650 to 2600 MHz in a metal case measuring 0.5 x 0.5 x 0.18 in. and shielded against unwanted signals and noise. It exhibits phase noise of –102 dBc/Hz offset 10 kHz from the carrier.

To simplify their use in PLL circuits, earlier this year Hittite Microwave Corp. (www.hittite.com) launched a pair of surface-mount PLLs with integrated VCOs, models HMC833LP6GE and HMC834LP6GE (**Fig. 2**). Model HMC833LP6GE is a fractional-N PLL and VCO that spans 1500 to 3000 MHz with an integral VCO divide by 1 through 64 output divider and frequency doubler, allowing the device to generate frequencies from 25 MHz to 6 GHz. The HMC834LP6GE also combines a PLL, VCO with range of 2.8 to 4.2 GHz, output divider, and doubler; it generates frequencies of 45 MHz to 1050 MHz, 1400 MHz to 2100 MHz, 2800 MHz to 4200 MHz, and 5600 MHz to 8400 MHz. The devices exhibit noise floor of –170 dBc/Hz and can operate from supply voltages of +1.8 to +5.2 VDC.

Additional suppliers of VCOs include Linear Technology (www.linear.com), Micronetics (www.micronetics.com), ON Semiconductor (www.onsemi.com), Phase Matrix (www.phasematrix.com), Raltron Electronics (www.raltron.com), RF Micro Devices (www.rfmd.com), Sivers IMA (www.siversima.com), Skyworks (www.skyworksinc.com), Spectrum Microwave (www.spectrummicrowave.com), TriQuint Semiconductor (www.triquint.com), and Z-Communications (www.zcomm.com).

When tuning speed is not critical, YIG-based oscillators provide broad frequency coverage with low phase noise. One of the longest-running YIG-based component suppliers, Omni YIG, Inc. (www.omniyig.com), in response to the growing demands for smaller oscillators, recently introduced a line of miniature YIG oscillators that includes the model YOM3824DD for applications from 2 to 6 GHz. It measures just

1.4 x 1.4 x 3.1 in. including an integral 12-b digital driver, and is capable of delivering +15-dBm typical output power across the frequency range. The YIG oscillator is usable at temperatures from −54 to +85°C with low spurious levels of typically −70 dBc and phase noise of −120 dBc/Hz offset 100 kHz from the carrier.

When even smaller YIG oscillators are needed, Micro Lambda Wireless (www.microlambdawireless.com) offers its MLTO series of TO-8-packaged oscillators in 2-GHz bandwidth models from 2 to 8 GHz. With a package height of only 0.27 in., these YIG sources are built for operating temperatures from 0 to +65°C. For example, YIG oscillator model MLTO-20204 tunes from 2 to 4 GHz (with a free-running frequency of 3 GHz) with +10-dBm typical output power. It operates from +8 V and −5 V supplies and exhibits 2-MHz pulling into a 12-dB return loss load and ±2 MHz/V pushing with power-supply variations.

It delivers −15 dBc minimum harmonics, −70 dBc minimum spurious levels, phase noise of −100 dBc/Hz offset 10 kHz from the carrier and −125 dBc/Hz offset 100 kHz from the carrier. The main coil sensitivity is 6 MHz/mA while the FM coil sensitivity is 300 kHz/mA. The TO-8 YIG oscillator draws 60 mA current from a +8-VDC supply and 15 mA at −5 VDC.

To overcome the characteristic slow tuning speeds of YIG oscillators, Giga-tronics (www.gigatronics.com) developed their model FTO-0408-540-01 source for use from 4 to 8 GHz. It offer phase noise of −104 dBc/Hz offset 10 kHz from the carrier with about five times the tuning speed of traditional YIG oscillators.

Teledyne Wireless (www.teledynewireless.com), which acquired the YIG component technology of Ferretec in 2004, maintains low phase noise in its higher-frequency oscillators through the use of bipolar transistor active devices. Its model FS2637 oscillators cover the frequency range from 8 to 18 GHz in a housing measuring 1.25 x 1.25 x 0.84 in. The typical phase noise is -128 dBc/Hz offset 100 kHz from the carrier. The oscillator is specified for +13 dBm output power at temperatures from 0 to +60°C and +11 dBm output power at temperatures from −55 to +85°C. The output-power flatness is within ±3.5 dB at temperatures from −55 to +85°C. Harmonics are typically −12 dBc while spurious levels are typically −60 dBc or better. The oscillator suffers maximum drift of 20 MHz with temperature, with 0.1% tuning linearity, and 0.5 MHz/V pushing. It draws 180 mA at +15 VDC and 30 mA at −5 VDC. Additional suppliers of YIG oscillators include Microwave Dynamics (www.microwave-dynamics.com) and Vida Products (www.vidaproducts.com). MWRF

JACK BROWNE | Technical Contributor

Producing Power The Solid-State Way

Discrete power transistors support RF and microwave large-signal applications with a variety of technologies, ranging from older silicon semiconductors to mixes of materials using gallium nitride.

HIGH-POWER RF and microwave signals are often associated with electron tubes, but solid-state devices have been gaining ground on their vacuum counterparts in recent years. With the maturation of gallium-arsenide (GaAs) power transistors, and as device designers continue to explore the capabilities of gallium nitride (GaN) and silicon-carbide (SiC) power-transistor technologies, solid-state devices offer noteworthy output-power levels.

The number of technologies supporting RF/microwave transistor developments has grown steadily over the years. Silicon bipolar transistors once handled the bulk of the solid-state amplification at radio frequencies. But over the last 30 years, GaAs field-effect transistors (FETs) have provided amplifier designers with higher-frequency performance while eventually matching the output-power levels of lower-frequency silicon bipolar transistors. In recent years, bipolar junction transistors based on SiC have established new marks for output power at lower microwave frequencies, while FETs and high-electron-mobility transistors (HEMTs) based on GaN have continued to boost solid-state power levels at higher microwave frequencies.

This transistor technological diversity is probably greatest for high-power applications around or below 1 GHz, such as in radio broadcast systems and in pulsed ultra-high-frequency (UHF) and very-high-frequency (VHF) radars. At these frequencies, silicon is still king, and a number of different transistor configurations have provided reliable results for many years. These include silicon bipolar transistors, silicon metal-oxide-semiconductor FETs (MOSFETs), and silicon lateral-diffused-MOS (LDMOS) FETs.

For example, model IB1011S1500 is a silicon bipolar power transistor from Integra Technologies (www.integratech.com) designed for L-band radars at 1030 and 1090 MHz.The firm offers a range of high-power devices for air-traffic-control (ATC) and avionics applications, based on different device technologies that include silicon LDMOS and GaN HEMT technologies. The IB1011S1500 is designed for

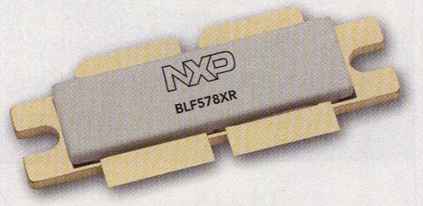

Model BLF578XR is developed for extremely severe load mismatch conditions. This 1400-W transistor (DC to 500 MHz) can handle a load mismatch of 125.0:1 through all phases at 1200 W output power. [Photo courtesy of NXP Semiconductors (www.nxp.com).]

pulsed applications, and when fed with a 150-W, 10-µs, 1%-duty-cycle signal at 1030 MHz, delivers 1432 W peak output power with better than 48% drain efficiency. The company also offers a more broadband model IB0912M600 bipolar transistor, designed for L-band TACAN systems from 960 to 1215 MHz. When supplied with a 90-W pulsed input signal, it can generate 845 W peak output power and more than 56% efficiency at 960 MHz. Both transistors are housed in beryllium-oxide (BeO) packages to aid thermal management.

Freescale Semiconductor (www.freescale.com) might be most closely identified with silicon LDMOS transistors, especially with that technology's ubiquitous use in cellular communications infrastructure applications. In addition to a wide range of silicon LDMOS transistors for cellular, ISM band, and commercial L- and S-band pulsed applications, and its extensive lines of integrated circuits (ICs), Freescale also offers RF power GaAs FET transistors through about 6 GHz). As an example of its L-band LDMOS technology, model MRF6VP121KHR6 is an L-band power transistor for applications from 965 to 1215 MHz. It is designed for a supply of +50 VDC (150 mA quiescent current) and can deliver 1000 W peak output power (and 100 W average output power) with a 128-µs pulse at 10% duty cycle. The power transistor achieves 20-dB power gain with 56% drain efficiency, but is only rated to handle a 5.0:1 VSWR maximum load mismatch. It is internally impedance matched to 50Ω with integrated electrostatic-discharge (ESD) protection and supplied in a flange package.

The company also supplies unmatched lateral N-channel broadband RF power MOSFETs for applications requiring broadband amplification. The model MRFE6VP61K25HSR6 power transistor, for example, is +50-VDC device (100 mA quiescent current) that operates from 1.8 to 600 MHz with 1250 W CW output power at

230 MHz, 24-dB gain, and 74% drain efficiency. It can also deliver 1250 W peak output power at 230 MHz with a 100-μs pulse at 20% duty cycle, 22.9-dB gain and 74.6% drain efficiency. This device has been designed for applications in industrial plasma exciters, broadcast, aerospace, land mobile communications and can tolerate a load mismatch as severe as 65.0:1 at +50 VDC.

In attempting to provide a more-robust LDMOS transistor, NXP Semiconductors (www.nxp.com) last year announced its XR family of "eXtremely Rugged" LDMOS RF power transistors **(see figure)**. Designed to withstand the severe conditions of applications such as industrial lasers, metal etching, and concrete drilling, these transistors are built to survive VSWR mismatches as severe as 125.0:1, which was the limit of the company's mismatch test system. One of the targets in developing the devices was to exceed a VSWR of 100.0:1, ruggedness thought to be necessary for many Industrial-Scientific-Medical (ISM) band applications. The first device in the product line is model BLF578XR, with 1400 W pulsed output power from DC to 500 MHz. It delivers 24-dB small-signal gain at 225 MHz with 70% drain efficiency, and can handle a load mismatch of 125.0:1 through all phases at 1200 W output power.

Transistor technological diversity is probably greatest for applications around or below 1 GHz.

Several years ago, devices based on SiC substrates showed great promise for use in high power continuous-wave (CW) and pulsed RF power applications. Device manufacturers including Cree (www.cree.com) and Microsemi Corp. (www.microsemi.com) developed RF power transistors based on the SiC material, including static induction transistors (SITs) for high-power pulsed radar applications working with UHF and VHF signals. Microsemi, for example, still offers the model 0405SC-2200M Class AB, common gate, depletion mode SIT for use at a drain voltage of +125 VDC. It provides 2200 W peak output power from 406 to 450 MHz with 7.5-dB typical gain when operating with 300-μs pulses at 6% duty cycle. It offers 55% drain efficiency and can handle load mismatches to 10.0:1. Suitable for UHF weather radar and long-range tracking radar, the power RF SiC transistor is supplied in a rugged flange-mount package.

SiC has excellent thermal properties, however, and is being used by many companies in conjunction with devices based on GaN epitaxial material, to form GaN-on-SiC power transistors. M/A-COM Technology Solutions (www.macomtech.com) is one of the growing list of suppliers for GaN-on-SiC power transistors. These devices offer unparalleled power densities at higher frequencies from smaller transistor cells, but require thoughtful thermal-management planning. For example, M/A-COM's model MAGX-000035-150000 is a GaN-on-SiC power transistor that can provide 150 W CW output power from 30 to 3500 MHz with as much as 30 dB gain. The firm's model MAGX-002735-180000 GaN-on-SiC transistor operates from 2700 to 3500 MHz with 180 W peak output power for a 500-μs pulse at 10% duty cycle. It can deliver 13-dB typical gain over that frequency range. In addition to these discrete transistors, the company also offers "pallet" circuits or amplifiers, such as the model MAPG-002731-330L0S which combines two discrete devices on a printed-circuit board (PCB) with coaxial input and output connectors matched to 50 Ωand bias connections for ease of use. The model MAPG-002731-330L0S pallet operates from 2700 to 3100 MHz with 330 W peak output power when running with a 300-μs pulse at 10% duty cycle; it yields 11-dB gain.

Rather than mounting GaN devices on SiC, Nitronex (www.nitronex.com) has developed its SIGANTIC® NRF1 GaN-on-silicon process to support high CW and peak output power levels from its devices. In addition to supporting high-performance levels, the process is economically attractive, since it is production qualified for fabrication of GaN-on-Si devices on standard 4-in. silicon semiconductor wafers. The firm's model NPT1007 GaN-on-SiC power transistor, for example, is a +28-VDC device that can be used from DC to 1200 MHz. It is designed for push-pull applications and can withstand load mismatches as severe as a 10.0:1 VSWR without damage or degradation. The transistor is rated for CW power levels to 200 W at 900 MHz with better than 18-dB small-signal gain and 63% typical drain efficiency. The company offers an excellent 25-page white paper on thermal management of GaN-based power transistors (application note AN-012) as a free download from its website.

In addition, Freescale offers an excellent application note on evaluating the temperature of RF transistors, "Thermal Measurement Methodology of RF Power Amplifiers." Copies are available for free download from www.freescale.com.

Late last year, Nitronex announced its move to +48-VDC GaN-on-silicon technology with a process designated NRF2. Intended to provide higher power densities and higher gain than the +28-VDC NRF1 process, the new process is also claimed to provide improved long-term reliability with a mean time to failure (MTTF) of more than one million hours (114 years) at an operating temperature of +230°C.

In addition to the firms mentioned, power transistors are available from a wide range of suppliers. These include Advanced Semiconductor, Inc. (ASI; www.advancedsemiconductor.com), which designs and fabricates a number of replacement devices for older broadcast and aerospace power transistors; Integra Technologies, Inc. (www.integratech.com), which provides silicon bipolar and MOSFETs and GaN HEMTs; IXYS RF (www.ixysrf.com), a supplier of silicon MOSFETs; Spectrum Devices (www.spectrumdevices.com), a source for silicon bipolars and MOSFETs; ST Microelectronics (www.st.com), which supplies silicon MOSFETs; TriQuint Semiconductor (www.triquint.com), which provides GaAs and GaN power FETs; and Richardson Electronics (www.richardsonrfpd.com), a distributor for numerous device manufacturers. MWRF

JACK BROWNE | Technical Contributor

Keep The Heat Under Control

Thermal management can involve choosing optimum circuit materials, making measurements, and developing accurate models that can predict the effects of heat on a design's ultimate reliability.

HEAT IS AN ENEMY to most electronic circuits. It can cause premature aging of active devices, deterioration of solder joints, and degradation of printed-circuit-board (PCB) performance. In power bipolar transistors, excess heat can even cause an undesirable effect known as "thermal runaway," in which energy from the device is released to feed a temperature-rise loop that ends in the device's destruction. Thermal management is a practical approach toward removing heat from electronic circuits, ideally without compromising electrical performance.

All electronic circuits generate heat to some degree, since efficiency levels are not close to 100%. The low efficiency of electronic circuits can be a particular problem at high power levels, such as in power amplifiers and the circuits that support them. The latter includes power combiners/dividers, filters, couplers, and terminations. Antenna circuits (on transmit) must also often handle high power levels. Managing the heat in an RF/microwave circuit requires a multipronged strategy that includes designing effective thermal paths to carry heat away from a circuit's heat sources, such as power transistors; measuring the heat produced by the circuit and its circuit elements; and modeling the circuit for heat. Many companies proficient in thermal design will perform measurements and create models before and after a circuit is packaged, since the packaging plays an instrumental role in handling the heat.

One of the first steps in designing for effective thermal management of an RF/microwave circuit (or any type of circuit, for that matter) is to carefully choose a PCB substrate material. RF/microwave circuit designers must find a circuit-board material that is not only stable with time and temperature and capable of dissipating a required amount of heat, but also has the proper dielectric and electrical properties needed for a particular high-frequency circuit design. High-frequency circuit-board materials are characterized by a large number of mechanical and electrical parameters, with permittivity (relative dielectric constant) and dissipation factor two of the critical barometers of electrical performance, while thermal coefficient of dielectric constant, coefficient of thermal expansion, and thermal conductivity are the three main measures of a PCB material's behavior with temperature.

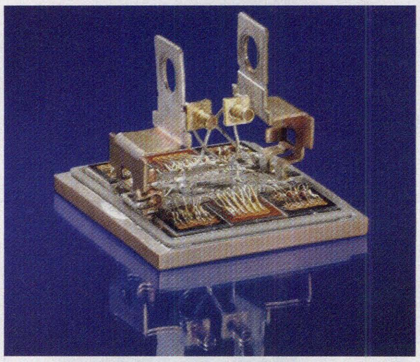

This electronic test module features a copper composite base plate to support accurate thermal measurements. [Photo courtesy of the Fraunhofer Institute for Manufacturing Technology and Advanced Materials (IFAM) (www.ifam-dd.fraunhofer.de).]

The thermal coefficient of dielectric constant is a measure (typically in ppm/°C) of the variability of permittivity as a function of temperature in the z direction or thickness of a circuit material, usually referenced to a specific test frequency, such as 10 GHz. The coefficient of thermal expansion (also in ppm/°C) is also measured in the z direction and is used to gauge the reliability of plated through holes (PTHs) with the temperature swings experienced in normal material processing. The PTHs are used not only to connect circuits to ground planes, but as thermal pathways that help dissipate heat. The thermal conductivity is a reading (in W/m/K) of the amount of power that can be dissipated by a material for a give rise in temperature, also measured in the material's z direction. By using circuit materials with enhanced thermal conductivity, for example, the temperatures at device junctions and solder joints can be minimized under high-power conditions.

While circuit materials based on fluoropolymers such as polytetrafluoroethylene (PTFE) are known for their low loss and general excellent electrical behavior, pure PTFE is subject to a great deal of expansion and contraction with changes in temperature. Thus, for use in PCBs, it is usually reinforced with some other material (such as glass fibers). In addition, some PCB material suppliers have developed circuit materials that combine PTFE and more thermally stable thermoset materials. For example, TMM® laminates

from Rogers Corp. (www.rogerscorp.com) are ceramic thermoset polymer composites designed for applications in which thermal management may be a concern. Available with various values of relative dielectric constant, these materials exhibit a low thermal coefficient of dielectric constant, typically less than 30 ppm/°C, electrical stability with changes in temperature. The material offers twice the thermal conductivity of traditional PTFE/ceramic laminates, at 0.70 W/m/K, with isotropic thermal expansion properties that are closely matched to those of copper, so that stress is minimized on PTHs even during the temperature changes of material processing cycles. For even more demanding thermal applications, the firm's RT/duroid® 6035HTC circuit material combines low loss with impressive thermal conductivity of 1.44 W/m/K to help manage heat flow away from a PCB's solder joints and device junctions.

> **The low efficiency of electronic circuits can be a particular problem at high power levels, such as in power amplifiers.**

Power transistors are predictable sources of heat in a high-frequency circuit, especially as demands for higher power levels push the capabilities of newer transistor designs, including gallium arsenide (GaAs), gallium nitride (GaN), and silicon-carbide (SiC) devices. With higher power levels come higher power densities, and the need for mounting and packaging materials with extremely high thermal conductivities to dissipate the excess heat. Transistor carriers have been developed from a variety of materials capable of conducting heat, including copper, beryllium oxide (BeO), copper-tungsten, and even diamond. BeO, for example, has thermal conductivity of about 285 W/m-K at room temperature, which is outstanding—except when compared to some diamond heatsinks, with thermal conductivity values as high as 1800 W/m-K.

While many power transistor suppliers develop their own packaging based on thermal needs, some organizations, such as the Fraunhofer Institute for Manufacturing Technology and Advanced Materials (IFAM) (www.ifam-dd.fraunhofer.de), specialize in developing custom materials and packages capable of dissipating a large amount of heat. The firm has developed heat sinks, packages, and even test fixtures **(see figure)** based on metal-phase-change-material (metal-PCM) composites which are designed to minimize the customary mismatch of CTE between different packaging materials for tailored thermal expansion behavior and enhanced packaging reliability at high power/temperature levels.

In addition to selection of packaging materials, the use of bonding films, such as organic adhesive films from American Standard Circuits (ASC; www.asc-i.com) can help enhance the thermal conductivity of PCBs as well as packages. The company offers PCBs with customer-specific heat management requirements based on the use of PCBs with PTHs and its proprietary adhesive bonding films. ASC manufactures PCBs based on circuit materials from leading laminate suppliers, including Arlon Materials for Electronics Div. (www.arlon-med.com), Nelco (Park Electrochemical Corp.; www.parkelectro.com), Taconic Advanced Dielectric Div. (www.taconic-add.com), and Rogers Corp. Measuring the temperatures of circuit designs or even simulating the operating conditions that can bring thermal stress to a PCB requires specialized test equipment capable of accurately detecting wide temperature extremes and, in some cases, generating such temperature extremes. The line of ThermoStream® benchtop and portable systems from Temptronic (www.temptronic.com), for example, are capable of creating and detecting temperatures from –90 to +225° using forced-air streams. Compact systems such as the model TPO4390A offer extremely fast temperature transition times for stress testing, with the capability of shifting from –55 to +125° in about seven seconds while maintaining 1°C accuracy. This system features a touchscreen for ease of control and four remote interface ports for system integration, including Ethernet, GPIB, and RS-232C ports. Khoury Industries (www.khouryindustries.com) is another supplier of thermal test equipment, along with test chambers and fixtures for thermal measurements. Microtek Laboratories (www.thetestlab.com) is an outside test laboratory for RF/microwave designers in need of outside test services for an extensive range of PCB tests, including thermal stress, thermal shock, and thermal analysis.

Once a design has been tested and analyzed for thermal hotspots, a computer model can help understand the modifications needed to better dissipate the heat from those critical points in a PCB or package. HyperLynx Thermal software from Mentor Graphics (www.mentor.com), for example, can perform thermal modeling on double-sided, multilayer PCBs with as many as 3000 components on each side. The software provides precise calculation of junction temperatures for improved reliability predictions. Another model tool is the QoolPCB™ thermal modeling software from Advanced Thermal Solutions (www.qats.com).

Docea Power (www.doceapower.com) recently released its AceThermalModeler™ (ATM) software for creating thermal models for PCBs, system-on-chip (SoC) designs, system-in-package (SiP) structures, and even three-dimensional (3D) integrated circuits (ICs). According to the firm's Chief Executive Officer, Ghislain Kaisler, "With it, system architects can perform both thermal steady state or coupled power and thermal analysis for dynamic application profiles running on different architecture configurations." The software's models are meant to help designers understand thermal gradients across a circuit and develop packaging and integration solutions quickly and effectively. MWRF

SAMIR KAMECHE
Assistant Professor

MOHAMMED KAMECHE
Researcher
Centre of Space Techniques, Algeria, P.O. Box 13, Arzew, 31200 Oran, Algeria

MOHAMMED FEHAM
Professor
Electronics and Electrical Engineering Department, STIC Laboratory, University of Tlemcen, P.O. Box 230, Chetouane, 13000 Tlemcen, Algeria; e-mail: samir.kameche@gmail.com.

OPTIMIZING PLL Performance Levels

Designing a PLL synthesizer for modern mobile communications systems involves achieving the proper balance among a number of tradeoffs, including spurious levels and frequency switching speed.

FREQUENCY SYNTHESIZERS based on phase-locked loops (PLLs) are widely used in radio communications systems. Such signal sources are known for their high frequency resolution and fast switching speed, while maintaining good frequency accuracy over time and changing temperatures. Of course, some communications systems have specific requirements in terms of performance, and it is sometimes necessary to optimize the performance of a frequency synthesizer for a particular parameter. As will be shown in Part 1 of this two-part article, it is possible to design a PLL frequency synthesizer for fast switching speed or low spurious noise, with those two parameters representing a tradeoff that depends upon the synthesizer's loop filter. By properly designing the loop filter, a desired balance can be achieved between PLL spurious levels and lock time.

Many wireless communications systems require a frequency synthesizer that can combine low-noise operation and high frequency resolution with short locking time.[1] Many systems require optimization of synthesizer locking time and reference spurious levels.[2,3] It is possible to design a PLL that is optimized for different performance parameters, often by trading off one or more of its performance parameters to improve another. **Figure 1** shows a conventional PLL frequency synthesizer.[4] It has been used for a variety of applications, including as a control oscillator for wireless transmitters and receivers and as a timing element for digital equipment. It consists of a high-stability crystal oscillator, phase detector, charge pump, lowpass filter (LPF), voltage-controlled oscillator (VCO), and programmable frequency dividers.

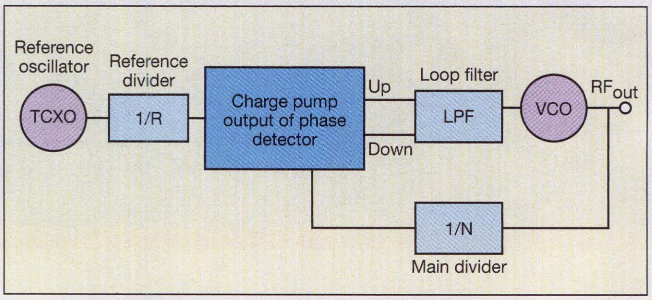

1. This simple block diagram shows the essential elements of the PLL frequency synthesizer.

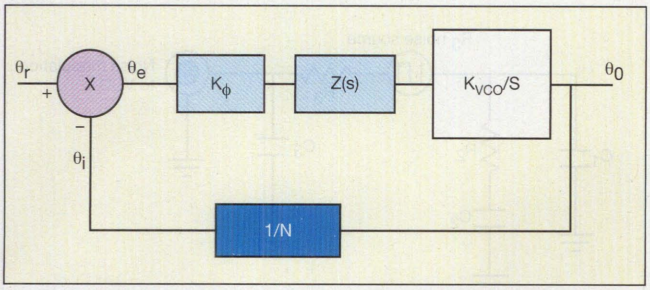

2. This block diagram represents a basic model for a PLL.

In the PLL frequency synthesizer, the phase/frequency detector (PFD) compares a fed-back frequency with a divided-down version of the reference frequency from the crystal oscillator. In an integer PLL frequency synthesizer, outputs are divided by integers. When a phase or time difference between the PFD's outputs is detected, the charge-pump circuit converts the difference into a voltage. The loop filter extracts the DC component of this voltage, which is then used to drive an external VCO to increase or decrease the output frequency and drive the average output of the PFD to zero.

In the PLL synthesizer, the input reference divider reduces the required reference input frequency, while the feedback divider reduces the output frequency required for comparison with the scaled reference frequency. The loop filter is a critical component in a PLL synthesizer, linking the VCO with the PFD. Because PFDs and VCOs can be somewhat more limited in their designs, it is the design of the loop filter that affords the main flexibility in determining a PLL's bandwidth. Although an active filter could be used, a passive filter is generally more desirable for practical applications.[5,6]

Figure 2 shows a linear mathematical model representing the phase of the PLL in its locked state,[4] where K_ϕ is the phase-detector/charge-pump gain (in mA/rad), S is the phase-detector gain factor, Z(s) is the transfer function of the loop filter, N is the main divider ratio, and K_{VCO} is the gain of the VCO (in MHz/V). The phase of the oscillator to be stabilized, θ_0, is compared with the phase of the reference, θ_r, and adjusted until the difference is driven to zero. The phases represented by θ_i and θ_e are the initial and error phases, respectively, of the oscillator to be stabilized.

In **Fig. 2**, the output is modeled as a phase rather than a frequency, which makes more sense considering the phase detector works in terms of phase rather than frequency. The VCO gain is multiplied by a factor of 1/s to convert it from a frequency to a phase. The PLL phase transfer functions are as follows.

The forward-loop gain can be shown as:

$$G(s)=\frac{\theta_0}{\theta_e}=\frac{K_\phi.Z(s).K_{VCO}}{s} \quad (1)$$

The reverse loop gain can be found from:

$$H(s)=\frac{\theta_i}{\theta_0}=\frac{1}{N} \quad (2)$$

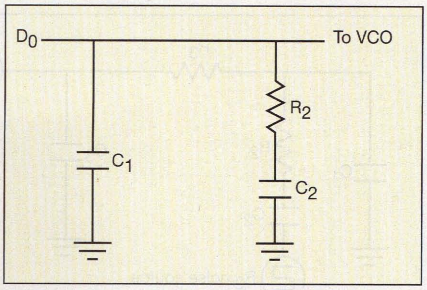

3. This schematic diagram represents a second-order loop filter.

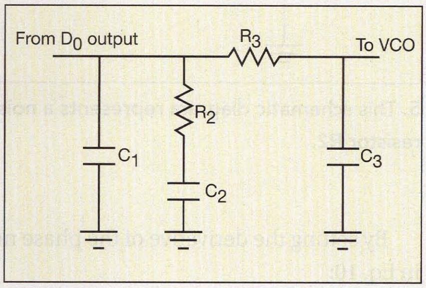

4. This schematic diagram represents a third-order loop filter.

The open-loop gain can be found from Eq. 3:

$$T(s)=H(s)G(s)=\frac{\theta_i}{\theta_e}=\frac{K_\phi.Z(s).K_{VCO}}{N.s} \quad (3)$$

By combining these transfer functions, the closed-loop gain can be found:

$$K(s)=\frac{\theta_0}{\theta_r}=\frac{G(s)}{[1+H(s)G(s)]} \quad (4)$$

Figure 3 shows the circuit for a second-order passive loop filter. Its transfer function, Z(s), can be found from:

$$Z(s)=\frac{s.C_2.R_2+1}{s^2C_1.C_2.R_2+s.C_1+s.C_2} \quad (5)$$

The time constants, T_1 and T_2, which determine the pole and zero frequencies of the filter transfer function, are defined by Eqs. 6 and 7:

$$T_1=R_2.\frac{C_1.C_2}{C_1+C_2} \quad (6)$$

$$T_2=R_2.C_2 \quad (7)$$

Thus, the third-order PLL open-loop gain can be calculated in terms of the frequency, ω; the filter time constants, T_1 and T_2; and the design constants, K_ϕ, K_{VCO}, and N:

$$G(s).H(s)\Big|_{s=j\omega}=\frac{-K_\Phi.K_{VCO}(1+j\omega.T_2)}{\omega^2.C_1.N(1+j\omega.T_1)}.\frac{T_1}{T_2} \quad (8)$$

The phase of the open-loop gain as a function of frequency depends upon the single pole and zero of the transfer function:

$$\phi(\omega)=\tan^{-1}(\omega.T_2)-\tan^{-1}(\omega.T_1)+180° \quad (9)$$

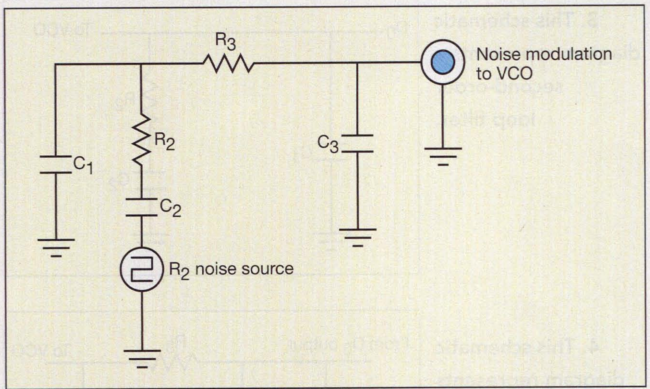

5. This schematic diagram represents a noise model for resistor R2.

By setting the derivative of the phase margin equal to zero, as in Eq. 10:

$$\frac{d\Phi}{d\omega}=\frac{T_2}{1+(\omega\cdot T_2)^2}-\frac{T_1}{1+(\omega\cdot T_1)^2}=0 \quad (10)$$

the frequency point corresponding to the phase inflection point can be found in terms of the filter time constants, T_1 and T_2. This relationship is given by Eq. 11:

$$\omega_p=\frac{1}{\sqrt{T_1.T_2}} \quad (11)$$

The values of the filter time constants, T_1 and T_2, can be found from Eqs. 12 and 13:

$$T_1=\frac{\sec\phi_p-\tan\phi_p}{\omega_p} \quad (12)$$

$$T_2=\frac{1}{w_p^2.T_1} \quad (13)$$

The component values for the filter can be found from T_1 and

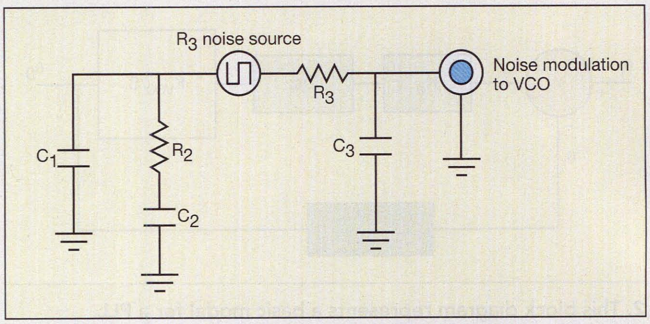

6. This schematic diagram represents a noise model for resistor R3.

T_2 and the loop bandwidth by applying Eqs. 14-16:

$$C_1=\frac{T_1}{T_2}\cdot\frac{K_\Phi.K_{VCO}}{w_p^2.N}\cdot\sqrt{\frac{1+(w_p.T_2)^2}{1+(w_p.T_1)^2}} \quad (14)$$

$$C_2=C_1(\frac{T_2}{T_1}-1) \quad (15)$$

$$R_2=\frac{T_2}{C_2} \quad (16)$$

Current switching noise in the dividers and the charge pump, at the reference frequency rate, F_{REF}, may cause unwanted frequency modulation (FM) sidebands at the RF output of the synthesizer. In a wireless communications system, the phase-detector comparison frequency is generally a multiple of the RF channel spacing. These spurious sidebands can cause noise in adjacent channels. Additional filtering of the reference spurs is often necessary, depending upon the width of the loop filter. This is often the case in modern time-division-multiple-access (TDMA) digital cellular communications systems, such as GSM cellular systems.[3]

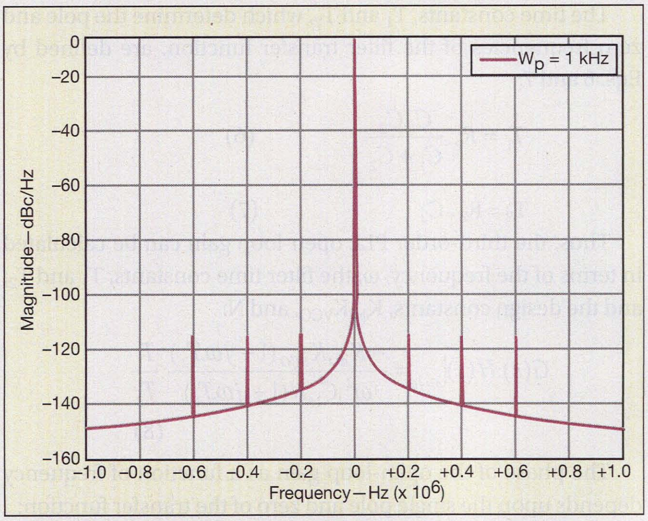

7. The PLL's output spectrum is shown here for a loop bandwidth of 1 kHz.

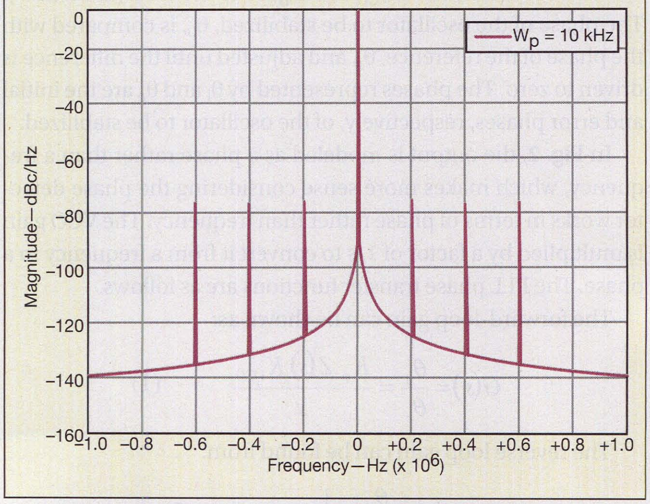

8. This plot shows the PLL's output spectrum for a loop bandwidth of 10 kHz.

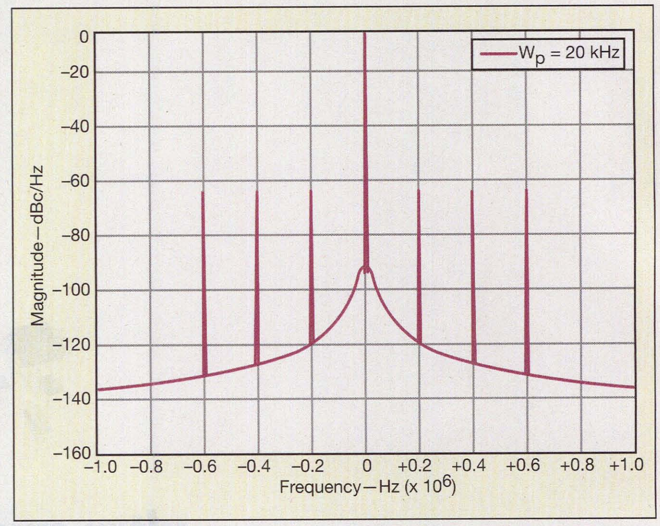

9. The PLL's output spectrum is shown here for a loop bandwidth of 20 kHz.

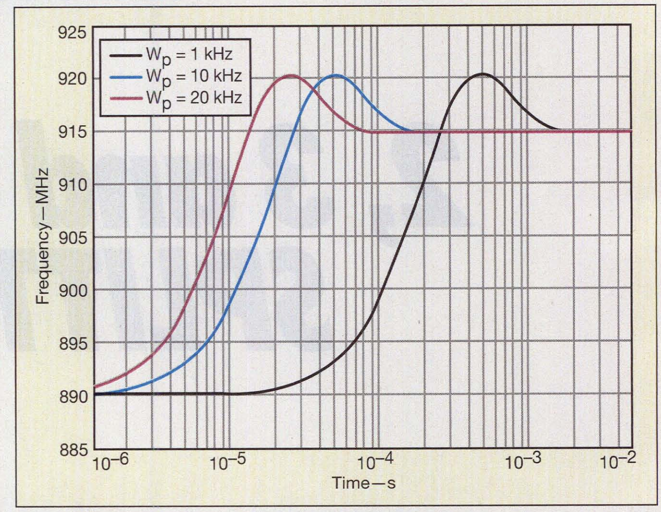

10. This plot shows the PLL transient response versus loop bandwidth.

A recommended filter configuration in such a case is the third-order filter shown in **Fig. 4**.[4] The attenuation added from its use is found from Eq. 17:

$$ATTEN = 20\log\left[(2\cdot\pi\cdot F_{ref}.R_3.C_3)^2+1\right] \quad (17)$$

The resulting third-order filter has a time constant for the added lowpass section, T_3, that can be found from Eq. 18:

$$T_3 = R_3 . C_3 \quad (18)$$

The transfer function of the loop filter in **Fig. 4** is given by Eq. 19:

$$Z_{fil3} = \frac{Z(s).\left(\frac{1}{C_3.s}\right)}{Z(s).+R_3+\left(\frac{1}{C_3.s}\right)} \quad (19)$$

where Z(s) is the transfer function for the second-order loop filter given by Eq. 5.

The cutoff frequency of the new filter, ω_c, can be found from Eq. 20 (see p. 59). Capacitor C_1 can be expressed by means of Eq. 21 (see p. 59).

Similar to what was done for the second-order filter, the component values can be found from Eqs. 22 and 23:

$$C_2 = C_1\cdot\left(\frac{T_2}{T_1}-1\right) \quad (22)$$

$$R_2 = \frac{T_2}{C_2} \quad (23)$$

For the loop filter in Fig. 4, it is necessary to calculate the voltage noise present at the output ports of resistors R_2 and R_3. The equivalent root-mean-square (RMS) noise voltage generated by the resistance can be found[7] by applying Eq. 24:

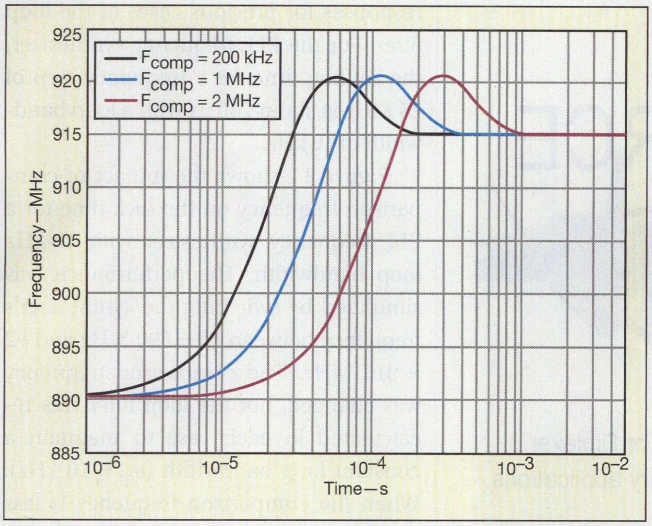

11. The PLL transient response is shown here versus comparison frequency.

$$V_{Noise}(R)=\sqrt{4.T_0.k.R.B} \quad (24)$$

where:

k = Boltzmann's constant;
T_0 = the device temperature (in°K);
B = the bandwidth (in Hz); and
R = the resistance (in Ω).

Figures 5 and 6 offer schematic-diagram noise models for resistances R_2 and R_3, respectively, as being equivalent sources of noise voltage appearing in series with each resistance. The derivation of the real noise voltage versus input frequency at the tuning port of the PLL synthesizer's voltage-controlled oscillator (VCO) is based on the basic circuit using the models of **Figs. 5 and 6**.[4]

Reference spurious products are also introduced in the simulation. The power levels of these can be calculated by the closed-loop transfer function evaluated at the spurious offset frequencies, F_{spur}. In general, spurious products are a result of either signal leakage or the impedance mismatch of the charge pump. In several studies, F_{spur} is assumed to be a multiple of the comparison frequency, F_{comp}. The power level of the reference spurious products can be found by applying Eq. 25[8]:

$$Spur_{Gain}(F_{Spur})=20\log\left[\frac{K_{VCO}Z(s)K_\phi}{s}\right] \quad (25)$$

In general, narrower loop bandwidths result in lower reference spurious levels but in longer frequency lock times.[9]

The loop bandwidth, the most critical system design parameter for a PLL, is determined by many factors, and is usually external to a PLL chip. A PLL user typical chooses a loop bandwidth and will design the PLL circuits for this parameter. As mentioned earlier, the classical design tradeoff in a PLL is lock time versus spurious performance. The spurious performance may look better for a narrower loop bandwidth, but the lock time is longer. For a large loop bandwidth, the lock time may be faster, but the spurious levels will increase.

To better understand the dynamics of a loop filter in a frequency synthesizer, a precise evaluation was undertaken to ensure the precision of the PLL frequency synthesizer design. **Figures 7, 8, 9, and 10** show the output spectra and transient

$$\omega_c=\frac{\tan\phi.(T_1+T_3)}{(T_1+T_3)^2+T_1.T_3}\cdot\left[\sqrt{1+\frac{(T_1+T_3)^2+T_1.T_3}{[\tan\phi\cdot(T_1+T_3)]^2}}-1\right] \quad (20)$$

$$C_1=\frac{T_1}{T_2}\cdot\frac{K_\Phi\cdot K_{VCO}}{\omega_c^2\cdot N}\cdot\left[\sqrt{\frac{1+\omega_c^2\cdot T_2^2}{(1+\omega_c^2\cdot T_1^2)\cdot(1+\omega_c^2\cdot T_3^2)}}\right] \quad (21)$$

responses for previous cases of the loop filter. For the PLL frequency synthesizer, the settling time for a frequency step of 25 MHz is about 240 μs with a loop bandwidth of 10 kHz.

Figure 11 shows the impact of comparison frequency on the lock time for a PLL frequency synthesizer with 10-kHz loop bandwidth. The performance was simulated by switching the synthesizer's frequency between F1 = 890 MHz and F2 = 915 MHz. The comparison frequency was changed, but the loop filter was recalculated in each case to maintain a constant loop bandwidth (ω_p = 10 kHz). When the comparison frequency is less than 20 times the loop bandwidth, the lock time obtained (about 240 μs) meets the requirements of most modern communications systems. However, when the comparison frequency is 1 MHz, the rise time of the synthesizer is greatly increased, which in turn increases the lock time. In the case where the comparison frequency, F_{comp}, is 2 MHz, the lock time becomes more degraded. MWRF

Editor's Note: The second part of this article will appear in the May issue of Microwaves & RF.

REFERENCES

1. G. Singh Patel and S. Sharma, "Comparative Study of PLL, DDS, and DDS-based PLL Synthesis Techniques for Communication System," International Journal of Electronics Engineering, Vol. 2, No. 1, 2010, pp. 35-40.
2. David Vye, "Performing Transient Analysis on PLL Frequency Synthesizers," Microwave Journal, Vol. 45, No. 1, January 2002, pp. 62-79.
3. William O. Keese, "An Analysis and Performance Evaluation of a Passive Filter Design Technique for Charge-pump PLLs," Application Note AN-1001, July 2001, National Semiconductor, Santa Clara, CA, 2006, www.national.com.
4. S. Kameche, M. Feham, and M. Kameche, "PLL Synthesizer Tunes DCS 1800 Band," Microwaves & RF, Vol. 46, No. 6, June 2007, pp. 84-90.
5. S. Kameche, M. Feham, and M. Kameche, "Simulating and Designing a PLL Frequency Synthesizer for GSM Communications," High Frequency Electronics, Vol. 7, No. 12, December 2008, pp. 36-41.
6. Jun Lee, "Phase Locked Loop Systems Design for Wireless Infrastructure Applications," Microwave Journal, Vol. 53, No. 5, May 2010, p. 74.
7. L. Lascari, "Accurate Phase Noise Prediction in PLL Synthesizers," Applied Microwave and Wireless, Vol. 12, No. 2, 2000, pp. 30-38.
8. D. Banarjee, PLL Performance, Simulation, and Design, 4th ed., National Semiconductor, Santa Clara, CA, 2006, www.national.com.
9. S. Kameche, M. Feham, and M. Kameche, "Optimizing Lock Time and Reference Spurs in PLL Frequency Synthesizer," IEEE International Conference on Electrical and Control Engineering ICECE 2011, Yichang, China, September 16-18, 2011.

More Power To You!

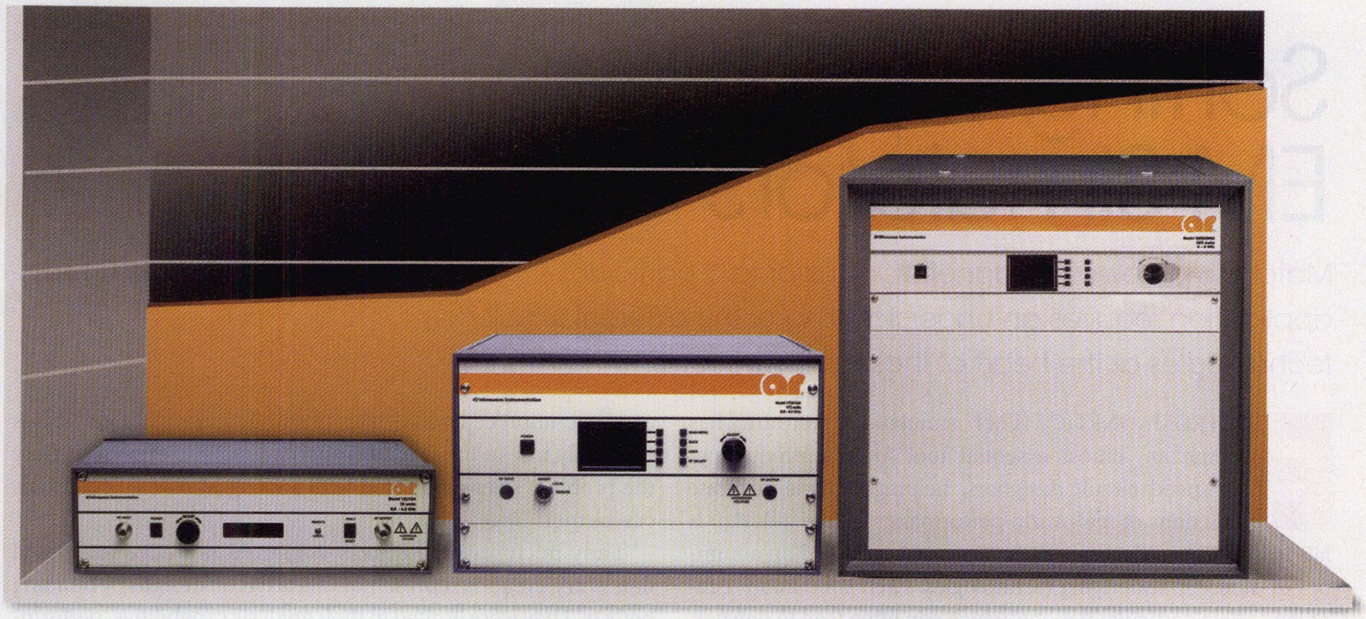

Our Newest "S" Series Amps Now Offers Powers From 20 To 1200 watts, And Everything In Between.

Once again AR has turned up the power on our "S" Series 0.8-4.2 GHz solid-state amplifiers. Recently we made them smaller and lighter, with more power. Now we've added *more* power without increasing size or weight.

One thing we didn't change was something we call **Subampability:**™ giving you expandable power. It's a unique money-saving feature that lets you add amplifiers when you need more power. And you can use these amps independently for tests that don't require as much power.

AR products are backed by the best and most comprehensive warranty in the industry. We back them better because we build them better. And we support our customers with a global network that reaches the far corners of the world.

So when you need a new power amplifier, there are some very powerful reasons to choose an "S" Series amp from AR.

www.arworld.us/sSeries

ISO 9001:2008
Certified

rf/microwave instrumentation

Other ar divisions: modular rf • receiver systems • ar europe

USA 215-723-8181. For an applications engineer, call 800-933-8181.

In Europe, call ar United Kingdom 441-908-282766 • ar France 33-1-47-91-75-30 • emv GmbH 89-614-1710 • ar Benelux 31-172-423-000

www.arworld.us

DAVE MORRIS
Application Engineer
Agilent Technologies, Lakeside, Cheadle Royal Business Park, Stockport 3K8 3GR, England; e-mail: david_morris@agilent.com, www.agilent.com.

Sorting Through EM Simulators

Matching an electromagnetic simulator to a particular application requires an understanding of the different simulation technologies at the heart of these software tools.

ELECTROMAGNETIC (EM) simulation software has become an almost essential tool for high-frequency/high-speed circuit designers, helping provide accurate predictions of real-world performance before a design is fabricated. EM analysis programs vary widely, based on a number of different underlying technologies. Each simulation technology offers particular benefits which can often lead to one particular type of EM simulator being better suited to solve a specific problem type. What follows is an outline of the three main EM simulation technologies found in commercial design tools today along with an outline of how they compare for different types of problems and applications.

A number of different EM simulation technologies have emerged over the years, including those based on the method of moments (MoM), finite-element method (FEM), and finite-difference-time-domain (FDTD) approaches. In principle, these technologies could be applied to solve the same problems, although there are practical reasons why one approach is better suited for solving a particular problem type. By reviewing these three key EM simulation technologies and comparing the relative merits of each, it may be possible to clarify those applications where an EM simulation based on one technology might be a better choice than software employing one of the other two EM simulation technologies.

The use of computer-aided-engineering (CAE) software developed specifically for RF and microwave circuit analysis has only been part of mainstream design processes for around 25 years, although such tools are now a much-relied-upon part of the high-frequency-circuit design process. Of course, computers have grown in power over that time, to currently efficient and powerful personal computers (PCs) capable of running compute-intensive CAE programs with fast processing speed. This dramatic improvement in computer power has been leveraged by CAE tool developers, resulting in today's designers having access to unprecedented levels of simulation capability. This is especially true in the field of computational EM analysis, where the problem sizes associated with solving Maxwell's equations can be quite large.

Early microwave CAE tools employed primitive text-based data entry, creating representations of circuit designs by building netlists. They were limited in their analysis capabilities, performing calculations only of linear scattering (S) parameters. In contrast, modern CAE tools provide designers with much more convenient design entry mechanisms that support schematic and layout design entry. This ease of design entry is combined with a host of analysis methods ranging from basic linear circuit analysis to advanced nonlinear frequency-domain simulation, time-domain simulation, hybrid frequency/time simulation methods (so-called "envelope" simulations), and EM simulation.

What limits the usefulness of a CAE simulation tool is generally not the speed or robustness of the simulation engine, but the accuracy or availability of the models within the simulation. Most microwave and high-speed digital designs can be divided into active or passive components or devices. Ideally, active devices would be represented by nonlinear models and passive devices by linear models. Of course, nothing is ideal—and even passive components such as cables and connectors exhibit nonlinear behavior—so complex models are often needed. Fortunately, nonlinear models have been in development for some time, with those based on X-parameters or the Cardiff model gaining popu-

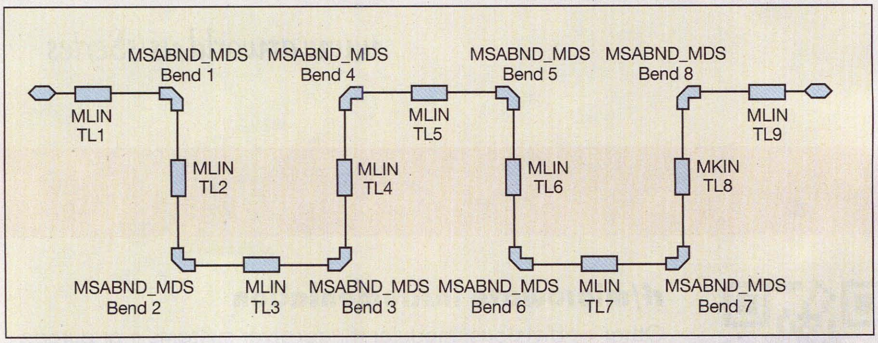

1. This is a schematic representation of a 500-mil-long, 50-Ω microstrip meander line.

larity among CAE users.

Modelling passive components and devices should be simpler than modelling active devices, since passive devices tend to be linear by nature and their behavior is typically independent of external factors, such as bias and RF drive level. For high-frequency design and modelling, passive components can be subdivided into discrete or lumped components [such as those formed of separate resistors (Rs), capacitors (Cs), and inductors (Ls)] and distributed components (such as those formed of microstrip transmission lines).

Lumped component models are generally available within most microwave CAE tools as either generic component libraries or as vendor libraries, based on specific commercial parts. Vendor models are often extracted from measurements. These component libraries also include models of standard building blocks for distributed components, such as microstrip and stripline elements. These distributed component models are typically closed-form types based on mathematical descriptions. They provide a useful starting point for a new design, but may be limited for some applications. Each of these distributed component models is calculated in isolation, without taking into account interactions (such as EM coupling) with other components in a circuit design. To illustrate this point, consider **Fig. 1** which shows a 0.5-in.-long 50-Ω microstrip meander line intended for fabrication on 10-mil-thick alumina substrate.

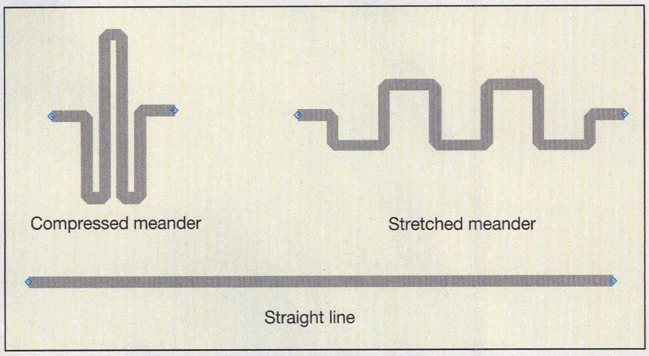

2. These three layouts represent alternative versions of the 500-mil-long, 50-Ω microstrip meander line.

In a schematic circuit simulation of **Fig. 1**, each of the microstrip components is modelled independently and cascaded with neighboring components through nodal connections defined in the schematic. Unintentional EM coupling between components, such as between TL2 and TL4, is not taken into account in the modelling process. Depending upon the aspect ratio of the meander line, this

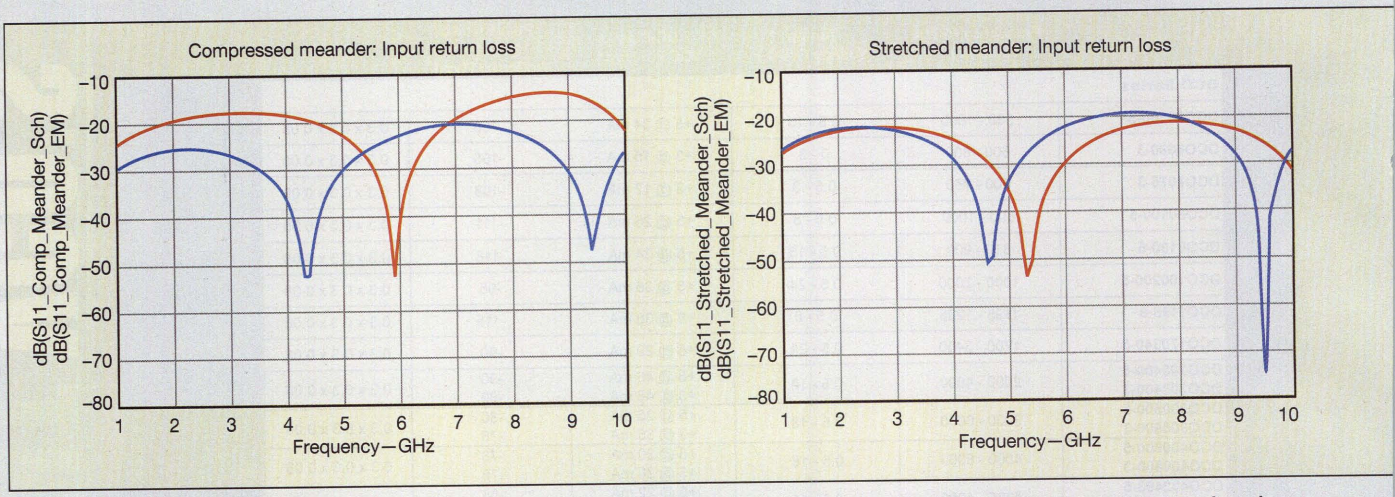

3. The results from schematic model representations and EM extracted models converge as unintentional EM coupling is reduced.

may or may not have a significant impact on the simulation accuracy.

Figure 2 shows three different layouts for a 0.5-in.-long 50-Ω microstrip line. Intuitively, it might be expected that the transmission line sections of the "compressed meander" design might result in the greatest unintentional EM coupling, leading to the largest discrepancy between a schematic simulation response and a measured or EM-simulated response. The simple "straight-line" design might be expected to most closely match the schematic simulation response to the measured or EM-simulated response.

Each of the three transmission-line variations has been simu-

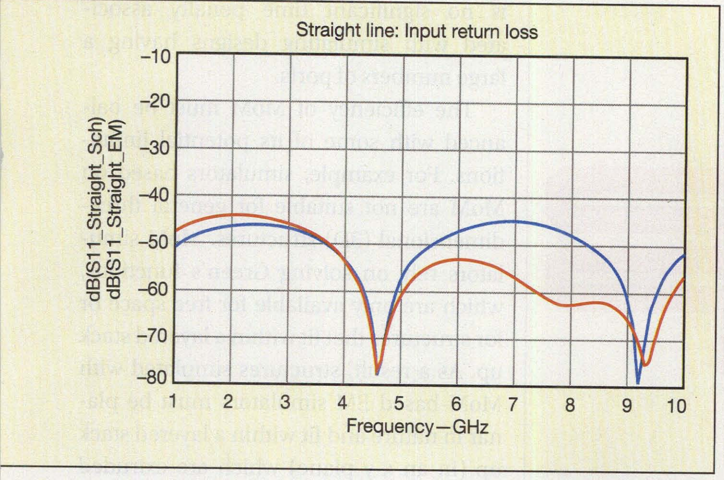

lated using schematic model representations and EM extracted models of the physical layout. **Figure 3** shows simulated S_{11} results and compares the schematic model response with the EM-extracted response. The results confirm that as the meander line is straightened and unintentional coupling is reduced, the responses of the two model types converge.

Although the meander line example is rather artificial, it does serve to illustrate that as interconnect densities on PCBs and ICs increase, the chances for unintentional EM coupling increase. Unless post-layout EM simulation is used to extract a model for interconnects in such cases, these unexpected problems may not be detected until the design has been fabricated and is tested.

EM simulators attempt to find solutions to Maxwell's equations for different circuit problems. A wide variety of commercial EM simulators has become available over the years, based largely on three key technologies: the aforementioned MoM, FEM, and FDTD methods. In general, these simulation methods use a similar approach to solving a particular problem.[1] They start with creating a physical model, which involves creating a layout geometry along with defining and assigning material properties to objects within the layout. The next step is to set up the EM simulator, which usually involves defining the extents of the simulation and the boundary conditions, as well as assignment of ports and specific simulation options.

Once the first two steps have been completed, the EM simulation can be performed; this involves transforming the physical model into discrete elements by means of mesh cells. The electric field/current across the mesh cells is then approximated using a local function, often referred to as an expansion or basis function. The function coefficients are then adjusted until the boundary conditions of the simulation are satisfied. The step after this involves post-processing, in which information about the design, including S-parameters and far-field radiation patterns, can be calculated. This process is similar for simulators based on MoM, FEM, and FDTD approaches, although differences among those technologies make each one best suited for particular applications.

Solvers based on the MoM simulation method are often referred to as "three-dimensional planar" (3D planar) solvers. This approach is one of the most difficult to implement EM simulation methods because it requires the careful evaluation of Green's functions and coupling integrals.[2]

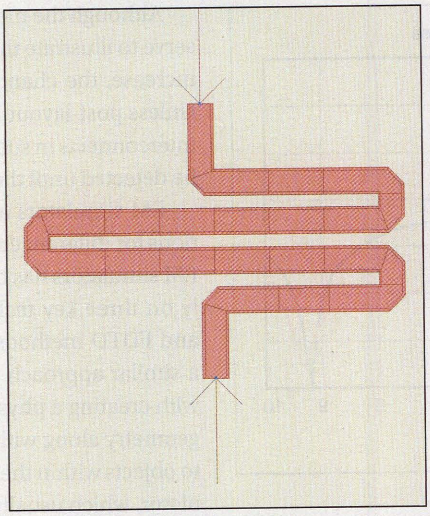

4. This is a typical conformal mesh for MoM simulations, where mesh cells are only applied at metal interconnects.

The key practical advantage of the MoM technique is that it is only necessary to discretize (mesh) the metal interconnects in the structure being simulated due to the fact that the current distribution on the metal surfaces emerge as the core unknowns. This is in contrast to other techniques which typically have the electric/magnetic fields (present everywhere in the solution space) as the core unknowns. The direct consequence of this is that a "planar" MoM mesh is simpler and smaller than the equivalent "3D volume" mesh required for an FEM or FDTD simulation. An efficient MoM mesh will be conformal (mesh cells are only created on the metal interconnects) and will typically consist of rectangles, triangles, and quadrilateral-shaped mesh cells **(Fig. 4)**.

A reduced number of mesh cells leads to fewer unknowns and an extremely efficient simulation. This makes MoM well suited for the analysis of complex (layered) structures. Another benefit of the MoM technique is that only one matrix solution is required for all port excitations; in other words, there is no significant time penalty associated with simulating designs having a large numbers of ports.

The efficiency of MoM must be balanced with some of its potential limitations. For example, simulators based on MoM are not suitable for general three-dimensional (3D) structures. MoM simulators rely on solving Green's functions, which are only available for free space or for structures that fit within a layered stack up. As a result, structures simulated with MoM-based EM simulators must be planar in nature and fit within a layered stack up (in an x-y plane) which are extruded vertically (along the z-axis) through the layered stack up. This is not a significant limitation in many cases since many RF/microwave designs are planar in nature. Even a multilayer PCB or monolithic-microwave-integrated-circuit (MMIC) structure can be considered planar when interconnects between dielectric and metal layers are considered as two-dimensional (2D) objects or cross sections extruded vertically through the substrate layers.

An example of an MoM-based analysis is the extraction of a multiport S-parameter model for the interconnections of a high-frequency PCB. **Figure 5** shows a relatively simple PCB layout that can be characterized by means of MoM. The resulting S-parameter model for that layout, when combined with the models that represent the discrete components used in the circuit, enables a simulation of the complete PCB.[3]

For analyzing arbitrarily shaped 3D structures, the FEM simu-

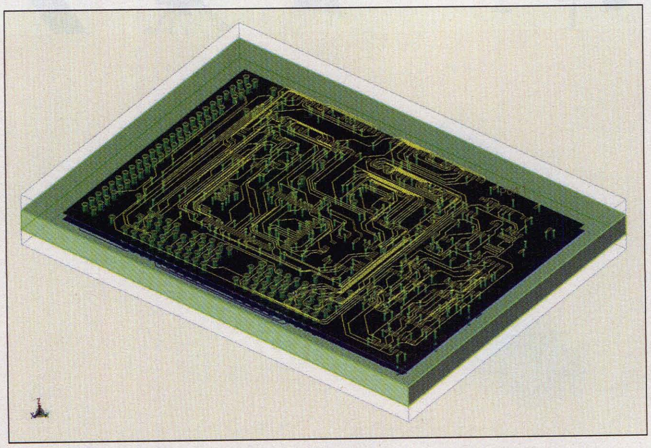

5. PCB layouts can typically be analyzed quite effectively by means of MoM simulation.

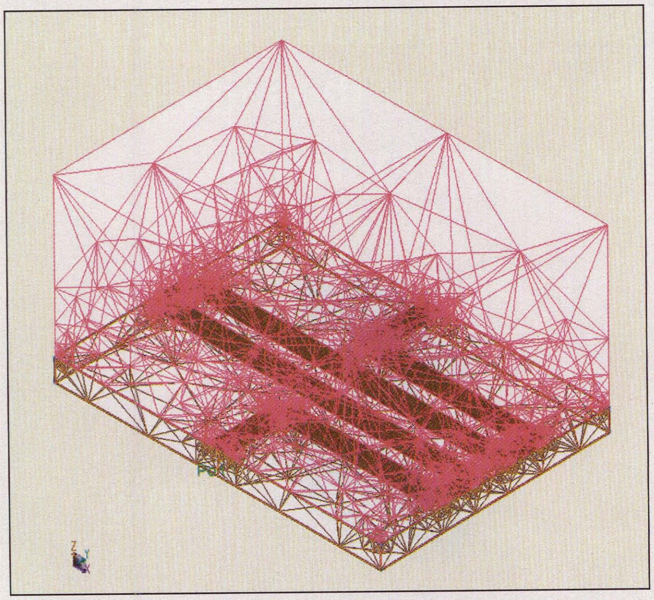

6. This is a typical tetrahedral mesh used in FEM-based EM simulations.

lation method is a true 3D field solver with an advantage over MoM simulators: it can be used for any type of 3D structure and is not confined to a layered stack up. FEM simulation requires that objects being simulated are placed into a "box" which truncates space and defines the simulation domain. The entire volume of the simulation domain is converted into discrete elements, usually tetrahedral mesh cells with a denser mesh being created around the geometric model being simulated (**Fig. 6**).

In an FEM analysis, the core unknown is usually a field quantity. The field is approximated over each tetrahedron as a sum of known expansion functions with unknown coefficients. The resulting sparse matrix is solved to determine the expansion function coefficients. As with an MoM simulator, only one matrix solving procedure is required for all port excitations in an FEM analysis. There is no time penalty associated with FEM when simulating designs requiring a large numbers of ports.

An application well suited to FEM analysis is the characterization of the parasitic circuit elements associated with packaging for RF/microwave ICs. **Figure 7** shows how an FEM-based EM simulator could be used to characterize the interconnect path from the PCB launch point to the bond pads on the MMIC within a QFN surface-mount package. The model extracted for the package and its interconnections could then be combined with a model for the MMIC to assess the impact of the packaging on the MMIC's performance. FEM may be the most flexible EM analysis method, but for geometrically complex and/or electrically large structures, the mesh can become very complex with many tetrahedral mesh cells. This results in large mathematical matrices, and a need for massive computer processing power.

Like FEM, the FDTD simulation method is a true 3D field solver which can analyze arbitrary shaped 3D structures. In contrast to MoM and FEM algorithms, which solve Maxwell's equations implicitly by solving for a matrix, FDTD algorithms solve Maxwell's equations in a fully explicit way. For an FDTD analysis, simulated objects are placed within a "box" with defined borders, to truncate the analysis space and define the simulation domain. The volume of the simulation domain is filled by means of discrete elements, usually hexahedral mesh cells, also known as "Yee" cells (**Fig. 8**).[4] FDTD employs a time-stepping algorithm which updates the field values across the mesh cell time-step by time-step, thereby explicitly following the EM waves as they propagate through the structure.

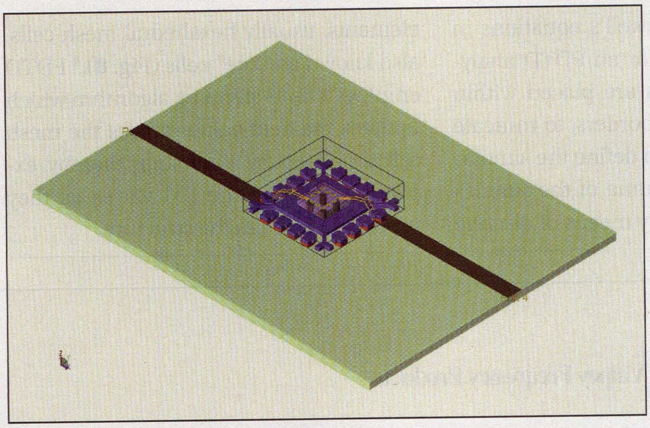

7. This is a typical tetrahedral mesh used in FEM simulations.

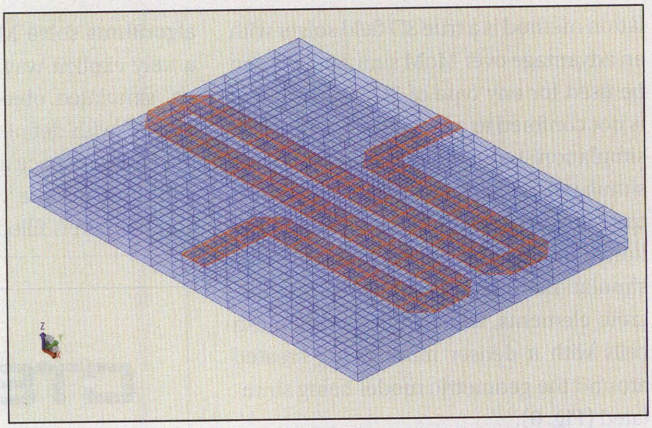

8. This is a typical hexahedral mesh used in FDTD simulations.

One significant benefit of the FDTD technique over the FEM method is that the former does not require a matrix solution, meaning that very large problems can often be addressed by using surprisingly small amounts of computer memory and processing power. FDTD also lends itself extremely well to parallelization, allowing modern multicore processors and graphical processing units (GPUs) to be leveraged to accelerate simulations. On the negative side, a single FDTD simulation must be run for each port placed onto simulation geometry. Since an N-port design requires N simulation runs, FDTD-based EM simulators are not ideal for analyzing designs with high port counts.

A typical application well suited to FDTD analysis is the characterization of an antenna embedded within a mobile telephone **(Fig. 9)**. The antenna(s) can become detuned when embedded in a handset or when the handset is in close proximity to the human body. Early evaluation of these effects and the assessment of additional legal requirements—such Specific Absorption Ratio (SAR) and Hearing Aid Compatibility (HAC)—is extremely useful.

When comparing EM simulators based on MoM, FEM, and FDTD analysis methods for applications, the first consideration is whether the geometry of the design to be simulated is planar or 3D. MoM-based simulators offer the most efficient simulation method for truly planar structures. For that reason, an MoM-based simulator would be recommended for analysis of PCB interconnects, on-chip passive elements and components, on-chip interconnects, and planar antennas. Either FEM- or FDTD-based EM simulators are usually more appropriate for true 3D structures, such as transitions (coaxial-to-waveguide and others), connectors, packages, cavities, waveguide, and 3D antenna structures.

9. The embedded antenna in a mobile phone can be evaluated by means of an FDTD-based EM simulation.

Another important consideration when selecting an EM simulator is the circuit response type. Both MoM- and FEM-based EM simulators solve natively in the frequency domain, which makes them more appropriate than FDTD for the analysis of circuits with high quality factor (high Q), such as filters, cavities, resonators, and oscillators. In contrast, FDTD-based EM simulators solve natively in the time domain, making them useful for time-domain-reflectometry (TDR) analysis on connector interfaces and transitions. TDR techniques are typically practiced more often in the high-speed digital domain than in RF/microwave circuit analysis.

Finally, if a structure to be simulated is truly 3D in nature, then the complexity of the structure and the problem size (the size of the mesh and the number of ports) must be taken into account when deciding whether an FEM- or FDTD-based EM simulator is more appropriate for the analysis. FEM-based EM simulators provide the most efficient solution to problems with large numbers of ports, such as IC packages and multichip modules (MCMs). For a structure that has a small number of ports but is electrically large, an FDTD-based simulator provides the most memory-efficient simulations. Applications well suited to FDTD-based simulations include analysis of antenna placement on vehicles, in addition to analysis of antenna performance in the presence of detailed human-body models. MWRF

REFERENCES

1. D.G. Swanson, Jr. and W.J.R. Hoefer, Microwave Circuit Modelling Using Electromagnetic Field Simulation, Artech House, Norwood, MA, 2009.
2. J. Van Hese, J. Sercu, D. Pissoort, and H-S. Lee, "State of the Art in EM Software for Microwave Engineers," Agilent Technologies, Application Note 5990-3225EN, February 2009.
3. D.J. Morris, "Virtual RF PCB Prototypes," Printed Circuit Design & Fabrication, June 2006.
4. K.S. Yee, "Numerical Solution of Initial Boundary-Value Problems Involving Maxwell's Equations in Isotropic Media," IEEE Transactions on Antennas and Propagation, Vol. AP-14, No. 5, 1996, pp. 302-307.

CHANG-FU-CHEN
Master

XIAO-JIAN TIAN
Professor
*Corresponding author

TANG-YANG
Doctor

College of Electronic Science and Engineering, Jilin University, Changchun, People's Republic of China; e-mail (Tang Yang): tangyang0816@163.com.

Two-Horn Antenna Aims At UWB Use

This compact antenna design features a simple, easy-to-manufacture structure with coplanar-waveguide feed that can achieve high peak gain from 3.0 to 13.9 GHz.

ULTRAWIDEBAND (UWB) communications from 3.1 to 10.6 GHz, the band made unlicensed by the United States Federal Communications Commission (FCC), is attractive for a wide range of commercial applications.[1] In support of UWB communications systems, antennas are an essential component. These antennas should provide high gain, wide-impedance bandwidths, and omnidirectional radiation patterns to make them suitable for UWB communications applications. Fortunately, all of these characteristics can be realized through the use of a coplanar-waveguide (CPW) feed and printed planar monopole structures.[2-5]

Some of these UWB antennas can achieve one of these properties by changing ground structures,[6,7] while others can gain the necessary properties and performance by changing the shape of their radiators.[8,9] The authors developed a two-horn planar monopole antenna structure for UWB applications which relies on a CPW feed. Computer simulations and measured results agree closely and indicate that the proposed two-horn antenna structure can achieve approximately omnidirectional radiation patterns at 5, 6, 7, 8, and 9 GHz, with high peak gain across the full bandwidth. The proposed antenna design provides an impedance bandwidth of about 10.9 GHz, from 3.0 to 13.9 GHz, with VSWR over that range of less than 2.0:1.

Figure 1 shows the geometry of the proposed two-horn antenna, which was fabricated on FR-4 circuit-board material with relative dielectric constant, ε_r, of 4.4 and dielectric loss tangent of 0.0018. The size of the proposed antenna is 34 x 26 x 1 mm. The antenna consists of two rectangular ground planes with a horn-shaped slot, while the feed line is designed by using a rectangular patch to connect with the horn-shaped patch as the main radiator.

The optimized dimensions of the two-horn antenna are: W1 = 26 mm, W2 = 18 mm, W3 = 10.6 mm, W4 = 6 mm, W5 = 8 mm, W6 = W8 = 11.3 mm, W7 = 2.8, L1 = 34 mm, L2 = 13 mm, L3 = 15 mm, L4 = 10 mm, and L5 = 11 mm. **Figure 2** shows a prototype of the proposed antenna, fabricated by hand according to these parameters.

The fabricated antenna was evaluated by means of measurements, as well as by using the commercial High-Frequency

(continued on p. 73)

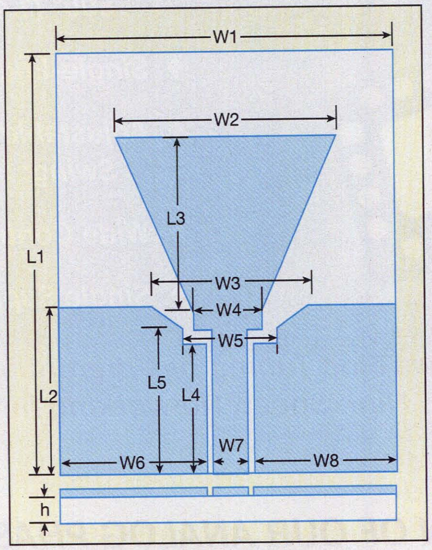

1. This is the basic geometry of the two-horn antenna for UWB communications applications from 3.0 to 13.9 GHz.

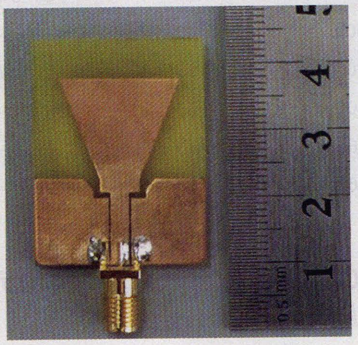

2. This photograph shows the prototype two-horn antenna fabricated on low-cost FR-4 circuit-board material.

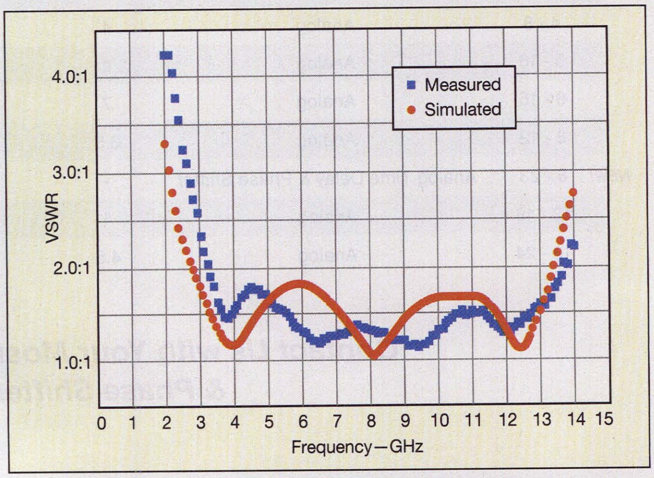

3. These plots show the measured and computer-simulated impedance bandwidths for the two-horn antenna design.

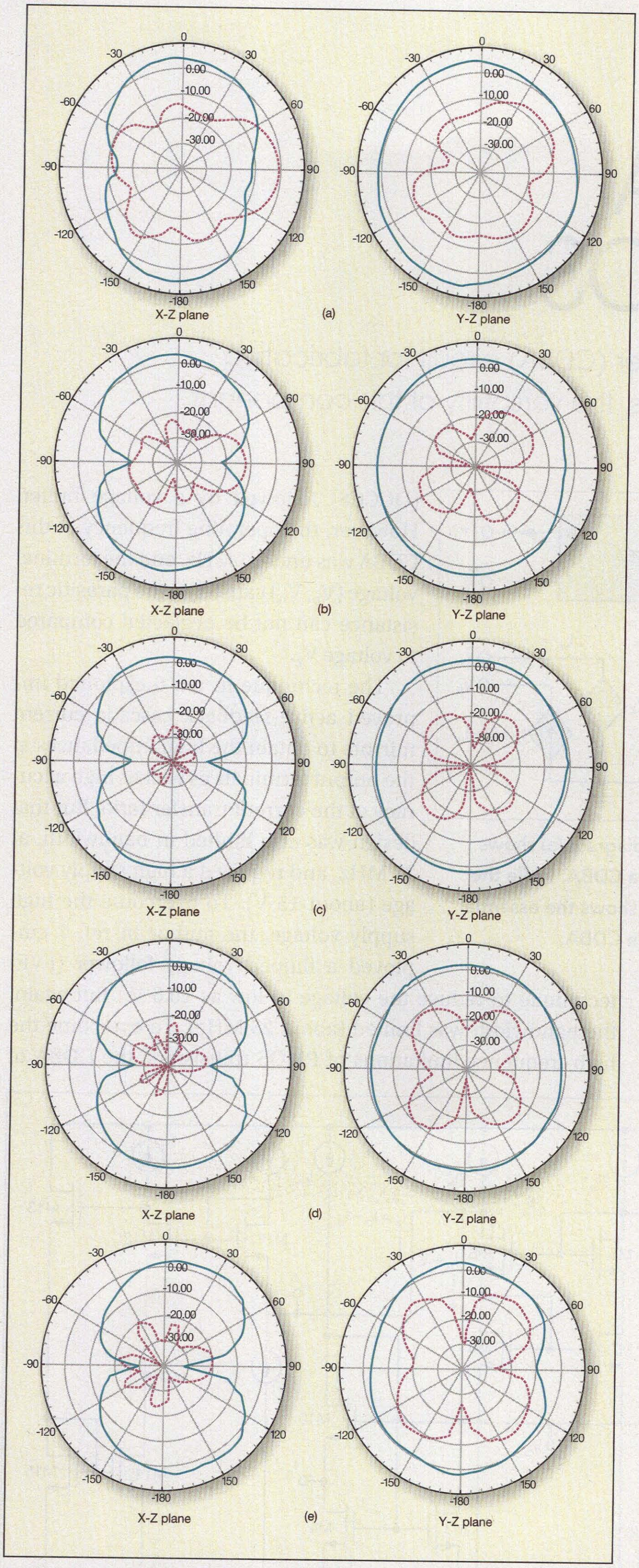

4. **These radiation plots show the far-field patterns for the two-horn antenna design at (a) 5 GHz, (b) 6 GHz, (c) 7 GHz, (d) 8 GHz, and (e) 9 GHz.**

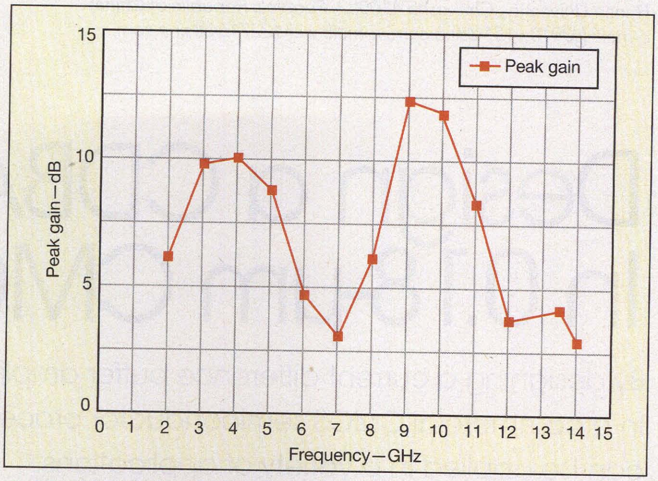

5. **This plot shows the peak gain of the two-horn antenna design as a function of frequency through 15 GHz.**

Structure Simulator (HFSS) electromagnetic (EM) simulation software from Ansoft Corp. (www.ansoft.com). Measurements were performed with a model 37269C microwave vector network analyzer (VNA) from Anritsu Co. (www.us.anritsu.com).

Figure 3 shows that the measured impedance bandwidth, which reached 10.9 GHz, is matched with the simulated results across a frequency range from 3.0 to 13.9 GHz (for a VSWR of less than 2.0:1). **Figures 4(a) through 4(e)** show the antenna's far-field radiation patterns at 5, 6, 7, 8, and 9 GHz, respectively.

These results demonstrate that the co-polar and cross-polar radiation patterns in the X-Z (ϕ = 0 deg.) and Y-Z (ϕ = 90 deg.) planes are consistent with the properties required for omnidirectional radiation patterns. Finally, **Figure 5** shows that the two-horn antenna achieves peak gains ranging from 2.8 to 12.5 dB, with gains across the entire impedance bandwidth always more than 2 dB. MWRF

REFERENCES

1. H. Schantz, The Art and Science of Ultrawideband Antennas, Artech House, Norwood, MA, 2005.
2. M. Ojaroudi, H. Ebrahimian, Ch. Ghobadi, and J. Nourinia, "Small microstrip-fed printed monopole antenna for UWB application," Microwave and Optical Technology Letters, Vol. 52, 2010, pp. 1756-1771.
3. Xu-Bao Sun and Mao-Yong Cao, "Wideband CPW-fed elliptical monopole antenna," Microwave and Optical Technology Letters, Vol. 52, 2010, pp. 1774-1776.
4. M.M. Sharma and V. Shrivastava, "Printed fractal elliptical monopole antenna for UWB applications," Proceedings of the International Conference on Microwaves, 2008, pp. 374-376.
5. A.A. Eldek, "Numerical Analysis of a Small Ultrawideband Microstrip-Fed Tap Monopole Antenna," Progress In Electromagnetic Resonators (PIER), Vol. 66, 2006, pp. 199-212.
6. Y.-B. Yang, F.-S. Zhang, F. Zhang, L. Zhang et al., "A Novel Compact CPW-Fed Planar Monopole Antenna with Modified Stair-Style Ground for Ultrawideband Applications," Microwave Optical Technology Letters, Vol. 52, 2010, pp. 2100-2104.
7. Shou-Tao Fan, Ying-Zeng Yin, Le Kang, Shi-Ju Wei, Yao- Zhao Wang, and Kun Song, "Bandwidth Enhancement of a Coplanar Waveguide-Fed Asymmetrical Slot Antenna with a Rectangular Patch," Microwave & Optical Technology Letters, Vol. 52, 2010, pp. 2259- 2261.
8. J. Liang, C.C. Chiau, X.D. Chen, and C.G. Parini, "Study of a Printed Circular Disc Monopole Antenna for UWB Systems, IEEE Transactions on Antennas & Propagation, Vol. 53, 2005, pp. 3500-3504.
9. Abdo Abdel Monem Shaalan and M.I. Ramadan, "Design of a Compact Hexagonal Monopole Antenna for Ultrawideband Applications," Journal of Infrared, Millimeter, & Terahertz Waves, Vol. 31, 2010, pp. 958-968.

JINJIANG LIU
Master's Degree Candidate

CHUNHUA WANG
Professor, Doctoral Supervisor

XIAODONG CAO
Student

JUN XU
Student

College of Information Science and Engineering, Hunan University, Changsha 410082, People's Republic of China; e-mail: ljj0910w131@sina.com, e-mail: wch1227164@sina.com.

Design a CDBA In 0.18-µm CMOS

By designing a current difference buffer amplifier (CDBA) circuit for fabrication in a commercial CMOS semiconductor process, the versatility of this component can be applied in a variety of applications.

CURRENT-MODE SIGNAL-PROCESSING techniques offer some advantages compared to voltage-mode techniques. Some of these advantages include increased linearity, simpler circuits, wider bandwidth, lower power consumption, and simple implementation of basic signal operations, such as addition and subtraction.[1] As a result, numerous active elements have been developed for current-mode use,[2,3] such as a current conveyor, current operational amplifiers (COAs), operational transconductance amplifiers (OTRAs), and current differencing buffered amplifiers (CDBAs).

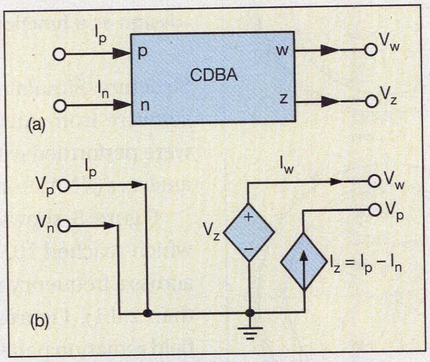

1. This simple block diagram (a) shows the basic concept of a CDBA, while the equivalent circuit (b) shows the essential circuit elements in the CDBA.

A CDBA can be constructed in a number of ways, provided that the current-mode components have been introduced. The benefits of using a CDBA in a signal-processing application include its high slew rate, freedom from parasitic capacitance, wide bandwidth, and relatively simple implementation. For example, the circuit in ref. 3 employed two commercial current-feedback amplifiers (CFAs), such as the model AD844 from Analog Devices (www.analog.com), where the CFAs functioned as second-generation current conveyors and voltage buffers.

In this CDBA design, however, the CDBA characteristics were dominated by the CFA properties. In ref. 4, a design approach included bipolar-junction-transistor (BJT) technology, based on a current subtractor and voltage buffer amplifier. In ref. 5, the circuit was designed for implementation in silicon CMOS technology with the CDBA consisting of a differential current-controlled current source (DCCCS) followed by a voltage buffer. However, the operating frequency of this CDBA was under 1 MHz, and the terminal voltage (V_p, V_n) caused by the parasitic resistance can not be neglected compared to voltage V_z.

The technique in ref. 6 exploited improved active-feedback cascade current mirrors to obtain the high impedances at the output terminals as well as high accuracy of the current transfer ratio. But that design was also limited in bandwidth, at 37 MHz, and required a high supply voltage (about ±5 V). To overcome the high supply voltage, the author in ref. 7 employed a flipped voltage follower (FVF) technique to reduce the voltage as low as ±0.6 V. But again, the bandwidth was limited (about 25 MHz). To overcome the high-frequency limitations of PMOS transistors, the CDBA of

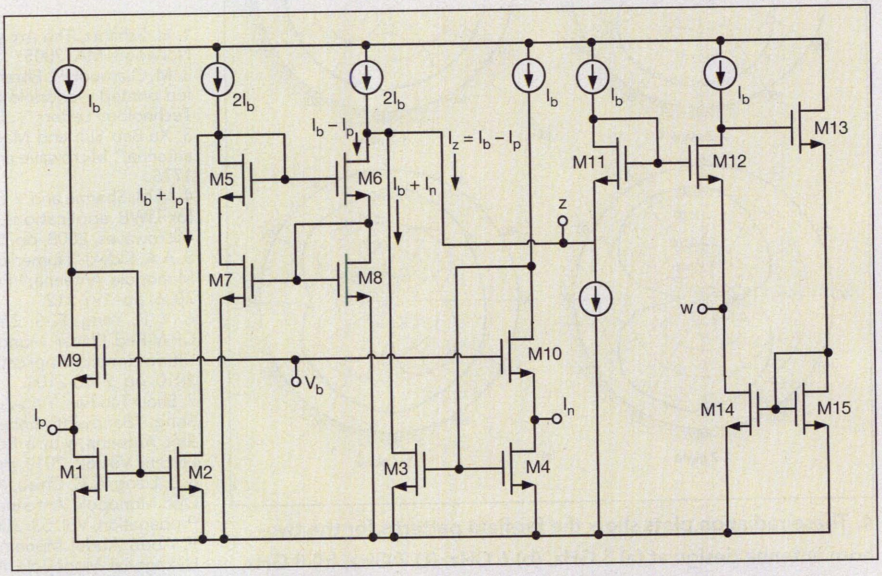

2. This schematic diagram details the key circuit elements in the CDBA.

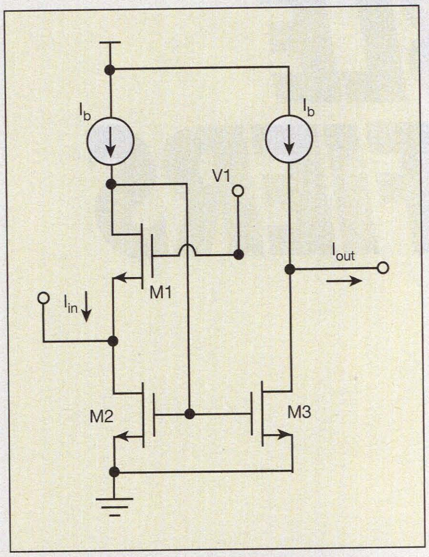

3. This circuit shows the low-voltage current mirrors in an FVFCS.

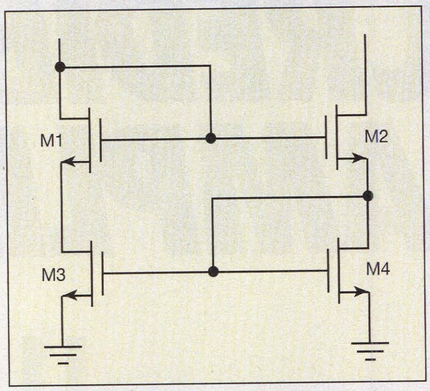

4. This is an improved version of the Wilson mirror.

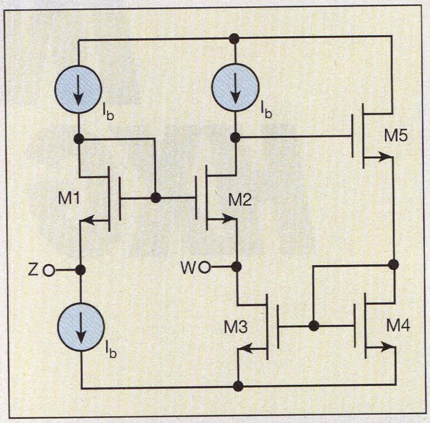

5. The output stage of the proposed CDBA is based on a voltage follower formed by a basic mirror and a Wilson mirror.

ref. 8 was designed such that the signal has an all NMOS signal path, and this design achieved a 3-dB bandwidth as wide as 500 MHz. This CDBA circuit also enjoys good voltage and current gain accuracies, and low resistance at both the current-input terminals (p, n) and the output-voltage terminal (w). Still, it suffers from high power consumption.

The current report focuses on designing a high-performance CDBA using all NMOS mirrors, with a current subtraction circuit and a voltage follower, and using only a few transistors. The current subtraction circuit exploits a low-voltage current mirror followed by an improved Wilson mirror to decrease the supply voltage and increase the bandwidth, respectively.

Compared with other design work, this proposed CDBA offers a wider dynamic range and lower resistance at both current input (p and n) terminals. It also operates with lower supply voltage and power consumption than the designs of refs. 5, 6, and 8.

Figure 1(a) shows the proposed CDBA circuit, where p and n are input terminals and w and z are output terminals. It is equivalent to the circuit of **Fig. 1(b)**, which uses dependent current and voltage sources. The current and voltage characteristics of the CDBA can be described by Eq. 1:

$$\begin{pmatrix} i_z \\ v_w \\ v_p \\ v_n \end{pmatrix} = \begin{pmatrix} 0 & 0 & 1 & -1 \\ 1 & 0 & 0 & 0 \\ 0 & 0 & 0 & 0 \\ 1 & 0 & 0 & 0 \end{pmatrix} \begin{pmatrix} v_z \\ i_w \\ i_p \\ i_n \end{pmatrix} \quad (1)$$

According to this matrix and the equivalent circuit of **Fig. 1(b)**, a CDBA can be considered as a transimpedance amplifier (TIA) that converts the difference of the input currents I_p and I_n at terminals p and n, and hence V_z is named as the current output, respectively; the voltage of the w terminal follows the voltage of the z terminal. The input terminals, through which I_p and I_n flow, are internally grounded. Finally, it can be further inferred that the terminal impedances of the p and n terminals must be very low. A CDBA of this design can be implemented with bipolar and CMOS technologies.

Figure 2 provides a schematic diagram of the proposed CDBA circuit. It employs all NMOS mirrors, and also contains the current subtraction circuit and the voltage follower. The current subtraction circuit provides the difference currents I_p and I_n, which flow into the current subtraction circuit through its low-impedance inputs (p, n) and lead away from the high-impedance terminal z. The z terminal is internally connected to the input of the voltage follower. The voltage, induced on an external impedance, connected with the z terminal, is copied to the low-impedance w terminal of the follower output.

The current subtraction circuit is formed by transistors M1 through M10. The circuit exploits the flipped voltage follower current sensor (FVFCS). The FVFCS has been used in the past for different applications, including as part of a power amplifier. For example, the first and simplest use of the FVFCS is as the input stage of

Table 1: Performance of the proposed CDBA.

Parameter	Simulation results
Supply voltage (V)	±0.8
Bias voltage, (V_{bl})	0.45
Power dissipation (mW) Static (@ $i_n = i_p = \mu A$) (mW) Max ($i_n = i_p = 30\mu A$) (mW)	 0.43 0.48
Offset current on terminal-z (μA)	0.23
Current transfer ratio, $\alpha = I_z/(I_p - I_n)$	1.02
Current transfer BW (MHz)	376
Voltage transfer ratio, $\beta_v = V_w/V_z$	0.988
Voltage transfer BW (MHz)	726
Terminal-p resistance (Ω)	12
Terminal-n resistance (Ω)	12
Terminal-z resistance (kΩ)	276
Terminal-w resistance (Ω)	46

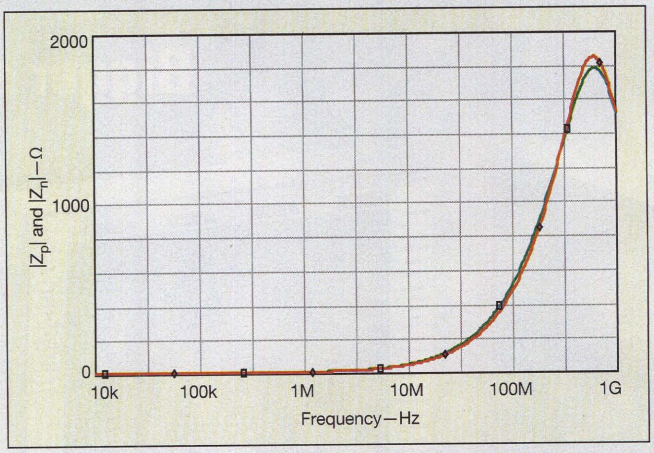

6. The input impedance remains fairly constant over a broad frequency range.

a low-voltage current mirror.[9-14] High-performance current mirrors with low input and output voltage requirements are needed as building blocks in mixed-mode very-large-scale-integration (VLSI) systems that operate from a single supply of 1.5 V or less. High accuracy requires very high output resistance and low input resistance.

The basic implementation of a FVFCS is given in **Fig. 3**, which has the lowest input resistance—as well as the lowest input voltage requirements—reported to date. The input voltage required for such current mirror is in the order of V_{ds}, which can be as small as 0.1 V, which is much smaller than the gate-source voltage (V_{gs}) drop required for a conventional low-voltage current mirror.

The input impedance is very low, on the order of 10 to 50 Ω, and can be expressed by Eq. 2:

$$r_{in} = 1/(g_{m1}g_{m2}r_{ol}) \quad (2)$$

The minimum voltage supply for the FVFCS can be found by Eq. 3:

$$V_{DDmin} = |V_{TN} + 2V_{DS} \quad (3)$$

From this, it can be seen that the mirror in **Fig. 3** operates with a low voltage supply and low power consumption.

A high-performance current mirror also requires high output resistance and low voltage requirements at the output stage. A simple approach for realizing the output stage is by means of a simple or cascade current source. Normally, two of the low-voltage current mirror circuits can be used to accept input currents I_p and I_n. Then, the differential current between I_p and I_n can be achieved by the use of an improved Wilson mirror, constituted by NMOS transistors **(Fig. 4)**.

More specifically, it is well known that a Wilson current mirror or an improved Wilson current mirror **(Fig. 4)** have better high-frequency behavior than a cascade current mirror without loss of the high-

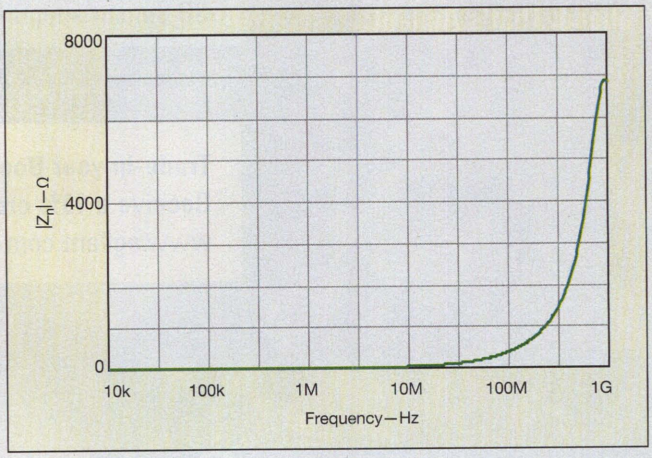

7. This plot shows the variations of the terminal w impedance with frequency.

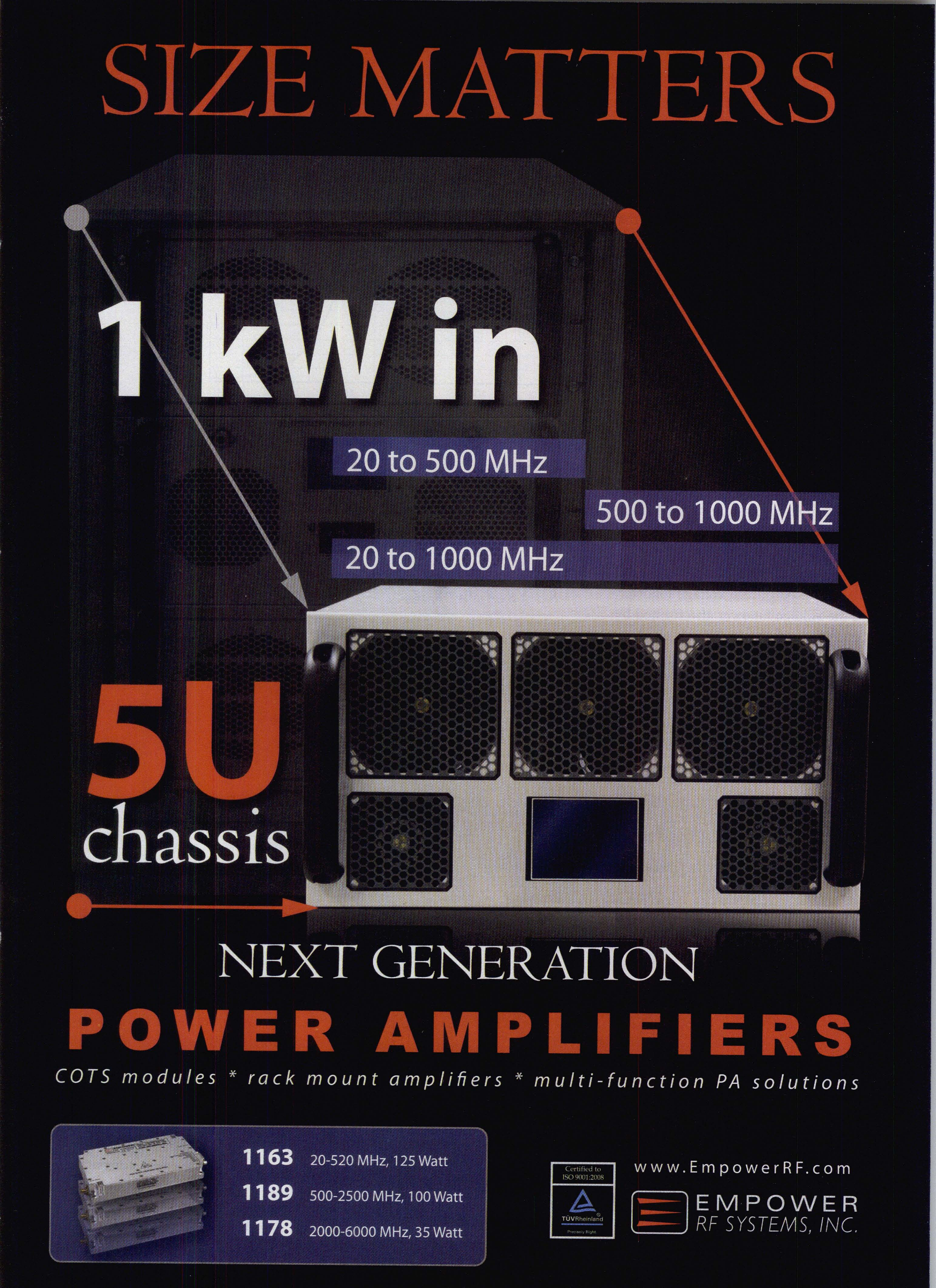
SIZE MATTERS
1 kW in
20 to 500 MHz
500 to 1000 MHz
20 to 1000 MHz
5U
chassis
NEXT GENERATION
POWER AMPLIFIERS
COTS modules * rack mount amplifiers * multi-function PA solutions
1163 20-520 MHz, 125 Watt
1189 500-2500 MHz, 100 Watt
1178 2000-6000 MHz, 35 Watt
Certified to ISO 9001:2008
TÜVRheinland
www.EmpowerRF.com
EMPOWER
RF SYSTEMS, INC.

output impedance and low static error features (having equal advantages with respect to the simple current mirror).[1] Moreover, the improved Wilson mirror also provides an increase in the output resistance, as shown by Eq. 4:

$$r_o = \frac{v_o}{i_o} = r_{ds2} + r_{ds4} + r_{ds2}r_{ds4}(g_{m2} + g_{mb2}) \qquad (4)$$

For this reason:

$g_{m2} \geq g_{mb2}$, $r_{ds2} + r_{ds4} \leq r_{ds2}\, r_{ds4}\, g_{m2}$

and:

$$r_o = r_{ds2}\, g_{m2}\, r_{ds4} \qquad (5)$$

Consequently, the output impedance of a Wilson mirror is more than just a simple mirror.

The output stage of the proposed CDBA is based on the voltage follower. And the voltage follower also formed by a basic mirror and a Wilson mirror **(Fig. 5)**. The impedance at mode w is very low and its voltage can be expressed by Eq. 6:

$$r_w = \left(\frac{1}{g_{m2}}\right)\left(\frac{g_{m5} + g_{m4}}{g_{m5}g_{m3}r_{ob} + g_{m5}g_{m4}}\right) \qquad (6)$$

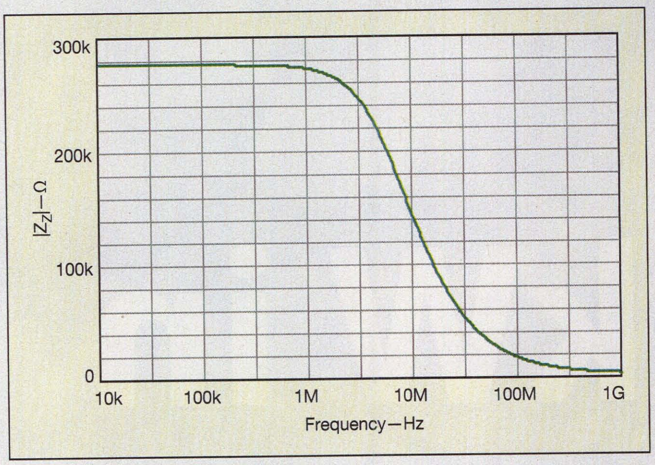

8. This plot shows the variations of the terminal z impedance with frequency.

with:

$$v_w = \beta_v v_z \qquad (7)$$

and:

$$\beta_v = \frac{g_{m1}r_{ob}}{1 + g_{m1}r_{ob}}\left(\frac{g_{m2}(1 + g_{m3}r_{ob}/2)}{g_w + g_{m2}(1 + g_{m3}r_{ob}/2)}\right) \qquad (8)$$

where R_w is the resistor connected to terminal w, if:

$g_{m1}r_{ob} \geq 1$

and:

$g_{m2}(1 + g_{m3}r_{ob}/2) \geq g_w$

then:

$v_w \approx v_z$.

The CDBA was designed for integrated-circuit (IC) fabrication in a CMOS process. It was simulated by PSPICE time-domain software based on a 0.18-μm CMOS process.

The aspect ratios of the current subtraction circuit elements (devices M1 through M10) are W/L = (30 μm)/(1 μm), and the voltage follower (devices M11 through M15) have an aspect ratio of W/L = (10 μm)/(1 μm). The supply voltages used are $+V_{DD} = -V_{SS} = 0.8$ V, and the constant bias current (I_b) of 30 μA was realized by employing basic current mirrors.

Figure 6 shows that the impedance of

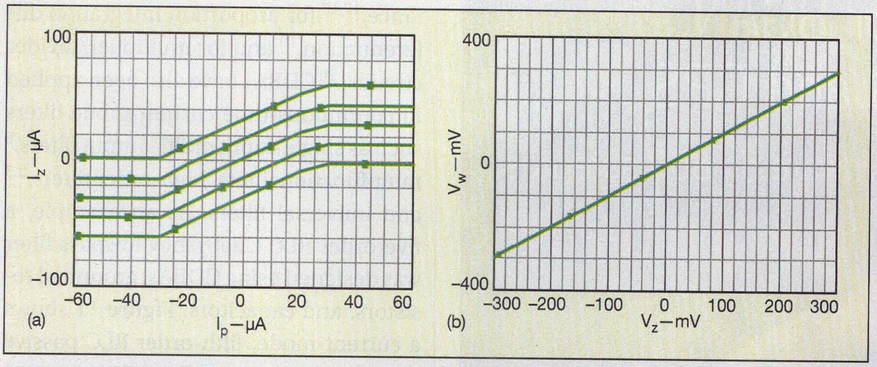

9. These are the DC transfer characteristics for the new CDBA, showing (a) current and (b) voltage.

terminals p and n are equal to 12 Ω for a wide frequency range. It can be seen from **Fig. 7** that terminal w has an impedance of 46 Ω. **Figure 8** shows the variation of z terminal impedance with frequency, which yields an impedance of 276 kΩ.

The device characteristics given in **Fig. 9** indicate that the CDBA circuit provides good performance and good potential for use in analog circuits. It has high linearity and accuracy over a wide dynamic range. As **Fig. 9(a)** shows, the maximum offset current on terminal z is equal to 0.23 μA. **Figure 9(b)** shows that the output voltage, V_w, follows voltage V_z. The power consumption for the CDBA circuit is 0.43 mW for $I_p = I_n = 0$ μA and 0.48 mW for $I_p = I_n = 30$ μA.

Figure 10 shows the CDBA's transfer characteristics. The current and voltage transfer ratios, α_p, α_n, and β_v, were found to be 1.020, 1.020, and 0.988, respectively. The 3-dB frequencies for I_z/I_p, I_z/I_n, and V_w/V_z are approximately 376, 376, and 726 MHz, respectively. **Table 1** summarizes the simulation results for the CDBA.

CDBA-based circuits offer excellent terminal characteristics and high common-mode rejection ratios for a variety of applications, including in oscillators,[16] integrators,[1] to simulate active induc-

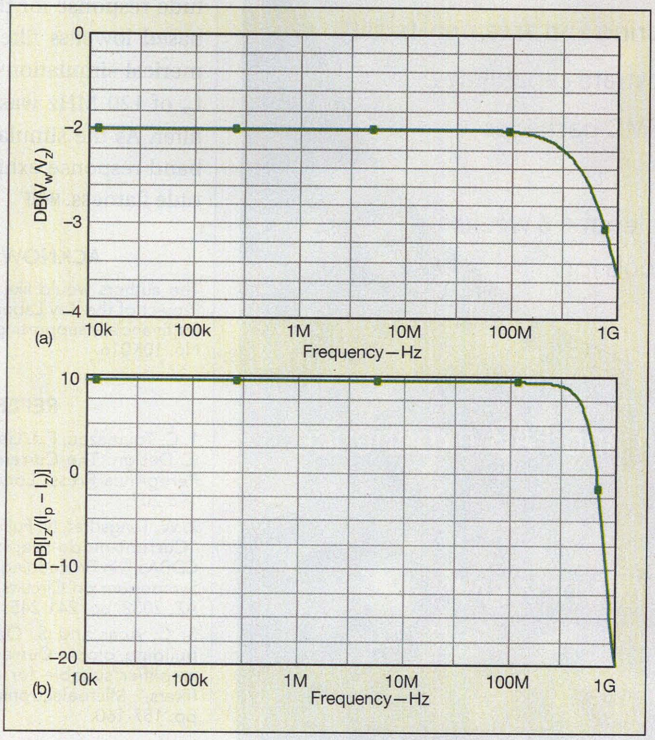

10. These are the AC transfer characteristics of the new CDBA, showing (a) the frequency response of the current transfer ratio and (b) the frequency response of the voltage transfer ratio.

tance,[17,18] for proportion integration differentiation,[19] and for multiplier/divider circuits.[20] CDBAs have also been applied in continuous-time current-mode filters such as single-input multi-output filters,[6] multifunction filters, high-order filters,[2,3] and universal filters. As an example, a five-order RLC Chebyshev lowpass filter was designed using CDBAs, grounded resistors, and capacitors. **Figure 11** shows a current-mode, fifth-order RLC passive ladder prototype, and a CDBA-based normalized filter.

The fifth-order current transfer function can be expressed by Eq. 9:

$$T(s) = \frac{I_{out}(s)}{I_{in}(s)} = \frac{a_0}{s^5 + b_4 s^4 + b_3 s^3 + b_2 s^2 + b_0} \quad (9)$$

where:

I_{in} = the input current and
I_{out} = the output current.

The numerator is a polynomial with positive and negative real coefficients. In this filter, $V_{DD} = V_{SS} = \pm 0.8$ V; resistors $R_S = R_L = R = 500\ \Omega$; and capacitors $C_1 = C_5 = 2.48$ pF and $C_2 = C_3 = C_4 = 1.22$ pF. **Figure 12** shows the simulated amplitude response for the fifth-order CDBA-based lowpass filter. Based on the numerical simulations, a cutoff frequency, f_c, of 120 MHz was determined for this filter. As the simulations show, its passband response exhibits excellent amplitude flatness. MWRF

ACKNOWLEDGMENT

The authors would like to thank the Open Fund Project of the Key Laboratory at Hunan University for financially supporting this research under grant No. 10K016.

REFERENCES

1. C. Toumazou, F.J. Lidjey, and D. Haigh, Analog IC Design: The Current-Mode Approach, Peter Peregrinus Press, London, England, 1990, pp. 195-207.
2. W. Tangsrirat, N. Fujii, and W. Surakampontorn, "Current-mode leapfrog ladder filters using CDBAs," in Proceedings of the IEEE International Symposium on Circuits and Systems, Scottsdale, AZ, 2002, pp. 241-245.
3. C. Acar and S. Ozuguz, "A new versatile building block: Current differencing buffered amplifier suitable for analog signal processing filters," Microelectronics Journal, Vol. 30, 1999, pp. 157-160.

Table 2: Comparing the performance levels of different CDBAs.

Parameter	Ref. 6	Ref. 7	Ref. 8	This work
Supply voltage	±5 V	±0.6 V	±1.25 V	±0.8 V
Power dissipation	NA	0.565 mW	1.15 mW	0.48 mW
Transistor count	45	18	28	15
Current offset	NA	0.05 µA	0.49 µA	0.23 µA
Terminal-p resistance	645 Ω	56.4 Ω	14 Ω	12 Ω
Terminal-n resistance	645 Ω	56.4 Ω	14 Ω	12 Ω
Terminal-z resistance	678 Ω	157 kΩ	290 kΩ	276 kΩ
Terminal-w resistance	49 Ω	270 Ω	14 Ω	46 Ω
Voltage gain	0.99	0.98	0.99	1.02
Current gain	0.99	0.98	0.99	0.99
Current transfer BW	70 MHz	25 MHz	NA	376 MHz
Voltage transfer BW	37 MHz	474 MHz	500 MHz	726 MHz

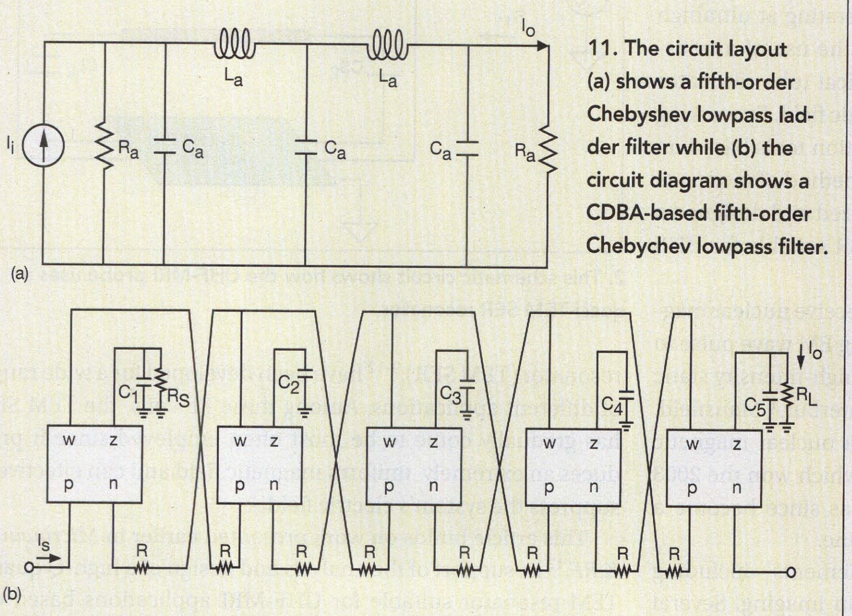

11. The circuit layout (a) shows a fifth-order Chebyshev lowpass ladder filter while (b) the circuit diagram shows a CDBA-based fifth-order Chebychev lowpass filter.

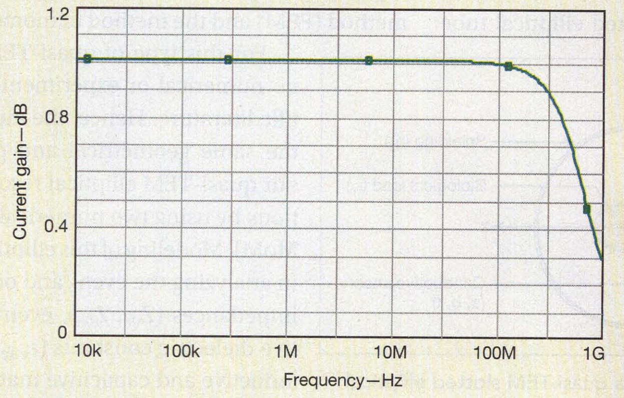

12. This curve shows the broad frequency range of the CDBA-based lowpass filter.

4. W. Tangsrirat, N. Fujii, and W. Surakampontorn, "Current-mode leapfrog ladder filters using CDBAs," in Proceedings of the IEEE International Symposium on Circuits and Systems, Scottsdale, AZ, 2002, pp. 241-245.

5. S. Ozoguz, A. Toker, and C. Acar, "Current-mode continuous-time fully-integrated universal filter using CDBAs," Electronics Letters, Vol.35, 1999, pp. 97-98.

6. Nil Tarim and Hakan Kuntmana, "A High Performance Current Differencing Buffered Amplifier," 13th International Conference on Microelectronics, Rabat, Morocco, October 29-31, 2001.

7. Cem Cakir, Shahram Minaei, and Oguzhan Cicekoglu, "Low voltage low power CMOS current differencing buffered amplifier," Analog Integrated Circuits and Signal Processing, Vol. 62, 2010, pp. 237–244.

8. Teerasilapa Dumawipata, Worapong Tangsrirat, and Wanlop Surakampontorn, "Low-voltage NMOS-based current differencing buffered amplifier and its application to current-mode ladder filter design," International Journal of Electronics, Vol. 93, No. 11, November 2007, pp. 777-791.

9. V. Peluso, M. Steyaert, and W. Sansen, Design of Low-Voltage Low-Power Sigma-Delta A/D Converters, Kluwer, Boston, MA, 1999, Chapter 4.

10. J.F. Riins, 54-MHz switched capacitor video channel equalizer," Electronics Letters, Vol. 29, No. 25, December 1993, pp. 2181-2182.

11. V.I. Prodanov and M.M. Green, "CMOS current mirrors with reduced input and output voltage requirements," Electronic Letters, Vol. 32, No. 2, January 1996, pp. 104-105.

12. T. Itakura and Z. Czarnul, "High output resistance CMOS current mirrors for low-voltage applications," IEICE Transactions on Fundamentals, Vol. E80-A, No. 1, January 1997, pp. 230-232.

13. J. Ramírez-Angulo, R.G. Carvajal, and A. Torralba, "Low supply voltage high-performance CMOS current mirror with low input and output voltage requirements," IEEE Transactions on Circuits and Systems II, Express Briefs, Vol. 51, No. 3, March 2004, pp. 124-129.

14. A. Torralba, R.G. Carvajal, J. Ramirez-Angulo, and F. Muñoz, "Output stage for low supply voltage, high-performance CMOS current mirrors," Electronic Letters, Vol. 38, No. 24, November 2002, pp. 1528-1529.

15. S. Özcana, A. Toker, C. Acar, H. Kuntmana, et al., "Single resistance-controlled sinusoidal oscillators employing current differencing buffered amplifier," Microelectronics Journal, Vol. 31, No. 3, 2000, pp. 169-174.

16. Winai Jaikla and Montree Siripruchyanun, "Voltage-Mode/Current-Mode Current Controllable Lossless/Lossy Integrators and their applications," in The 21st International Technical Conference on Circuits/Systems, Computers, and Communications, Thailand, 2006, pp. 733-736.

17. Ali Ümit Keskin and Erhan Hancioglu, "CDBA-Based Synthetic Floating Inductance Circuits with Electronic Tuning Properties," ETRI Journal, Vol. 27, No. 2, 2005, pp. 239-242.

18. Winai Jaikla and Montree Siripruchyanun, "Current Controlled CDBA Based Novel Floating and Grounded Negative Inductance Simulators," in The 21st International Technical Conference on Circuits/Systems, Computers, and Communications, Thailand, 2006, pp. 701-704.

19. Ali Ümit Keskin, "Design of a PID controller circuit employing CDBAs," International Journal of Electrical Engineering Education, Vol. 43, No. 1, 2003, pp. 113-122.

20. Ali Ümit Keskin, "A Four Quadrant Analog Multiplier Employing Single CDBA," Analog Integrated Circuits and Signal Processing, Vol. 40, No. 1, 2004, pp. 99-101.

KAMILA ALIANE
Physics Engineer
aliane_kamila@yahoo.fr

NASREDDINE BENAHMED
Professor of Microwaves
n_benahmed@yahoo.fr

NADIA BENABDALLAH
Assistant Professor of Physics
n_benabdallah@yahoo.fr

FETHI TARIK BENDIMERAD
Professor of Communications Systems
ftbendimerad@gmail.com

ABDELKADER BENKADDOUR
Assistant Professor of Electronics

University of Abou Bekr Belkaid-Tlemcen, B.P. 119, (13000) Tlemcen, Algeria

Resonators Support UHF MRI Systems

These numerical methods, backed by various simulation methods, helped develop a high-Q resonator that is well suited for magnetic resonance imaging applications at UHF.

MAGNETIC RESONANCE IMAGING (MRI) is widely used for noninvasive exploration inside the human body. It can provide clear images of organs and tissues, especially those with high water content like muscles and brain tissue. MRI systems operating at ultrahigh frequency (UHF) can benefit greatly from the use of a transverse electromagnetic (TEM) slotted elliptical tube resonator (SER), which can produce a uniform magnetic field. By working with electromagnetic (EM) software simulation tools based on the finite-element method (FEM) and the method of moments (MoM), the authors have successfully analyzed and designed a high-quality-factor (high-Q) quasi-TEM SER suitable for UHF MRI applications.

The fundamental principle of MRI is to receive nuclear magnetic resonance signals induced by radiating EM wave pulse to a human body, which is placed inside the high-intensity static magnetic field. MRI was developed by Lauterbur,[1] Mansfield, and Grannell,[2] and is based on applying a nuclear magnetic resonance (NMR) technique. Their work, which won the 2003 Nobel Prize in physiology or medicine, has since become a standard clinical method in modern medicine.

An MRI system is composed of various elements—including an RF coil, which plays an essential role in imaging. Several types of RF coils, such as a saddle coil,[3] transverse electromagnetic (TEM) birdcage coil resonator (TEM BCR),[4,5] TEM slotted tube resonator (TEM STR),[6-8] and TEM slotted elliptical tube resonator (TEM SER),[9-12] have been developed for a wide range of different applications. Among these RF coils, the TEM SER has gradually come to be most often employed since it produces an extremely uniform magnetic field and can effectively suppress the system's electric field.

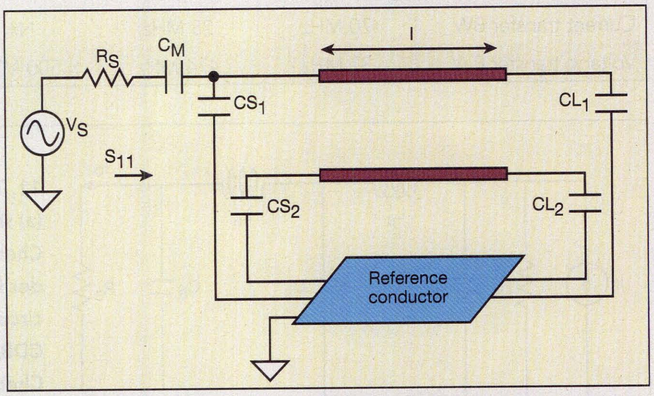

2. This schematic circuit shows how the UHF-MRI probe uses a quasi-TEM SER resonator.

This article builds on work presented earlier in *Microwaves & RF*.[12] In support of the analysis and design of a high-Q quasi-TEM resonator suitable for UHF-MRI applications based on loaded slotted elliptical tube resonator, the authors have adapted effective approaches based on the use of the finite-element method (FEM) and the method of moments (MoM).

For this type of quasi-TEM resonator, there are no numerical or experimental results in the scientific literature. Hence, the authors were obliged, for the same geometrical and physical parameters of our quasi-TEM elliptical resonator, to make simulations by using two numerical approaches (FEM and MoM). Modeling of this elliptical resonator consisted in analyzing the even- and odd-mode characteristic impedances (Z_{0e}, Z_{0o}), even- and odd-mode effective dielectric constants (ε_{effe}, ε_{effo}), and the primary inductive and capacitive matrices ([L], [C]), yielding the frequency response for the return loss, S_{11}, at the

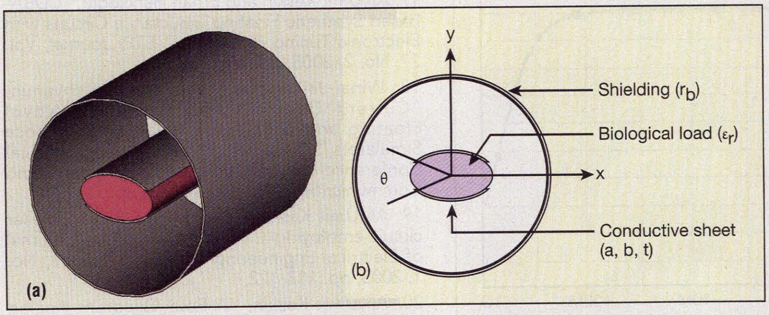

1. This figure shows (a) a 3D representation of a quasi-TEM slotted elliptical tube resonator with its (b) cross-sectional view.

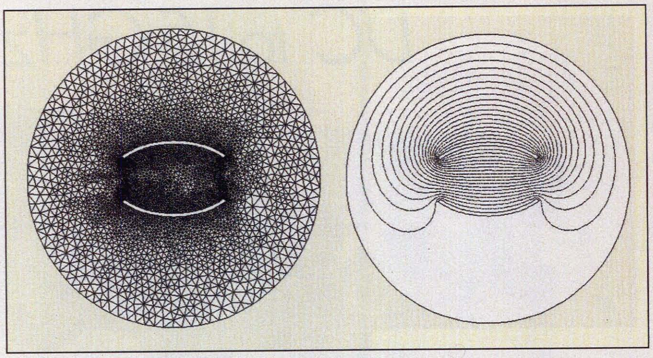

3. These illustrations present (left) the FEM meshes used to analyze the cross section of the quasi-TEM SER resonator and (right) the potential distribution obtained by solving for Laplace's equation.

RF port of the designed inhomogeneous MRI probe using the transmission-line method (TLM).[13]

As an application, the authors present the design results of a UHF-MRI probe loaded with a human head model[14] of average relative dielectric constant of 64 and using the optimum configuration of the TEM SER. The probe with high quality factor (Q) operates at 340 MHz (proton imaging at 8 T) and has minimum reflection of –139.5 dB. The UHF-MRI probe using quasi-TEM SER is easy to construct, inexpensive, and simple to operate. Furthermore, the elliptical coil presented here may be constructed to work at different resonant frequencies.

Figure 1(a) shows a schematic depiction of the quasi-TEM slotted elliptical tube resonator. As shown in **Fig. 1(b)**, this coil consists of two conductive bands containing a biological load (having a relative dielectric constant of ε_r) with thickness, t, carrying opposite currents on each side of a cylinder. The two conductive bands can be mounted on the long (a) or short (b) axes of the ellipse. The conductive sheets are connected at the ends with capacitors to the cylindrical outer shield of radius r_b **(Fig. 2)**. **Figure 1(b)** shows an elliptical cross section of the quasi-TEM SER. Angle θ is called the "window angle." The quasi-TEM SER structure generally performs as well as inhomogeneous cylindrical birdcage coils, with the advantages of being easier to construct and operate.

For the analyzed TEM SER (i.e., unloaded resonator) of ref. 11 with a/b = 1.8 and r_b/a = 2.4, the optimum field homogeneity was obtained for a window angle of 72 deg. In ref. 12, the current authors presented the design results of a UHF-MRI probe with high Q, operating at 7 T (i.e., 300 MHz) and using the optimum configuration of the slotted elliptical tube-line TEM resonator. Unfortunately, changes introduced by human biological loads with high dielectric constants in the quasi-TEM resonator were not negligible, because of the nonhomogeneity of the structure. For this reason, the authors adapted the previous numerical tools based on FEM and MoM approaches from ref. 12 to analyze a slotted elliptical tube resonator loaded with biological material.

The EM properties of the quasi-TEM SER can be described in terms of its primary parameters [L], [C] and its secondary parameters: the even- and odd-mode characteristic impedances, Z_{0e} and Z_{0o}, the even- and odd-mode effective dielectric constants, ε_{effe} and ε_{effo}, and the loaded quality factor, Q, where the primary parameters can be found from:

$$[L]=\begin{bmatrix} L_{11} & L_{12} \\ L_{21} & L_{22} \end{bmatrix} \quad [C]=\begin{bmatrix} C_{11} & C_{12} \\ C_{21} & C_{22} \end{bmatrix}$$

The inductance matrix [L] contains the self-inductances of the sheets on the diagonal, and the mutual inductances between sheets in the off-diagonal terms. Matrix [C] accounts for the capacitative effects between the two conductive sheets, characterizing the electric field energy storage in the quasi-TEM SER.

The coefficients for these matrices are obtained by solving a two-dimensional static field problem using the FEM[15,16] and MoM methods.[17]

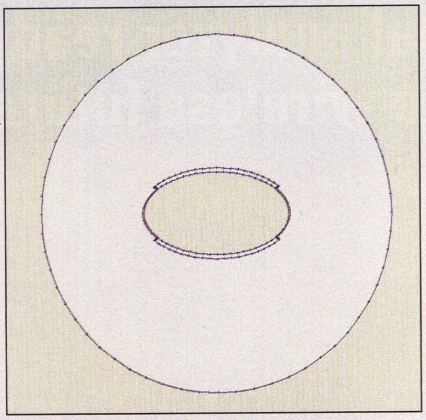

4. This view shows the segmentation of the charged surfaces used to analyse the cross section of the elliptical tube-line quasi-TEM resonator.

For the FEM approach and under the FreeFEM environment,[18] the solution can be obtained by solving the Laplace equation as shown in Eq. 1 **[Fig. 3(a)]**:

$$div\,[\varepsilon_r \nabla_t V(x,y)] = 0 \qquad (1)$$

where:

V = 1 V on the ith conductor's surface, and
V = 0 V on all other conductors.

This solution represents the distribution of the potential, V, at the different mesh nodes of the structure **[Fig. 3(b)]**.

When the potential V is known, it is possible to calculate the ith row of the [C] matrix from the electrical charge on each conductor, as in Eq. 2:

$$C_{ij} = \frac{1}{V_0}\oint_{lj} q_s dl \qquad (2)$$

where:

$V_0 = 1$ V;
$q_s = \varepsilon_0 \varepsilon_r E_N$;
1j represents the contour around the jth conductor; and
E_N = the normal component of the electric field.

In the high-frequency limit—i.e., the skin depth is sufficiently small such that current flow occurs only on the surface of the conductors—the inductance matrix [L] can be obtained from the matrix $[C_0]$.[8] The inductance matrix in terms of $[C_0]$ calculated for $\varepsilon_r = 1$ is:

$$[L] = \mu_0 \varepsilon_0 [C_0]^{-1} \quad (3)$$

For the MoM approach described in ref. 12, the numerical calculations of the EM-parameters of the studied resonator were carried out with LINPAR for Windows (Matrix Parameters for Multiconductor Transmission Lines), a two-dimensional (2D) software program for numerical evaluation of the quasistatic matrices for multiconductor transmission lines embedded in piecewise-homogeneous dielectrics.[17] For the slotted elliptical tube-line quasi-TEM resonator, the authors were obliged to supply the cross section of the structure and all relevant dielectrics characteristics including the segmentation by using our programs in FORTRAN **(Fig. 4)**.

When the EM-parameters are determined, it was possible to estimate the resonance spectrum (S_{11}) of the quasi-TEM resonator shown in **Fig. 2** using programs based on the TLM or other numerical tools.

The UHF-MRI probe developed for this article consists of an SER resonator with length l, matching capacitor, C_M, and terminating capacitors, C_{Si} and C_{Li} (with I = 1, 2). The loaded Q of the quasi-TEM elliptical resonator can be estimated from the reflection-parameter (S_{11}) sweep with frequency[12]:

$$Q = \frac{f_r}{f_u - f_l} \qquad (4)$$

where:

f_r = the resonant frequency of the circuit;
f_u = the 3-dB frequency above the resonant frequency; and
f_l = the 3-dB frequency below the resonant frequency.

To design a loaded UHF-MRI probe operating at 8 T (i.e., 340 MHz) and using the optimum configuration of the TEM SER (for θ = 72 deg.), the authors applied modified and coherent FEM- and MoM-based numerical modeling tools to the structure of **Fig. 2** with the following set of features:

A short b axis of 10 cm;
A long-to-short-axis ratio (a/b) of 1.8;
An outer radius-to-long-axis ratio (r_b/a) of 2.4;
A sheet thickness-to-short-axis ratio (t/b) of 0.1; and
A window angle (θ) of 72 deg.

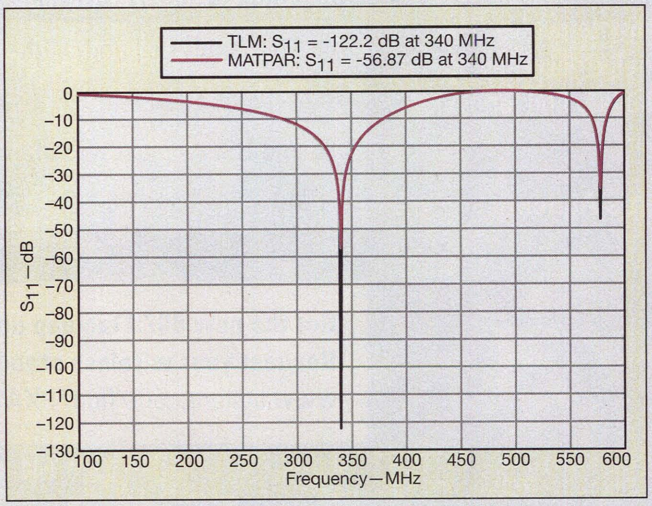

5. These curves show the scattering parameters of the designed UHF-MRI probe operating at 8 T and using the unloaded TEM SER resonator.

The numerical approaches make it possible to simulate the performance of a design and decide if a given set of constraints makes it possible to realize the UHF-probe.

The authors' FEM and MoM approaches were employed as shown in **Figs. 3 and 4** to determine the EM parameters of the quasi-TEM elliptical resonator. As discussed above, the integration of the normal flux over the conductor contours determines the per-unit-length parameter matrices. For instance, **Table 1** lists the elements of the [L]

EQAM INTEGRATION

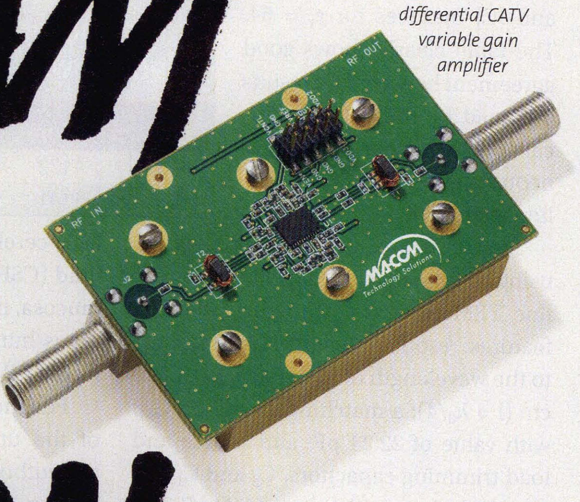

M/A-COM Tech Edge QAM VGA

MAAM-010399: Delivering the complete Edge QAM voltage variable attenuator solution

Part Number	MAAM-010399
Variable Gain Amplifier	
Package (PQFN)	5x7 mm, 40-lead
Gain	28 dB
Attenuation Range	25 dB
ACPR	
@ max output N=1, 67 dBmV	62 dBc
@ max output N=2, 63 dBmV	60 dBc
@ max output N=4, 59 dBmV	60 dBc
P1dB	28 dBm
OIP3	48 dBm
2nd and 3rd Harmonic	-65 dBc
CTB	78 dBc
CSO	78 dBc
Current, Voltage	900 mA, 6 V

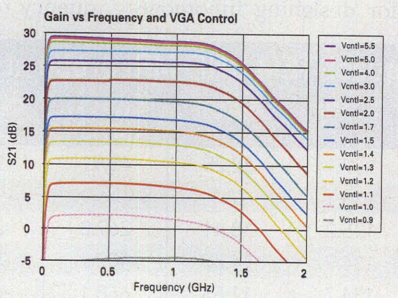

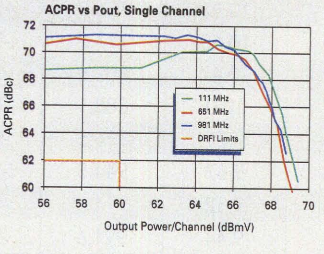

M/A-COM Technology Solutions announces our new MAAM-010399 EQAM variable gain amplifier. This highly linear differential VGA is characterized in 75 ohms and packaged in a small 5x7 mm QFN. The MAAM-010399 reduces real estate requirements, simplifies the RF implementation and exceeds DOCSIS DRFI specifications with 7 dB typical performance margin.

Our MAAM-010399 VGA features:

- 28 dB gain
- 25 dB attenuation range
- 62 dBc ACPR*
- 65 dBc 2nd harmonic
- 48 dBm OIP3
- 20 dB output return loss

* See table for details

SIGN UP FOR NEWS

To sign up for more news and new product announcements, visit macomtech.com

MACOM Technology Solutions
THE FIRST NAME IN MICROWAVE®

and [C] matrices for $\varepsilon_r = 64$. The table clearly shows good agreement between the results obtained by the two numerical approaches for inhomogeneous slotted elliptical tube-line resonator.

First, a UHF-MRI probe was designed using an unloaded slotted elliptical tube-line TEM resonator with the following features: resonator length, l (with respect to the wavelength of free space, λ_0), of 20 cm ($l \approx \lambda_0/4$); a matching capacitor, C_M, with value of 22.24 pF; and source and load trimming capacitors, C_S and C_L, respectively, both with value of 1.44 pF. The simulated S_{11} responses at the RF port for the designed unloaded MRI probe are shown in **Fig. 5** for both TLM programs and for MATPAR software.[19]

In practice, for UHF-MRI proton imaging at 8 T, such results remain valid when the quasi-TEM SER is filled by an inhomogeneous biological load (such as a human head). In ref. 14, 18 tissue types (in addition to air) were identified in the images given in **Fig. 6** in order to obtain a detailed human head structure. These included blood, bone-cancellous material, bone-cortical material, cartilage, cerebellum, cornea, cerebro spinal fluid (CSF), dura, fat, gray-matter (GM), mucosa, muscle, nerve, skin, tongue, vitreous-humor, white-matter (WM), and mixed-GM-WM.

Table 1: Primary EM parameters for the inhomogenous SER loaded with biological element with relative dielectric constant of 64.

	$C_{11} = C_{22}$ (pF/m)	$C_{12} = C_{21}$ (pF/m)	$L_{11} = L_{22}$ (nH/m)	$L_{12} = L_{21}$ (nH/m)
FEM	1172	-1152	311.2	133.3
MoM	1141	-1116	319.0	144.7

For the same length (i.e., l = 20 cm) of the unloaded elliptical MRI probe, the authors introduced a biological load having a relative dielectric constant (ε_r)[20] into the MRI resonator and numerically tuned matching capacitor C_M and terminating capacitors C_{Si} and C_{Li} until achieving resonance. At 340 MHz, the values obtained for these capacitors are shown in **Table 2**, along with the EM parameters of the elliptical resonator, for each biological load. From **Table 2**, the value of the matching capacitor varies between 1 and 2.06 pF for MRI use when applying the optimum configuration of the quasi-TEM SER. The values shown in **Tables 1** (for the element of matrix [L]) **and 2** are essential for designing inhomogeneous elliptical UHF-MRI probes operating at 8 T. **Table 2** provides the key parameter values for the wide range of load types in the MRI probe at 340 MHz, including blood, bone, cartilage, cornea, muscle, nerve, and skin materials.

Considering that the average relative dielectric constant of the human head is 64,[14] the wavelength inside the head is approximately 11 cm. As a result, the EM parameters of the quasi-TEM SER loaded with the human head model obtained from the authors' MoM analyses include even- and odd-mode characteristic impedances, Z_{0e} and Z_{0o}, of 134.6 Ω and 8.8 Ω, respectively, and effective dielectric constants, ε_{effe} and $(\varepsilon_{effo}$, of 1.066 and 35.36, respectively, and primary inductive and capacitive matrices, [L] and [C], respectively, as follows:

$$[L]=\begin{bmatrix} 319 & 144.7 \\ 144.7 & 319 \end{bmatrix} \left(\frac{nH}{m}\right);$$

$$[C]=\begin{bmatrix} 1141 & -1116 \\ -1116 & 1141 \end{bmatrix} \left(\frac{pF}{m}\right)$$

Figure 7 shows the simulated frequency responses of S_{11} at the RF port

Table 2: Parameters for the quasi-TEM UHF-MRI probe at 340 MHz.

Load type	ε_r [20]	ε_{effe}	ε_{effo}	Z_{0e} (Ω)	Z_{0o} (Ω)	$C_{11}=C_{22}$ (pF/m)	$C_{12}=C_{21}$ (pF/m)	C_M (pF)	$C_{Si} = C_{Li}$ (pF)
Air	1	1	1	139.1	52.25	43.91	-19.94	22.24	1.44
Fat	5,14	1.043	3.27	136.1	28.9	116.9	-91.91	20.0	1.0
Bone-Cortical	13,91	1.058	8.06	135.2	18.41	269.8	-244.5	28.57	1.43
Bone-Cancellous	21,84	1.062	12.38	134.9	14.85	407.9	-382.4	27.15	1.08
Nerve	36,80	1.065	20.54	134.7	11.53	668.1	-642.6	21.13	2.06
White-Matter	41,85	1.065	23.29	134.7	10.83	756.0	-730.4	20.11	1.69
Skin	43,07	1.065	23.96	134.7	10.68	777.2	-751.6	24.89	1.49
Cartilage	44,82	1.065	24.91	134.7	10.47	807.6	-782.0	27.33	1.37
Mixed-GM-WM	49,45	1.066	27.43	134.7	10.0	888.1	-862.6	21.18	1.47
Dura	52,23	1.066	28.95	134.6	9.71	936.5	-910.9	24.89	1.29
Mucosa	52,69	1.066	29.2	134.6	9.67	944.5	-918.9	25.0	1.28
Cerebellum	54,40	1.066	30.13	134.6	9.52	974.2	-948.7	23.25	1.32
Cornea	55,40	1.066	30.68	134.6	9.44	991.6	-966.1	26.23	1.21
Gray-Matter	57,05	1.066	31.58	134.6	9.30	1020	-994.7	20.41	1.41
Blood	57,50	1.066	31.82	134.6	9.27	1028	-1003	21.42	1.38
Tongue	59,64	1.066	33.0	134.6	9.10	1065	-1040	29.34	1.10
Muscle	65,57	1.066	36.22	134.6	8.68	1169	-1143	25.55	1.03
Vitreous-Humor	68,30	1.066	37.71	134.6	8.51	1216	-1190	21.16	1.13
CSF	69,08	1.066	38.13	134.6	8.46	1230	-1204	21.45	1.09

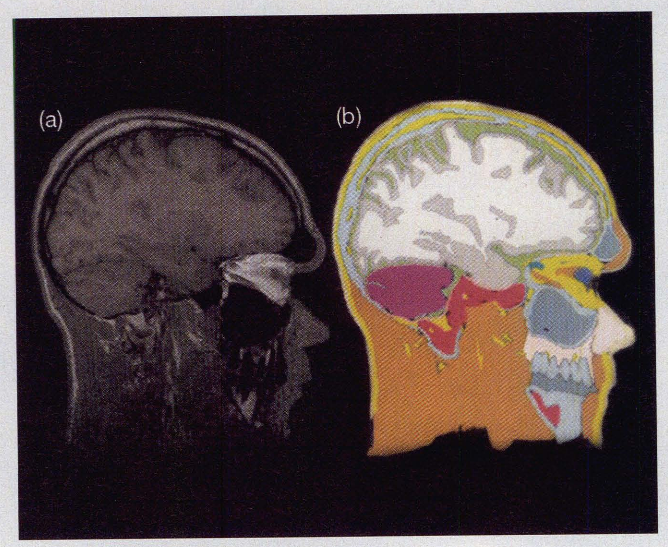

6. These views show (a) an MRI image of the inhomogeneous biological load that is a human head and (b) its equivalent anatomically detailed human head model used in ref. 14.

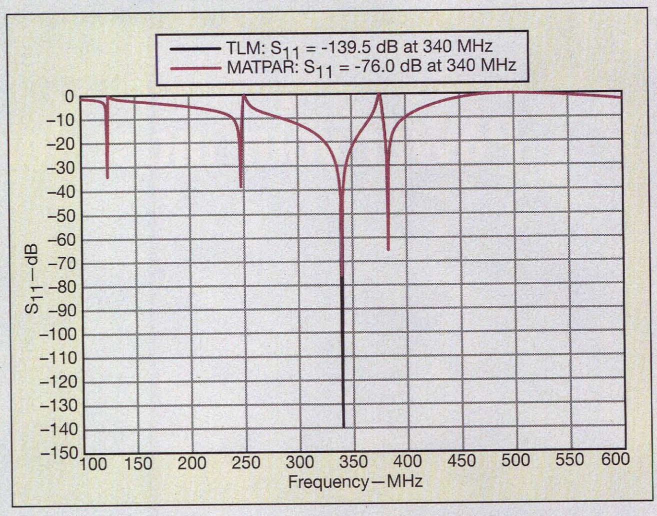

7. Measurements of reverse transmission, S_{11}, at the RF port of the designed UHF-MRI probe using quasi-TEM SER loaded with the human head model are plotted here as a function of frequency.

for the designed UHF-MRI probe using quasi-TEM SER loaded with the human head model, using both of the authors' TLM programs and commercial MATPAR software. From this figure, it appears that the biological load introduced into the SER improves the value of the reverse transmission, indicated by the response of parameter S_{11}, at 340 MHz. For matching capacitor C_M with value of 20.83 pF and terminating capacitors C_{Si} and C_{Li}, both with capacitance value of 1.31 pF, the loaded UHF-probe operates at 340 MHz (proton imaging at 8 T) and has −139.5 dB minimum reflections. Using Eq. 4, Q was estimated to be very superior to 500.

This report has presented the analysis and the design of a UHF-MRI probe with high Q, operating at 8 T (i.e., 340 MHz) and using the optimum configuration of the slotted elliptical tube-line quasi-TEM resonator. The EM parameters of the elliptical quasi-TEM resonator were characterized using modified FEM and MoM programs. When the EM parameters were determined, it was possible to simulate the frequency response of S_{11} at the RF port of the designed quasi-TEM resonator loaded with any biological element having any combination of relative dielectric constants. The high-Q quasi-TEM UHF-MRI probe that was designed operated at 340 MHz. Using a SER loaded with a human head model having average relative dielectric constant of 64, minimum reflections of −139.5 dB were measured. The UHF-MRI probe described in this report is inexpensive, easy to construct, simple to operate, and can be easily modified to work at different resonant frequencies. It can be effectively applied to research on organs and tissues with high water content, including muscles and brain tissues. MWRF

REFERENCES

1. P.C. Lauterbur, "Image formation by induced local interactions: examples employing nuclear magnetic resonance," Nature, Vol. 242, 1973, pp. 190-191.
2. P. Mansfield and P.K. Grannell, "NMR diffraction in solids?" Journal of Physics C, Vol. 6, 1973, pp. L422–L426.
3. C.E. Garrido Salmon, E.L. G´ea Vidoto, M. J. Martins, and A. Tann´us, "Optimization of Saddle Coils for Magnetic Resonance Imaging," Brazilian Journal of Physics, Vol. 36, No. 1A, March 2006, pp. 4-8.
4. G. Bogdanov and R. Ludwig, "A Coupled Microstrip Line Transverse Electromagnetic Resonator Model For High-Field," Magnetic Resonance Medicine, Vol. 47, 2002, pp. 579-593.
5. R. Ludwig, G. Bodgdanov, J. King, A. Allard, and C.F. Ferris, "A dual RF resonator system for high-field functional magnetic resonance imaging of small animals," Journal of Neuroscience Methods, Vol. 132, 2004, pp. 125-135.
6. D.W. Alderman and D.M. Grant, "An efficient decoupler coil design which reduces heating in conductive samples in superconducting spectrometers," Journal of Magnetic Resonance, Vol. 34, 1979, pp. 425-433.
7. S. Li, Q.X. Yang, and M.B. Smith, "RF coil optimization: Evaluation of B1 field homogeneity using field histograms and finite element calculations," Magnetic Resonance Imaging, Vol. 12, 1994, pp. 1079-1087.
8. N. Benabdallah, N. Benahmed, B. Benyoucef, R. Bouhmidi, and M'. Khelif, "EM analysis of the slotted-tube resonator with circular cross section for MRI applications," Journal of Physics in Medicine and Biology, Vol. 52, August 2007, pp. 4943-4952.
9. S. Crozier, L.K. Forbes, W.U. Roffmann, K. Luescher, and D.M. Doddrell, "A methodology for current density calculations in high-frequency RF resonators," Concepts in Magnetic Resonance, Vol. 9, 1997, pp. 195-210.
10. M.C. Leifer, "Theory of the quadrature elliptic birdcage coil," Journal of Magnetic Resonance Medicine, Vol. 38, 1997, pp. 726-732.
11. S. Bobrof and M.J. McCarthy, "Variations on the slotted-tube resonator: Rectangular and elliptical coils," Journal of Magnetic Resonance Imaging, Vol. 17, 1999, pp. 783-789.
12. N. Benabdallah, N. Benahmed, and B. Benyoucef, "Analyzing a resonator for MRI applications," Microwaves and RF, Vol. 46, No. 11, November 2007, pp. 92-98.
13. R.P. Clayton, Analysis of Multiconductor Transmission Lines, Wiley, New York, 2008.
14. T.S. Ibrahim, R. Lee, B.A. Baertlein, A.M. Abduljalil, H. Zhu, and P.L. Robitaille, "Effect of RF coil excitation on field inhomogeneity at ultra high fields: A field optimized TEM resonator," Magnetic Resonance Imaging, Vol. 19, 2001, pp. 1339-1347.
15. R. Bouhmidi, N. Benabdallah, N. Benahmed, and M'. Khelif, "Design coupled microstrip resonators for MRI," Microwaves and RF, Vol. 46, No. 3, March 2007, pp. 59-66.
16. N. Ben Ahmed, M. Feham, and M'. Khelif, "Analysis and design of a coupled coaxial line TEM resonator for magnetic resonance imaging," Journal of Physics in Medicine and Biology, Vol. 51, April 2006, pp. 2093-2099.
17. A.R. Djordjevic, M. B. Bazdar, and T.K. Sarkan, LINPAR for Windows: Matrix parameters of multiconductor transmission lines, Software and user's manual, Artech House, Norwood, MA, 1999.
18. www.Freefem.org.
19. A.R. Djordjevic, M. Bazdar, G. Vitosevic, T. Sarkar, and R. F. Harrington, Scattering parameters of microwave networks with multiconductor transmission lines, Artech House, Norwood, MA, 1990.
20. C. Gabriel, "Compilation of dielectric properties of body tissues at RF and microwave frequencies," AL/OE-TR-1996-0037 1996.

PROBING PROBLEMS BASED ON EMI

ELECTROMAGNETIC INTERFERENCE (EMI) has long been a concern for design engineers. EMI stems from unintentional radio-frequency transmitters or emitters, which can be the result of unexpected signal leakage, unplanned-for harmonic frequencies, and even high-level spurious signal products. The consequence is usually interference with a receiver that is operating within the frequency band of the EMI leakage. EMI levels in electronic products are limited by regulatory agencies, including the American National Standards Institute (ANSI; www.ansi.org) and Comite International Special des Perturbations (CISPR; www.iec.ch), which require that well-established measurements be used to certify that those products comply with standardized limits for EMI. Fortunately, a 12-page application note from Tektronix, "Real-Time Spectrum Analysis for EMI Diagnostics," explains how EMI measurements can be made with a real-time spectrum analyzer (RSA), including the types of filters that must be applied for accurate results.

The note explains that many of the EMI standards are based on how interference affects analog electronic communications systems, and thus were not written for the needs of modern digital communications systems. For systems employing digital modulation, even a short burst of interference can result in a loss of data. Fortunately, modern test instruments, such as Tektronix's lines of RSAs, can view wide spans of frequency spectrum instantaneously, making it possible to detect even transient interferers. General-purpose spectrum analyzers are often used early in the design stages of a product, ensuring proper electromagnetic compatibility (EMC) of different circuits within a design. However, once all those circuits have been integrated (with the potential to interfere with each other), the measurement power of an RSA can help not only to find EMI problems, but to troubleshoot the overall performance of the design.

The application note addresses the flexibility offered by an RSA in terms of changing receiver filters to comply with different EMI measurement systems. In addition to the filter bandwidths, the shapes of the filters are also defined by different standards, including MIL-STD-461E for military applications. In addition, the note reviews how detectors are used in EMI measurements, so as to find a single point that represents a signal at any instant in time. Detection methods can reveal positive or negative voltage peaks, average or root-mean-square (RMS) values of voltage, or even quasi-peak values of voltage. Quasi-peak detectors read the weighted peak value of a signal envelope. These detectors, which are available in an RSA, have fast attack times with slow decay times, and read higher levels for signals that are more frequent than for those that are less frequent. The 12-page application note provides an excellent overview of EMI measurements and how an RSA serves as a versatile tool for making these measurements. A free PDF is available for download from the Tektronix website.

Tektronix, Inc., 14150 SW Karl Braun Dr., P.O. Box 500, Beaverton, OR 97077; (800) 833.9200, www.tek.com.

EXTEND THE RANGE OF EVM MEASUREMENTS

MODERN COMMUNICATIONS SYSTEMS rely on digital modulation techniques to transfer large amounts of information wirelessly. These modulation methods typically rely on vector signals with in-phase (I) and quadrature (Q) signal components. One of the key tests for evaluating the performance of a wireless digital communications system is an error-vector-magnitude (EVM) measurement, which can be performed with a vector signal analyzer (VSA) and a vector signal generator (VSG). But no test instruments are perfect, and noise and other imperfections from the test equipment can degrade the quality of EVM measurements. Fortunately, a five-page application note from ZTEC Instruments, "Extending the Useable Range of Error Vector Magnitude (EVM) Testing," helps testers get the most from the VSAs and VSGs when making EVM measurements.

The application note uses the IEEE 802.11 wireless-local-area-network (WLAN) standard as an example of a digitally modulated communications system that requires EVM for evaluation. The various iterations of the IEEE 802.11 WLAN standard employ orthogonal frequency-division-multiplexing (OFDM) modulation, which encodes digital data simultaneously on multiple subcarrier frequencies for enhanced signal robustness. The standard's number of carriers varies by channel bandwidth, with 802.11 channel bandwidths ranging from 20 to 160 MHz.

ZTEC Instruments, 7715 Tiburon St. NE, Albuquerque, NM 87109; (866) ZTEC-NOW, (505) 342-0132, FAX: (505) 342-0222, www.ztecinstruments.com

Such factors as signal instability and noise in a VSA and VSG can hinder the effectiveness of EVM measurements performed with these instruments. Signal noise and distortion can limit the minimum and maximum modulated signal levels that can reliably be measured with a VSG and VSA. For example, test signal phase noise and spurious levels can impact EVM measurement quality.

Fortunately, the application note provides several equalization techniques, as well as noise and distortion optimization methods, that can be used to improve the quality of EVM measurements with a VSA and VSG. A free PDF of the application note is available for download from the ZTEC Instruments website.

PRECISION TEST

CABLES

now up to 40 GHz

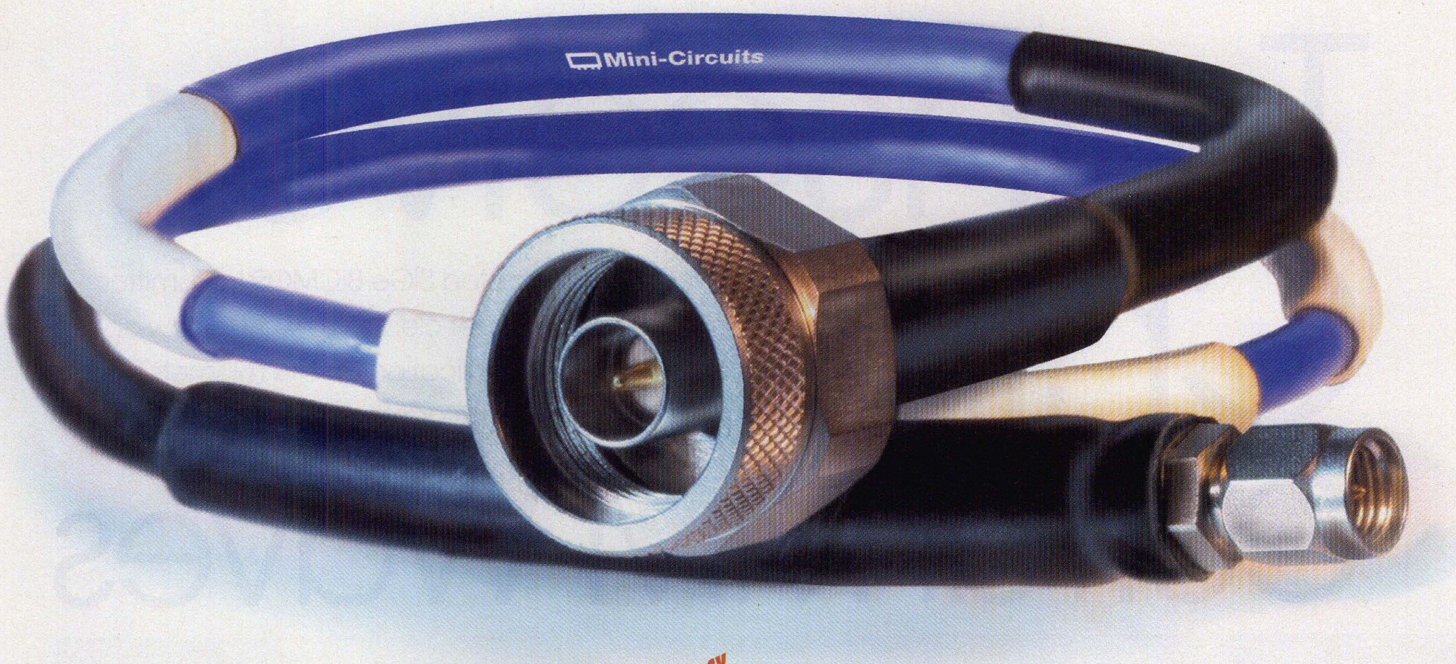

from **$68.95** ea. (qty.1-9) **IN STOCK**

High-quality data requires high-quality cables — and different models to meet different needs. Mini-Circuits Precision Test Cables have been designed with our 40 years of industry experience in mind, and tested beyond any others on the market. It's why we can back them with an unprecedented 6-month guarantee,* and customers can save time and money with fewer false rejects and less retesting.

Flex Test™ Our standard, triple-shielded CBL cables are so tough, we had to invent a new way to test them: Flex Test™. Even after more than 20,000 flex cycles, these cables deliver unimpaired performance from DC-18 GHz. Ideal for design labs or test benches, they're available in lengths up to 25 feet with SMA or N-type connectors.

Quick Lock For high-speed production efficiency and superior electrical & mechanical performance, our QBL cables are the answer. Just push them onto a standard female SMA connector and slide the collar forward to lock. You'll get proven high-integrity DC-18GHz connections, even after 20,000 flex and 20,000 mating cycles!

Armored For harsh, abusive, outdoor environments, our APC cables can't be beat. Even 1,000 crush cycles with a 440-lb nitrogen tank had minimal effect: attenuation increased only 0.15 dB, while return loss in/out remained ≥20 dB from DC-18 GHz. N-type connectors are standard, with lengths from 6 to 15 feet in stock.

Our new 40 GHz cables are proven through 20,000 flex cycles, and are fitted with high-performance connectors that mate with K®- and SMA-equipped DUTs. Standard lengths range from 1.5 feet to 2 meters.

Low Loss For design work requiring long cable runs or whenever Ka-band signal strength is key, our KBL-LOW cables are ideal. Insertion loss is only 2.46 dB/m at 40 GHz, with a velocity ratio of 84%.

Phase Stable When phase stability is a concern, as in many high-frequency production tests, try our KBL-PHS cables. They offer a phase change ≤0.1°/GHz when wrapped a full turn around a 3" diameter mandrel, and a shielding effectiveness of 110 dB!

RoHS compliant

See minicircuits.com for cable lengths, specifications, performance data, and surprisingly low prices!

* Mini-Circuits will repair or replace your test cable at its option if the connector attachment fails within six months of shipment. This guarantee excludes cable or connector interface damage from misuse or abuse.

K-Connector is a registered trademark of Anritsu Company.

Mini-Circuits...we're redefining what VALUE is all about!

Mini-Circuits®

ISO 9001 ISO 14001 AS 9100

P.O. Box 350166, Brooklyn, New York 11235-0003 (718) 934-4500 Fax (718) 332-4661

HITTITE MICROWAVE CORP.
2 Elizabeth Dr., Chelmsford, MA 01824;
(978) 250-3343, FAX: (978) 250-3373; e-mail: sales@hittite.com, www.hittite.com.

Transceiver Chips Corral MM Waves

This highly integrated SiGe BiCMOS transmitter and receiver chipset clears the way for low-cost, high-data-rate applications in the millimeter-wave frequency spectrum centered at 60 GHz.

DATA AND BANDWIDTH ARE TWO AREAS where wireless communications customers have seemingly insatiable needs. No matter their wireless device of choice—be it a cellular telephone or a personal computer (PC)—users want faster data rates, and thus require more bandwidth. Unfortunately, bandwidth is finite. But, thanks to a 7-GHz millimeter-wave-frequency block from 57 to 64 GHz set aside by the United States' Federal Communications Commission (FCC; www.fcc.gov) in 2001, bandwidth is still available for wireless services. In general, throughout the world a 5-GHz millimeter-wave band is available for wireless services.

Of course, this assumes the development of practical transceiver components for radios at those frequencies. Fortunately, the model HMC6000 transmitter integrated circuit (IC) and the model HMC6001 receiver IC, both from Hittite Microwave Corp. (www.hittite.com), are those practical transceiver component solutions. Hittite's HMC6000/6001 chipset not only solves many of the key technical challenges encountered at millimeter-wave frequencies, but also enables turnkey multi-Gb/s communication links at 60 GHz.

A 5-GHz portion of that millimeter-wave bandwidth, 59 to 64 GHz, is available for unlicensed applications in the US and in many locations around the world. The large block of spectrum enables the use of simple modulation schemes to achieve multi-Gb/s communication links, working with simpler transceiver designs at lower power levels than required for wireless applications at lower, more crowded frequencies.

The small wavelengths at 57 to 64 GHz also allow for extremely small antennas and overall miniaturization of radio system solutions. The short wavelengths support direct line-of-sight communications with low interference. At 60 GHz, signals propagate in an oxygen absorption band with approximately 15 dB/km attenuation; signals in that band also do not penetrate walls, which can be an aid in densely deployed short-range applications and in smaller wireless communications cell deployments enabling significant fre-

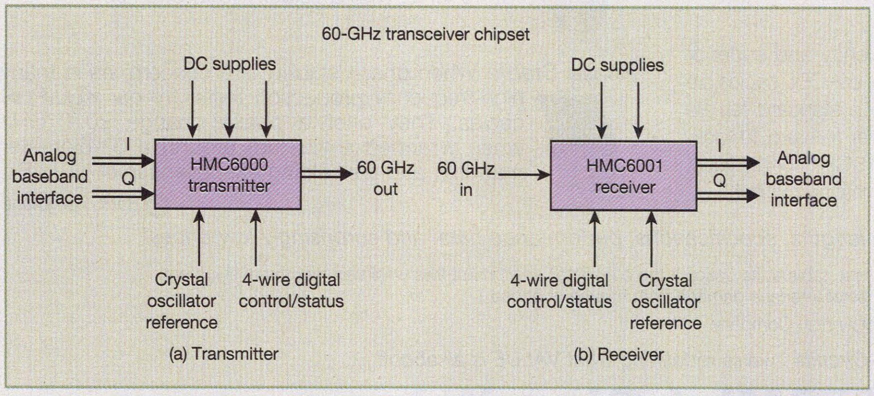

1. This low-cost solution for license-free 60-MHz wireless communications consists of the model HMC6000 transmitter IC and a model HMC6001 receiver IC.

quency reuse. At 60 GHz, the short wavelength means that, for a given antenna aperture, a very narrow beam is transmit, with such beams capable of high isolation even in dense signal environments.

Because of the high isolation, the FCC allows for high transmit powers in this frequency band (to 500 mW) and an effective isotropic radiated power (EIRP) level to +40 dBm. This is 10 dB more than allowed at 900 MHz outdoors, 2.4 dB more than allowed at 5 GHz indoors, and 6 dB higher than the 5-GHz UNII band outdoors. The limits set by the European Telecommunications Standards Institute (ETSI; www.etsi.org) allow for a power density of +13 dBm/MHz and a maximum EIRP of +40 dBm for wireless-local-area-network (WLAN) and wireless-personal-area-network (WPAN) applications and +55 dBm maximum EIRP for outdoor point-to-point fixed wireless systems.

The signal propagation properties, along with the wide bandwidth and high available EIRP, make the 60-GHz band an attractive frequency range for short-range applications requiring multi-Gb/s data rates. These include outdoor point-to-point radio solutions for metrocell/picocell backhaul, and indoor datalink applications such as wireless Gb/s cable replacement (HDMI, USB 3.0, Thunderbolt, etc.), wireless docking stations,

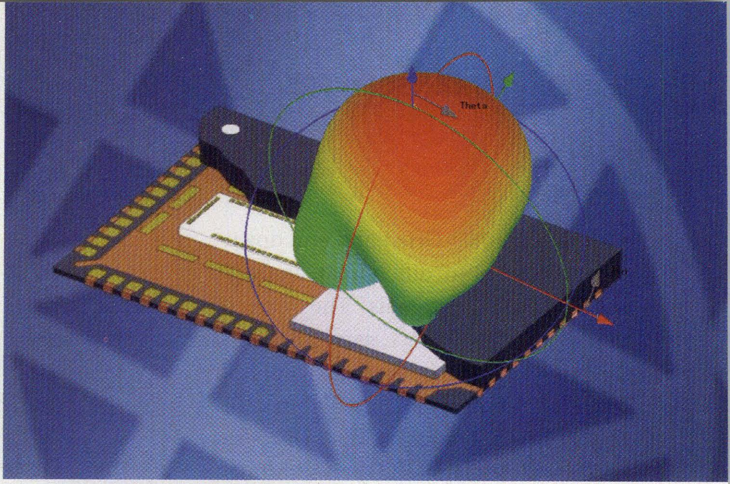

2. This is a 60-GHz antenna-in-package (AiP) solution which can include either the HMC6000 transmitter or the HMC6001 receiver.

and video/magazine kiosks. The bandwidth also holds great promise for millimeter-wave wireless sensor applications. Several standards and industry groups have emerged to address the use of these millimeter-wave frequencies, including the Institute of Electrical and Electronics Engineers (IEEE; www.ieee.org) with their IEEE 802.11ad and IEEE 802.15.3c standards, as well as the WirelessHD and Wireless Gigabit Alliance (WiGig; www.wirelessgigabitalliance.org) consortiums.

Of course, millimeter-wave signal processing poses many challenges. Achieving low-loss performance on printed circuit boards (PCBs) and with interconnections can be difficult without the use of advanced materials and sophisticated topologies. For low-cost solutions, millimeter-wave interconnections (to give one example), must be incorporated into the ICs themselves or into their packages. Hittite, a contributing member of the WiGig consortium, is providing the HMC6000/6001 chipset to translate low-frequency baseband signals directly to and from 60 GHz, minimizing the need for expensive or complex millimeter-wave interconnection components on the PCB.

For example, the HMC6000 transmitter IC **[Fig. 1(a)]** can translate baseband in-phase (I) and quadrature (Q) signals to a selected channel in the 60-GHz band, requiring only an external reference oscillator to execute the frequency translation. Model HMC6000 is fabricated with silicon-germanium (SiGe) BiCMOS semiconductor process technology. It provides analog I and Q (differential) input ports with DC coupling for cancellation of DC offsets and carrier feedthrough. The transmitter IC includes a low-noise frequency synthesizer for tuning across the 57-to-64-GHz band using 500- or 540-MHz steps (a quarter of the IEEE channel spacing) depending on the reference input frequency. It features as much as 38-dB gain (with 17-dB gain-control range) to achieve as much as +12 dBm linear output power and as much as +17 dBm saturated output power. The differential RF output provides a low-loss RF transition with high output efficiency.

The HMC6001 receiver IC **[Fig. 1(b)]** works with input signals from a selected

The 60-GHz transceiver solution at a glance.

Parameter	HMC6000 transmitter	HMC6001 receiver
Operating frequency range	57 to 64 GHz	57 to 64 GHz
Linear output power	+12 dBm	---
Noise figure	---	6 dB
Maximum gain	38 dB	67 dB
Gain control range	17 dB	65 dB in 1-dB steps
Phase noise (offset 1 MHz)	-86 dBc/Hz	-86 dBc/Hz

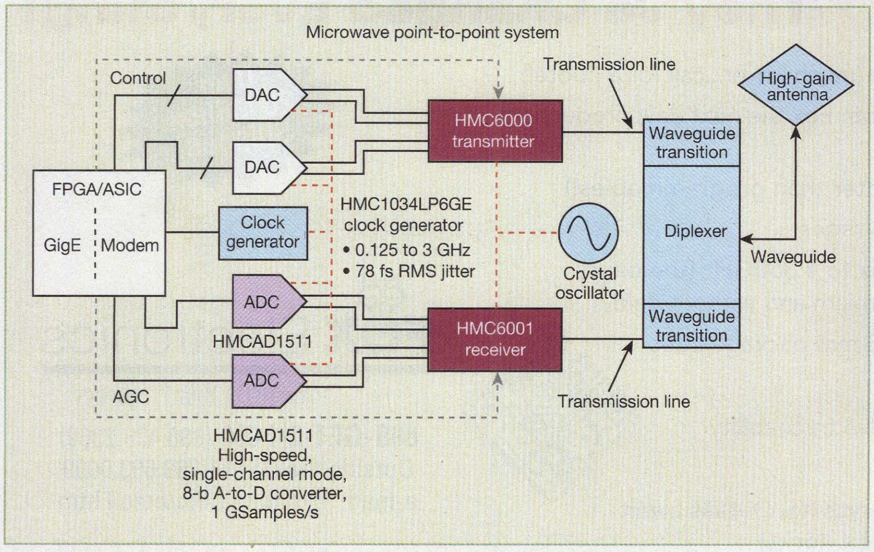

3. This is a 60-GHz Gigabit Ethernet point-to-point microwave backhaul solution.

channel in the 60-GHz band and downconverts them to differential analog I and Q baseband signals. The receiver chip includes all necessary frequency generation, filtering, and gain control, including a programmable highpass filter that helps remove residual DC offset and local-oscillator (LO) feedthrough signals. The HMC6001 exhibits a 6-dB noise figure at the maximum gain setting; it provides a 65-dB gain control range in 1-dB steps **(see table)**. A simple four-wire digital serial interface provides full control and status reporting for these ICs, including frequency channel selection, gain control, circuit bias, and filter bandwidths.

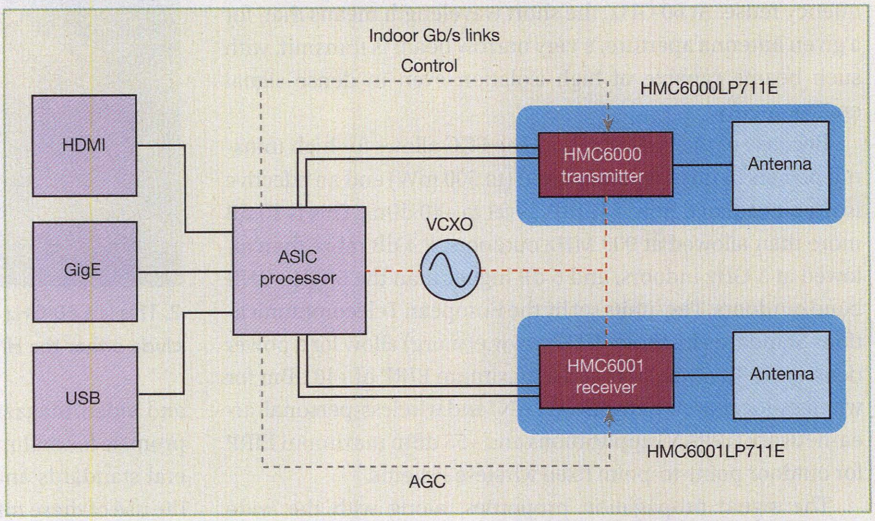

4. This is a consumer-oriented multi-Gb/s solution that adheres to the WiGig standard.

Because reference and voltage-controlled-oscillator (VCO) signals (and their noise) are multiplied up in frequency to achieve 60-GHz signals, phase noise can be a limiting factor for a millimeter-wave receiver. To avoid degrading the HMC6001's receiver noise figure, its integrated phase noise is maintained at typically 10 dB below the thermal noise of the applicable modulation format. Fortunately, with the faster symbol rates used at 60 GHz, the integrated phase noise of concern is much further from the carrier. Both the HMC6000 and HMC6001 have integrated phase noise of roughly –25 dBc at 1.76-GHz WiGig symbol rates, enabling modulation formats to 16-state quadrature amplitude modulation (16QAM).

Both the HMC6000 and HMC6001 exhibit phase noise of typically –86 dBc/Hz offset 1 MHz from the carrier.

To assist customers with 60-GHz system solutions, Hittite offers both connectorized and antenna-in-package (AiP) solutions based on the HMC6000 and HMC6001 millimeter-wave transceiver ICs. **Figure 2** shows the model HMC6000LP711E solution, which combines a 60-GHz antenna with the HMC6000 transmitter IC in a low-cost, 7 x 11 mm QFN plastic package. This surface-mount-compatible solution supports low-cost PCB assembly and requires no experience in handling millimeter-wave devices. Similarly, the HMC60001LP711E combines a 60-GHz antenna with the HMC6001 receiver IC, also in a 7 x 11 mm QFN plastic package.

A typical point-to-point 60-GHz microwave radio link **(Fig. 3)** might transport one or more Gigabit Ethernet data streams. These are full-duplex connections so a diplexer is commonly used to provide the necessary isolation between the transmit and receive channels while sharing a common, high-gain antenna. In contrast to earlier system designs with numerous discrete components, a design based on the HMC6000 and HMC6001 ICs reduces the radio portion of the system to a pair of chips and a crystal reference oscillator; in addition, the interconnect challenge is reduced to two short transmission lines to the diplexer. The block diagram includes compatible analog-to-digital-converter (ADC) and clock-generator products from Hittite.

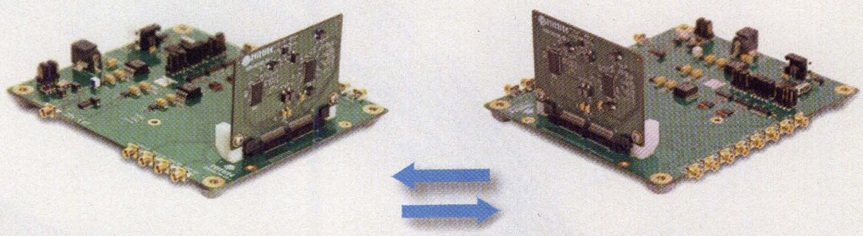

5. This is the model HMC6450 AiP transceiver evaluation kit, with both the HMC6000 transmitter and HMC6001 receiver in antenna-in-package (AiP) format.

Figure 4 shows the block diagram for a multi-Gb/s indoor link adhering to the WiGig standard that is based on the HMC6000 and HMC6001. A variety of high speed digital interfaces can be used for such a link, including GigE, USB, HDMI, or even PCIe. But to compete in consumer markets, this design integrates all network processing, Media Access Control (MAC), and Physical Layer functionality into a single application-specific integrated circuit (ASIC). The ADCs and digital-to-analog converters (DACs) in this system design typically operate at multi-Gb/s sampling rates, or at least twice the symbol rate of the modulation format. To minimize power and cost in a consumer application, the ADCs and DACs might even be integrated as part of the ASIC. Since WiGig employs time-division-duplex (TDD) multiplexing, this system can operate without a diplexer. Since its communications path distance is limited to the size of a room, the high-gain antenna used with outdoor millimeter-wave point-to-point links can typically be replaced by a much smaller, lower-gain antenna. To minimize transmission-line losses at 60 GHz, the radio chipset should be located as close to the antenna as possible. The differential baseband interface for the transceiver ICs simplifies this placement by allowing separation between the ASIC and the ICs.

To try out these 60-GHz ICs, evaluation kits are available with coaxial connectors and in AiP configurations. For example, model HMC6450 is a 60-GHz AiP Transceiver Evaluation Kit **(Fig. 5)** comprised of two boards, with each board including the model HMC6000LP711E transmitter and the model HMC6001LP711E receiver. With its configuration software, a user has everything needed to set up a bidirectional millimeter-wave link at 60 GHz with universal analog I and Q interface. For those preferring coaxial connectors, model HMC6451 is a 60-GHz MMPX Transceiver Evaluation Kit with the same functionality and software but with snap-on MMPX 60-GHz connectors. MWRF

HITTITE MICROWAVE CORP., 2 Elizabeth Dr., Chelmsford, MA 01824; (978) 250-3343, FAX: (978) 250-3373; e-mail: txrx@hittite.com, www.hittite.com.

JACK BROWNE | Technical Contributor

TWTAs Power Satcom Systems

Vacuum-tube amplifiers are still alive and well, providing high gain and output-power levels in a wide range of satellite systems—both in space and on the ground.

HIGH-POWER MICROWAVE systems still depend on a variety of vacuum electronic devices to reach their required output levels. While vacuum tubes may have long ago departed from consumer radios, they are alive and well in many satellite communications (satcom) and military electronics systems. In fact, in deep space where reliability is essential, microwave traveling-wave tubes (TWTs) and traveling-wave-tube amplifiers (TWTAs) are often the signal-boosting subsystems of choice at microwave through millimeter-wave frequencies.

TWTs and TWTAs are both associated with high-output-power levels and gain. But in recent years, the performance levels of these devices has improved in terms of a number of performance parameters, including gain flatness with frequency, linearity, and phase distortion. At one time, "linearity" in a TWT or TWTA was considered equivalent to its continuous-wave (CW) output power level backed off by at least 3 dB. But with more and more TWT and TWTA manufacturers complying with the requirements of MIL-STD-188-164A interoperability and performance standards for C-band, X-band, and Ku-band satcom earth terminals, an increasing amount of data are available on the performance levels of TWTAs under a variety of operating conditions.

In addition to the motivation to save weight and volume on satellites that has helped reduce the size of newer TWTAs, military customers have pushed TWT and TWTA designers and suppliers for smaller products as part of military size, weight, and power (SWaP) initiatives. And the requirements of modern conflicts have demonstrated the need to transfer an increasing amount of data quickly and securely from the tactical edge of a conflict to command centers. Hence, TWTs and TWTAs have gotten smaller while maintaining high output-power levels.

1. This satcom trailer, powered by a Ku-band TWTA from MCL, was used for mobile satcom applications in Iraq during Operation Iraqi Freedom. [Photo courtesy of MCL, Inc. (www.mcl.com).]

As an example, **Fig. 1** shows a US Army satcom trailer that was deployed in Iraq, incorporating a Ku-band TWTA from MCL (www.mcl.com). The high-frequency tube amplifier is one of a wide range of TWTAs designed and produced by the company for satcom applications, meeting both MIL-STD-188-164A/B (proposed) and Army Forces Strategic Command (ARSTRAT) requirements.

In keeping with the need for increased linear power in smaller packages, MCL has developed lines of antenna-mountable TWTAs, including its outdoor amplifier models MT2300 and MT3600, for Ka-band satcom uplinks **(Fig. 2)**. The MT2300 TWTAs weigh just 33 lbs while the MT3600 TWTAs weigh 47 lbs. MT2300 TWTAs can be specified for Ku-band frequencies from 13.75 to 14.50 GHz as well as for Ka-band frequencies from 27.5 to 31.0 GHz. The Ku-band models deliver 100 W linear output power and 175 W peak output power. The Ka-band models provide 60 W linear output power and 150 W peak output power, or 120 W linear output power with 215 W peak output power. The MT3600 TWTA

is available in Ka-band (27.5 to 31.0 GHz) and Q-band (43.5 to 45.5 GHz) versions, the latter with an integral frequency block upconverter (BUC) and solid-state driver amplifier. The Ka-band models offer either 8 W linear output power with 150 W peak output power, or 120 W linear output power with 215 W peak output power. The Q-band TWTAs can be specified for either 55 W linear output power or 80 W linear output power.

To simplify upgrades of the AN/USC-60A fly-away triband satellite terminal (FTSAT), L-3 Communications Narda Satellite Networks (www.nardamicrowave.com) has developed its model 1.2 Ka-60A upgrade system, which can be integrated with other military multiband super-high-frequency (SHF) satcom systems. The upgrade hardware is designed to meet ARSTRAT certification when integrated with the base system. It consists of a 1.2-m segmented carbon fiber reflector, adapter plate, and linearized 175-W TWTA.

Bosch Telecom GmbH (www.bosch-telecom.com) emphasizes the importance of TWTAs for space-based communications in its brochure, "Traveling Wave Tube Amplifiers (TWTAs) for Space Applications," available as a free PDF download from the firm's website. The company's TWTAs, which are available for use from 1.5 to 30.0 GHz at power levels from 10 to 450 W CW, have been integrated into a wide range of satellite systems, including PIONEER 1, PIONEER 2, the Ka-band and Ku-band Astra satellites, Eutelsat III, and Intelsat 9. The company's TWTAs feature high-performance electronic power conditioner (EPC) subassemblies that provide the high voltages needed by TWTs.

Comtech Xicom Technology (www.xicomtech.com) offers a number of TWTAs that cover more than one satcom band within a single unit, such as the model XTRD-2000CX TWTA with at least 500 W output power at C-band (5.850 to 6.425 GHz) and X-band (7.90 to 8.40 GHz) frequencies. It uses a TWT rated for 2 kW output power.

The firm's model XTD-750KHE TWTA **(Fig. 3)** is designed for antenna mounting in Ku-band satcom links. It is based on a high-efficiency TWT with dual-stage collector. The TWTA delivers 270 W linear output power, 355 W maximum CW output power, and 750 W peak output power from 13.75 to 14.50 GHz with large- and small-signal gain of at least 70 dB. It weighs only 56 lbs and draws only 1450 W power at its full output rating. Level control is accomplished by means of a 30-dB attenuator circuit that can be adjusted in 0.1-dB steps. The amplifier is also available as model XTD-750KHE-B1 with a BUC that accepts input signals from 950 to 1700 MHz. Both amplifier versions are equipped with an Ethernet interface for remote control.

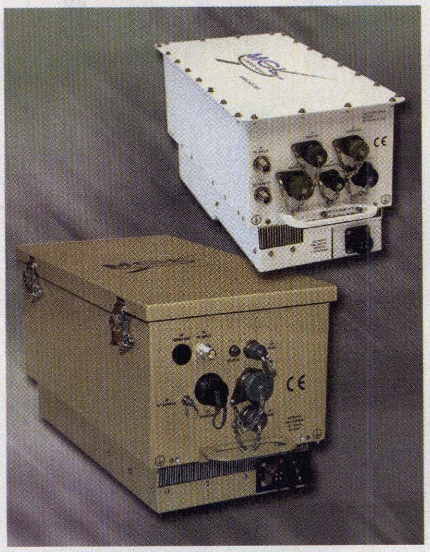

2. Models MT2300 and MT3600 are antenna-mountable TWTAs for use in satcom band through Q-band frequencies (43.5 to 45.5 GHz). [Photo courtesy of MCL, Inc. (www.mcl.com)]

3. Model XTD-750KHE is an antenna-mount TWTA with 750 W peak output power from 13.75 to 14.50 GHz. [Photo courtesy of Comtech Xicom Technology (www.xicomtech.com)]

Communications & Power Industries (www.cpii.com) offers a range of indoor and outdoor TWTAs for fixed and mobile satcom applications covering C-, Ku-, X-, and Ka-band frequencies at power levels from 200 to 750 W. For example, the TO-1TO series of outdoor TWTAs is intended for use at C-band (5.85 to 6.425 GHz), X-band (7.9 to 8.4 GHz), and Ku-band (14.0 to 14.5 GHz) frequencies, with 85 W minimum output power at the amplifier flange at C-band, 120 W minimum output power at X-band, and 80 W minimum output power at Ku-band frequencies. The TWTA offers 41-dB small-signal gain at the lower frequencies and 45-dB small-signal gain at X- and Ku-band frequencies.

TMD Technologies Ltd. (www.tmd.co.uk) offers high-power tubes of different types, including TWTAs for laboratory test applications. Supplied in 19-in. rack-mount enclosures, these TWTA-based systems include the model PTX7437 transmitter subsystem optimized for radar testing from 9.0 to 9.5 GHz. The subsystem generates 8000 W peak output power at a 2% pulse duty cycle and 20-μs pulse width. It boasts 60-dB gain to boost pulsed input signals, and measures 355 x 430 x 155 mm and weighs 20 kg.

Another well-known name in TWTAs for test applications is AR RF/Microwave Instrumentation, with narrowband and broadband TWTAs for use at frequencies through 45 GHz, and with as much as 10 kW pulsed output power from 8 to 10 GHz for high-power RF/microwave test applications. For example, model 200T2Zz-5G40A is a rack-mount TWTA with forced-air cooling for test applications from 26.5 to 40.0 GHz. It provides 200 W CW minimum output power minimum with 50 W linear output power at 1-dB compression.

Finally, in addition to TWTs and TWTAs, some vacuum-tube manufacturers supply compact assemblies that include EPCs, linearizer circuits, and the TWTA circuits. Known as microwave power modules (MPMs), these compact units can not only save space in mobile and fixed satcom earth stations, but also support simplified connections for rapid installation. MWRF

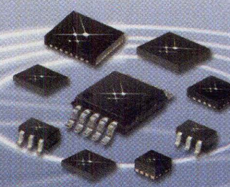

SKYWORKS

Digital Attenuators

Select Digital Attenuators Available from Stock for Prototype or High Volume Production

- High Attenuation Range and Accuracy
- Broadband GaAs 1 Bit–7 Bit Designs
- Low Cost, Small Form Factor Packaging
- Integrated CMOS Controllers for Low Current and Low Frequency Operation
- Integrated Serial Port Interface (SPI) and Decode Functions
- Monotonic Step Response with Flat Broadband Attenuation
- Low Reference Insertion Loss and High IIP3

Digital Attenuators for IF/UHF/VHF and Broadband RF Applications

Part Number	Frequency Range	Number of Bits	Least Significant Bit (dB)	Control Interface	Maximum Attenuation (dB)	Typical Insertion Loss (dB)	Typical IIP3 (dBm)	Package (mm)
AA103-72LF	10–2500 MHz	1	10	Parallel	10	0.3	41	SOT-23 5L 2.9 x 2.7 x 1.16
SKY12406-360LF	50–600 MHz	1	12	Parallel	12	0.3	46	DFN 8L 2 x 2 x 0.9
SKY12407-321LF	50–600 MHz	1	12	Parallel	12 (100 Ω Differential I/O)	0.3	48	QFN 12L 3 x 3 x 0.75
AA116-72LF	4–2000 MHz	1	15	Parallel	15	0.35	41	SOT-23 5L 2.9 x 2.7 x 1.16
AA104-73LF	0.3–2500 MHz	1	32	Parallel	32	0.9	41	SOT-23 6L 2.9 x 2.7 x 1.16
SKY12324-73LF	500–4000 MHz	2	4	Parallel	12	0.9–1.3	43	SOT-23 6L 2.9 x 2.7 x 1.16
SKY12338-337LF	350–4000 MHz	2	6	Parallel	18	0.55–1.3	45	QFN 12L 3 x 3 x 0.9
SKY12325-350LF	500–4000 MHz	3	1	Parallel	7	0.7–1.3	47	QFN 16L 3 x 3 x 0.75
SKY12348-350LF	100–3000 MHz	4	1	Parallel	15	0.8–1.2	45	QFN 16L 3 x 3 x 0.75
SKY12340-364LF	300–2000 MHz	5	0.5	SPI	15.5	1.4–1.8	45	QFN 32L 5 x 5 x 0.9
SKY12322-86LF	500–4000 MHz	5	0.5	Parallel	15.5	1.4–3.0	45	MSOP 10L 5 x 3 x 1.1
SKY12323-303LF	500–3000 MHz	5	1	Parallel	31	1.4–2.3	48	MSOP 10L 5 x 3 x 1.1
SKY12328-350LF	500–4000 MHz	5	0.5	Parallel	15.5	1.1–2.3	45	QFN 16L 3 x 3 x 0.75
SKY12339-350LF	400–3000 MHz	5	1	Parallel	31	1.2–2.0	39	QFN 16L 3 x 3 x 0.75
SKY12345-362LF	700–4000 MHz	5	0.5	SPI	15.5	1.2–2.0	42	QFN 24L 4 x 4 x 0.9
SKY12347-362LF	DC–3000 MHz	6	0.5	SPI or Parallel	31.5	1.2–2.0	50	QFN 24L 4 x 4 x 0.9
SKY12343-364LF	100–4000 MHz	7	0.25	SPI or Parallel	31.75	1.8	50	QFN 32L 5 x 5 x 0.9

Skyworks Green™ products are compliant to all applicable materials legislation and are halogen-free. For additional information, refer to Skyworks Definition of Green™, document number SQ04-0074.

All parts are lead (Pb)-free and RoHS-compliant.

Samples and Evaluation Boards Available at www.skyworksinc.com

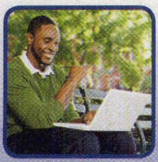
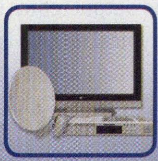




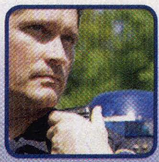

USA: 781-376-3000 • Asia: 886-2-2735 0399 • Europe: 33 (0)1 43548540 • Email: sales@skyworksinc.com

www.skyworksinc.com • NASDAQ: SWKS

Low-Noise Amplifiers Feature Bias Flexibility

These compact amplifiers are fit for a variety of small-signal applications from 30 to 3000 MHz, allowing users to "play" with the bias current to improve on efficiency and intercept-point performance.

LOW-NOISE AMPLIFIERS (LNAs) are essential for receiver front ends when signal sensitivity is important. The models SKY67012-396LF, SKY67013-396LF, SKY67014-396LF, and SKY67015-396LF (the latter available in June) surface-mount LNAs from Skyworks Solutions (www.skyworksinc.com) are four such notables. They operate across frequency ranges of 300 to 600 MHz, 600 to 1500 MHz, 1500 to 3000 MHz, and 30 to 400 MHz respectively. Based on advanced GaAs pseudomorphic-high-electron-mobility-transistor (pHEMT) process technology, they are ideal for use in a wide variety of wireless systems.

All four amplifiers are housed in miniature DFN 8-pin 2 x 2 mm DFN packages **(see figure)**, and all incorporate on-die stability structures and integrated active bias circuitry for superior performance. The amplifiers allow users to adjust quiescent supply current (I_{ddq}) over a range of 5 to 50 mA. This provides the flexibility, for example, to achieve higher input third-order-intercept points (IIP3s).

The output power at 1-dB compression for each amplifier will follow the level of supply voltage while the IP3 performance will more closely follow the supply current. The amplifiers feature the capability to set supply current independent of supply voltage. For a given bias control voltage, the choice of external resistor will set the available supply current for a given application.

As an example, model SKY67012-396LF covers 300 to 600 MHz, with typical midband (at 450 MHz) gain of 16.5 dB and noise figure of 0.85 dB. It can be used with supply voltages from +1.5 to +5.0 VDC, with a typical power supply of +3.3 VDC and 15 mA. In terms of linearity, the LNA exhibits typical IIP3 of +7.5 dBm and typical OIP3 of +24 dBm, although supply current can be adjusted for improved intercept-point performance. The input 1-dB compression point is typically +3.5 dBm while the output 1-dB compression point is typically +12 dBm, when the amplifier is run at its nominal power-supply (15 mA at +3.3 VDC) setting. The low-current amplifier achieves input return loss of typically 20 dB and output return loss of typically 12 dB, with 26-dB typical reverse isolation.

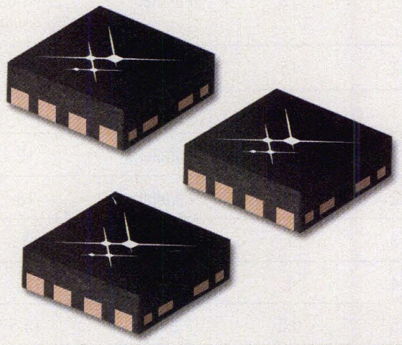

Models SKY67012-396LF, SKY67013-396LF, SKY67014-396LF, and SKY67015-396LF are GaAs pHEMT low-noise amplifiers that are designed for use from 30 to 3000 MHz, with adjustable linearity performance depending upon how the power supply is set.

Model SKY67013-396LF can be used from 600 to1500 MHz, with typical midband (900 MHz) noise figure of 0.85 dB and typical midband small-signal gain of 14 dB. It can also be run on bias voltages of +1.5 to +5.0 VDC, with a typical supply of 15 mA at +3.3 VDC. Over its 900-MHz bandwidth, SKY67013-396LF delivers typical IIP3 of +12 dBm and IP3 of +26 dBm, with input 1-dB compression point of typically +2.5 dBm and output 1-dB compression point of typically +15.5 dBm. The input return loss is typically 23 dB while the output return loss is typically 16 dB, with typical return isolation of 22 dB.

The SKY67014-396LF is well suited for 500 to 3000 MHz. With I_{ddq} at 15 mA, the typical small-signal gain is 12.5 dB at 2.35 GHz with 0.9-dB associated noise figure. At 15 mA and +3.3 VDC, it offers typical IIP3 of +13.5 dBm and typical OIP3 of +26 dBm, with input 1-dB compression point of typically +3.5 dBm and output 1-dB compression at typically +15 dBm. The input return loss is typically 17 dB while the output return loss is typically 13 dB, with a typical reverse isolation of 22 dB.

Last but not least, model SKY67015-396LF is suitable for 30 to 400 MHz. With quiescent drain current set to 15 mA, it boasts typical small-signal gain of 17 dB at 200 MHz, with 0.85 dB noise figure at that same frequency. At 15 mA and +3.3 VDC, the typically IIP3 is 3 dBm and typical OIP3 is +20 dBm, with typical input 1-dB compression point of –1 dBm and typical output power at 1-dB compression of +15 dBm. The input return loss is typically 16 dB while the output return loss is typically 14 dB, with a typical reverse isolation of 24 dB.—*JB*

SKYWORKS SOLUTIONS, INC., 20 Sylvan Rd., Woburn, MA 01801; (781) 376-3100, FAX: (781) 376-3300, *www.skyworksinc.com*.

Coaxial Cables Are Phase Stable

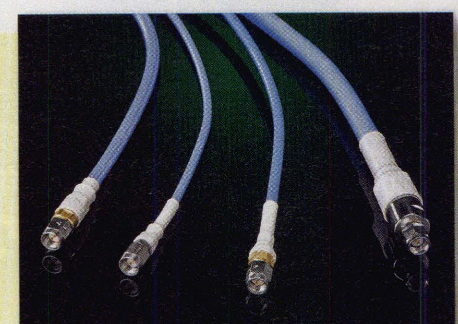

The Phase Critical Product Line from Times Microwave Systems features an expanded range of PhaseTrack® cable assemblies based on the company's low-loss cable assemblies. The cables are designed to provide extremely stable phase characteristics over broad temperature and frequency ranges. The PhaseTrack-210 cable assemblies, for example, which are usable through 30 GHz, feature insertion loss of only 0.43 dB per foot at 18 GHz. The exhibit a velocity of propagation of 83% with typical VSWR of 1.35:1 across the frequency range and better than –100 dB shielding effectiveness (SE). These cables are usable at temperatures from –55 to +125°C. This is just one example of the PhaseTrack product line, which includes cables in standard flexible, low smoke flexible, in-the-box flex and semi-rigid versions.
TIMES MICROWAVE SYSTEMS, 358 Hall Ave., Wallingford, CT 06492; (203) 949-8400, FAX: (203) 949-8423, *www.timesmicrowave.com.*

Model Services, Library Expand

Microwave modeling professionals Modelithics have announced an expansion of their X-parameter (nonlinear) measurement-based modeling services to include conversions of nonlinear equivalent-circuit models to X-parameter models. This service should be of particular interest to users of the Genesys high-frequency modeling software from Agilent Technologies (www.agilent.com), who can now use this service to acquire X-parameter models that enable accurate as well as computationally efficient nonlinear simulations. Modelithics has also released the latest version of their Modelithics COMPLETE Library™ of accurate and scalable models for the Genesys® software program from Agilent. This latest release adds 17 capacitive-resistive-inductive (CRL) library models, more than 20 nonlinear diode and transistor models, and introduces Modelithics SLC library models formatted for use with the Genesys software. The new library release also includes a measurement-based substrate library. The upgrade will be forwarded, free of charge to all Modelithics COMPLETE Library customers currently under a Platinum Maintenance contract. In addition, visitors to the Modelithics website can experience a free trial by clicking on a link found at the website.
MODELITHICS, INC., 3650 Spectrum Blvd., Tampa, FL 33612; (888) 359-6359, FAX: (813) 866-6334, e-mail: sales@Modelithics.com, *www.Modelithics.com.*

Portable Analyzer Scours Radio Waves

Invisible Waves X™ is a personal-computer (PC) -based spectrum analyzer capable of scanning for signals from 9 kHz to 1.8 GHz. The spectrum analyzer is built around a direct-digital synthesizer (DDS) and superheterodyne receiver architecture. The portable monitoring system can work with the firm's RF Coordinator™ software to identify open and usable portions of RF spectrum as well as the UFO Alert™ software to identify interfering signals. It features ±dB amplitude accuracy over a typical amplitude range of –130 to 0 dBm, connecting to a PC by means of a standard 2.0 Universal Serial Bus (USB) interface. It exhibits 10 PPM frequency stability and provides filter bandwidths from 1 kHz to 50 MHz to isolate and analyze signals of interest.
KALTMAN CREATIONS LLC, 651 Amberton Crossing, Suwanee, GA 30024; (678) 714-2000, FAX: (678) 714-2092; e-mail: sales@kaltmancreationsllc.com, *www.kaltmancreationsllc.com.*

Bluetooth Modules Integrate Controllers

The PAN1321i Series of Bluetooth RF modules feature a Bluetooth transceiver, antenna, integrated controller, and AT Command Set Application Program Interface (API). The modules are qualified to the Bluetooth 2.0 standard and offer a highly integrated, cost engineered solution for Bluetooth applications using Serial Port Profile (SPP). The modules interface with the Apple authentication coprocessor and support the iPod Accessory Protocol (iAP). The Bluetooth transceiver features transmit output power of +3 dBm and receiver sensitivity of –86 dBm for 10^{-3} bit error rate (BER). Each module measures just 15.6 x 8.7 x 2.8 mm and incorporates a reference clock. It operates from an external supply of +2.7 to +3.6 VDC and is designed for operating temperatures from –40 to +85°C.
PANASONIC INDUSTRIAL DEVICES SALES COMPANY OF AMERICA, 1 Panasonic Way, Secaucus, NJ 07094; (201) 558-0901, *www.panasonic.com/rfmodules.*

Omni Antenna Pulls In IBW

Model CMS69273 is a ceiling-mount broadband omnidirectional antenna with linear vertical polarization which provides indoor cellular coverage for GSM, DCS, UMTS, and LTE/WiMAX standards in the frequency ranges from 698 to 960 MHz, 1575 MHz, and 1710 to 2700 MHz, with peak gains of 1, 2, and 3

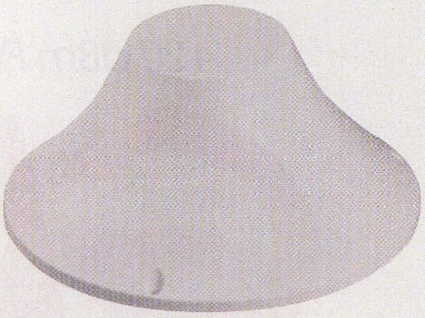

dBi, respectively, over those three frequency bands. Suitable for use by in-building-wireless (IBW) service providers, the antenna features a uniform, symmetrical pattern that enables system integrators to precisely determine cell size. The antenna is available in a low profile, aesthetically neutral housing made with UL 94 V-0 materials. Mounting options include a flush mount with screws and anchors or a threaded stem. The antenna weighs 0.34 kg and can handle 25 W power.
LAIRD TECHNOLOGIES, 3481 Rider Trail S., Earth City, MO 63045; (636) 898-6000, FAX: (636) 898-6100, *www.lairdtech.com.*

Mixer Translates Signals To 6 GHz

Model LTC is a wide-dynamic-range downconverting mixer from Linear Technology designed to translate input signals from 4 to 6 GHz to intermediate-frequency (IF) signals to 1 GHz. The mixer has single-ended 50-Ω RF and local-oscillator (LO) input ports. It features an input third-order intercept point (IIP3) of +25.9 dBm (at 5250 MHz) and is ideal for wireless systems such as point-to-point broadband microwave links, 5-GHz license-free band WiMAX radios, satellite receivers, radar systems, avionics, public safety radios, and RF test systems. It also delivers high conversion

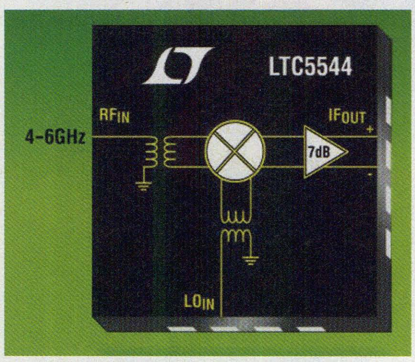

gain of 7.4 dB at 5250 MHz thanks to an integrated IF amplifier and a noise figure of 11.3 dB, also at 5250 MHz. It operates on a single +3.3-VDC supply drawing typically 194 mA current. It includes an LO buffer amplifier which requires only +2-dBm LO drive level. It also has a power-down feature with 0.6-microsecond turn-on/turn-off time. The mixer is supplied in a 16-lead, 4 x 4 mm plastic QFN package. P&A: $8.50 each in 1000 qty.; stock. **LINEAR TECHNOLOGY CORP.**, 1630 McCarthy Blvd., Milpitas, CA 95035-7417; (408) 432-1900, FAX: (408) 434-0507, ***www.linear.com/product/LTC5544***.

Duo of ICs Drive Automotive GPS

A pair of integrated-circuit (IC) solutions are ideal for in-automobile Global Navigation Satellite System (GNSS) applications. Model MAX2670 is a dual-stage, low-noise amplifier (LNA) while model MAX2769B is a universal GPS receiver qualified to AC-Q100 automotive requirements. The receiver IC is driven by a fractional-N frequency synthesizer and provides programmable intermediate-frequency (IF) output with cumulative noise figure of 1.4 dB. The receiver features an integrated crystal-oscillator reference and can operates from a supply voltage of +2.7 to +3.7 VDC. It is supplied in a 28-pin RoHS-compliant lead-free QFN package. The LNA IC, model MAX2670, features 1 dB noise figure and 34.8 dB gain at the GPS frequency of 1575 MHz. It suffers gain variations of less than 0.3 dB with temperature and offers adjustable gain, controllable in 3.4-dB steps. The LNA, which can be used a supply voltages of +3.0 to +5.5 VDC, is supplied in a 3 x 3 mm surface-mount package that is electrostatic-discharge (ESD) protected to a ±2-kV human-body model (HBM). Both ICs are based on the firm's low-power SiGe BiCMOS process technology. **MAXIM INTEGRATED PRODUCTS, INC.**, 120 San Gabriel Dr., Sunnyvale, CA 94086; (408) 737-7600, FAX: (408) 774-9139, ***www.maxim-ic.com.***

Hybrid Couplers Span 1.4 To 26.5 GHz

A pair of broadband 90-deg. hybrid couplers are suitable for splitting and combining signals over broad frequency ranges through 26.5 GHz. Model 3014265 provides frequency coverage from 1.4 to 26.5 GHz while model 3014265 features outstanding performance from 1.4 to 26.5 GHz. The lower-frequency model 3014265 suffers less than 3-dB insertion loss from 1.4 to 26.5 GHz with better than 13-dB isolation between ports. It achieves amplitude unbalance of ±1.2 dB across the full frequency range with phase unbalance of typically ±12 deg. The maximum VSWR for this 3-dB hybrid coupler is 1.80:1. The higher-frequency model 3017265 has less than 3.4-dB insertion loss from 1.7 to 26.5 GHz, with better than 14-dB isolation between ports. It offers amplitude unbalance of ±1.5 dB and phase unbalance of ±10 deg. The maximum VSWR for model 3017265 is 1.85:1. Each of the hybrid couplers handles 20 W average power and 3 kW peak power across operating temperatures from –54 to +85°C. Model 3014265 measures 2.62 x 1.00 x 0.49 in. while model 3017265 measures 2.60 x 0.625 x 0.50 in. They are both supplied with SMA female connectors but available with Type N female connectors as an option. **KRYTAR, INC.**, 1288 Anvilwood Ave., Sunnyvale, CA 94089; (408) 734-5999, (877) 734-5999, FAX: (408) 734-3017, e-mail: sales@krytar.com, ***www.krytar.com.***

Switches Handle DC To 12.4 GHz

The 2N and 2NH Series of single-pole, double-throw (SPDT) switches are designed for signal-control applications from DC to 12.4 GHz. The break-before-make, 50-Ω switches are supplied with high-power Type N connectors for large-signal use, and are rated for operating lifetimes of 1 million switching cycles or more. The switches weigh 8.5 oz. and are designed for ambient operating temper-

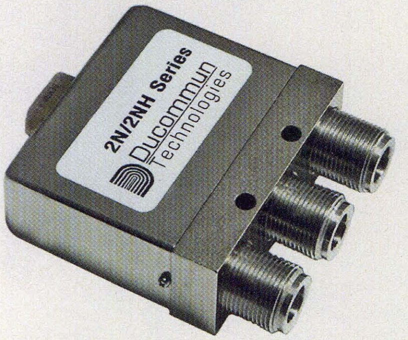

atures from –55 to +85°C. Both switch series are available with failsafe, latching self cut-off, or pulse latching functions. **DUCOMMUN LABARGE TECHNOLOGIES**, 23301 Wilmington Ave., Carson, CA 90745; (310) 513-7200, FAX: (310) 513-0206, ***www.ducommun.com.***

Front-End Module Serves AMR Systems

Model RF6559 is an integrated transmit/receive front-end module for use in 915-MHz automated-metering-system (AMR) applications. It helps reduce the circuit-board size by minimizing the number of required external components. It features a three-stage power amplifier with 42 dB gain from 902 to 928 MHz and typical output power of +28 dBm over that same frequency range. The module includes a pair of single-pole, double-throw (SPDT) switches that allow transmission and reception with a single antenna. It is housed in a 28-pin, 6 x 6 mm laminate package. **RF MICRO DEVICES**, 7628 Thorndike Rd., Greensboro, NC 27409-9421; (336) 678-5570, e-mail: customerservice@rfmd.com, ***www.rfmd.com.***

**Domestic Edition only   **International Edition only   This index is provided as an additional service by the publisher, who assumes no responsibility for errors or omissions.*

MARKETING & ADVERTISING STAFF

VICE PRESIDENT & MARKET LEADER
Bill Baumann
T: (201) 845-2403
F: (201)845-2484
E: bill.baumann@penton.com

GROUP SALES MANAGER
Paul Milnamow
T: (312)-840-8462
F: (312)-514-3957
E: paul.milnamow@penton.com

NORTHEAST
David Madonia
T: (212)-204-4331
E: dave.madonia@penton.com

WEST
Gene Roberts
T: (408) 268-5414
F: (408) 268-8045
E: gene.roberts@penton.com

SOUTH
Bill Yarborough
T: (713) 636-3809
T: (713) 523-8384
E: bill.yarborough@penton.com

CENTRAL
Tracy Smith
T: (913) 967.1324
F: (913) 514.6881
E: tracy.smith@penton.com

DIRECT CONNECTION ADS CLASSIFIED ADVERTISING
Phyllis L. Schroder
E: phyllis.schroder@penton.com
Kevin Dern
E: kevin.dern@penton.com

Penton Electronics Group

EUROPEAN SALES REP
Mark Durham
T: +44 (0)7958 564137
E: mark.durham@penton.com

TAIWAN, R.O.C.
Charles C.Y. Liu
T: (886)-2-2727-7799
F: (886)-2-2728-3686

JAPAN
Hiro Morita
T: 81-3-3261-4591
F: 81-3-3261-6126

KOREA
Jo Young Sang
T: 011-82-2-739-7840
F: 011-82-732-3662

CUSTOMER SERVICE - SUBSCRIPTIONS
New/Renew/Cancel/Change Address/Missing and Back Issues
T: 866-505-7173 F: 847-763-9673
E: microwaves&rf@halldata.com

Subscription Assistance and Information: Microwaves & RF (ISSN 0745-2993) is published monthly, except semi-monthly in December. **Microwaves & RF** is sent free to individuals actively engaged in high-frequency electronics engineering. In addition, paid subscriptions are available. Subscription rates for U.S. are $95 for 1 year ($120 in Canada, $150 for International). Published by Penton Media, Inc., 9800 Metcalfe Ave., Overland Park, KS 66212-2216. Periodicals Postage Paid at Shawnee Mission, KS and at additional mailing offices.
POSTMASTER: Send change of address to Microwaves & RF, Penton Media Inc., P.O. Box 2095, Skokie, IL 60076-7995. For paid subscription requests, please contact: Penton Media Inc., P.O. Box 2100, Skokie, IL 60076-7800. Canadian Post Publications Mail agreement No. 40612608. Canadian GST# R126431964. Canada return address: Bleuchip International, P.O Box 25542, London, ON N6C6B2.

Back issues of **MicroWaves** and **Microwaves & RF** are available on microfilm and can be purchased from National Archive Publishing Company (NAPC). For more information, call NAPC at 734-302-6500 or 800-420-NAPC (6272) x 6578.

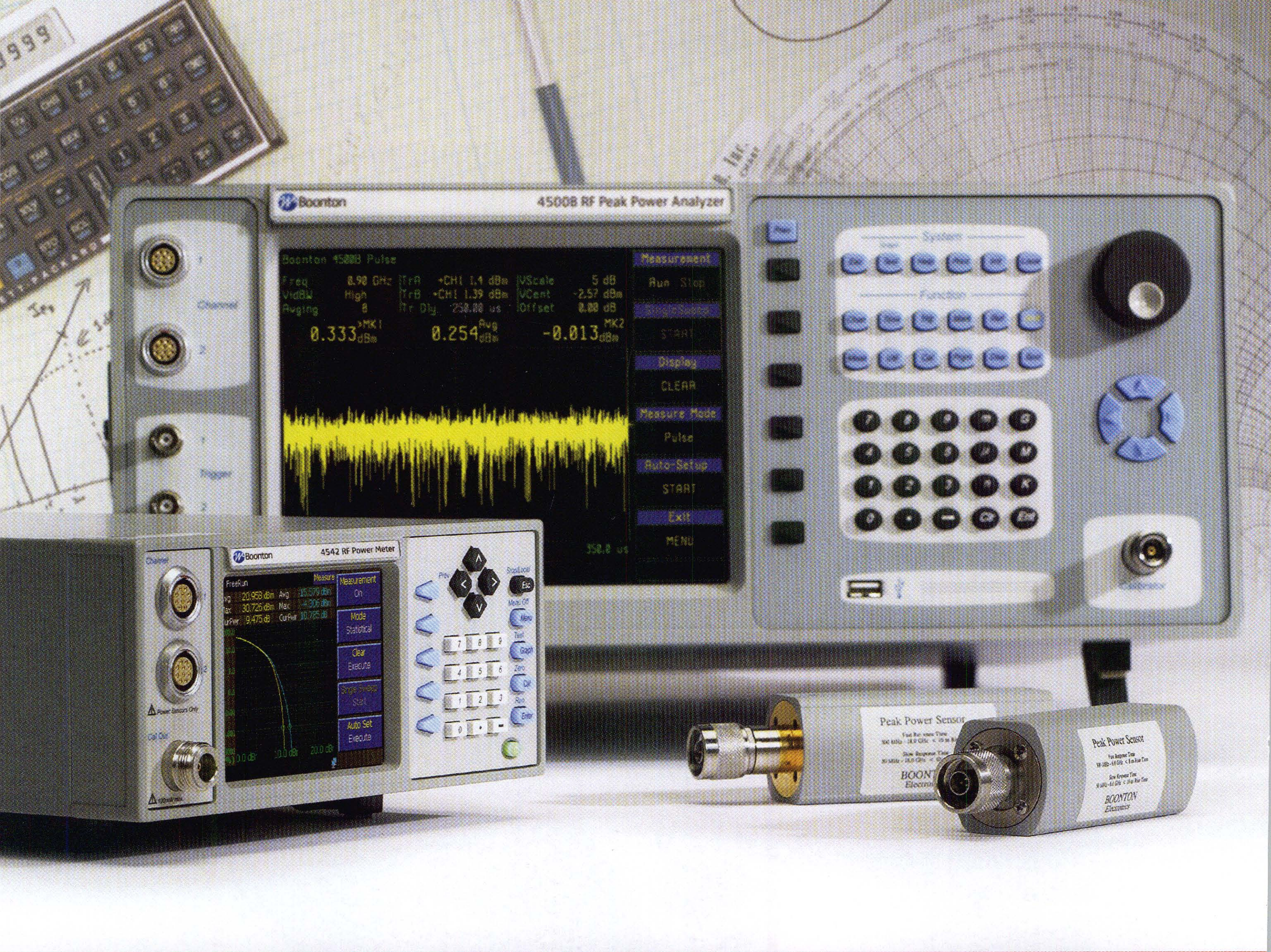
Boonton
4500B RF Peak Power Analyzer
Boonton 4500B Pulse
Measurement
Display
CLEAR
Measure Mode
Pulse
Auto-Setup
START
Exit
MENU
Boonton
4542 RF Power Meter
Peak Power Sensor
Peak Power Sensor